

ABSTRACT

Title of Thesis: CALIBRATING CAPACITANCE SENSORS TO ESTIMATE WATER CONTENT, MATRIC POTENTIAL, AND ELECTRICAL CONDUCTIVITY IN SOILLESS SUBSTRATES

Félix Rubén Arguedas Rodríguez, MS, 2009

Directed By: John Lea-Cox, PhD. Associate Professor,
Department of Plant Science and
Landscape Architecture

The nursery and greenhouse industry requires precise methods to schedule irrigations, since current practices are subjective and contribute to water and nutrient runoff. Capacitance sensors were calibrated to precisely estimate substrate water content, matric potential, and pore water electrical conductivity (EC) in five soilless substrates. Regression coefficients (R^2) ranged from 0.29 – 0.88 and 0.16 – 0.79 for water content in 5-cm and 20-cm column heights; matric potential R^2 ranged from 0.10 – 0.98 and 0.79 – 0.98, respectively. Pore water EC calibrations were investigated, contrasting two sensor types and two prediction models. Results were applied to an empirical greenhouse dataset. Better precision and accuracy were achieved with ECH₂O-TE sensor and Rhoades model. Capacitance sensors provide precise estimates of plant-available water in most soilless substrates, while pore water EC accuracy and precision depends on the sensor-model combination. These results will enable growers to precisely schedule irrigations based on water content and pore water EC.

CALIBRATING CAPACITANCE SENSORS TO ESTIMATE WATER CONTENT,
MATRIC POTENTIAL, AND ELECTRICAL CONDUCTIVITY IN SOILLESS
SUBSTRATES

By

Félix Rubén Arguedas Rodríguez

Thesis submitted to the Faculty of the Graduate School of the
University of Maryland, College Park, in partial fulfillment
of the requirements for the degree of

Masters in Science
2009

Advisory Committee:

John D. Lea-Cox, PhD., Chair
Associate Professor, Department of Plant Science and Landscape Architecture

Andrew G. Ristvey, Ph.D.
Agent, University of Maryland Extension

David S. Ross, PhD.
Professor, Department of Environmental Science and Technology

© Copyright by
Félix Rubén Arguedas Rodríguez
2009

Dedication

I was raised with integrity, passion, patience, and most importantly, endless love.

Thanks to her sacrifice and wisdom.

“She instilled in me the value of intellectual work rather than purely physical work”

Dedicated to Lilliam Rodriguez Cordero.

Acknowledgements

Firstly, I would like to thank Dr. John Lea-Cox for his guidance and advice throughout my time at the University of Maryland. I would also like to thank Dr. Andrew Ristvey and Dr. David Ross for all their wise advice and help.

I am very grateful to the Chesapeake Bay Trust, The Horticultural Research Institute, and the University of Maryland Agricultural Experiment Station for financial and research support.

I am also grateful to Dr. William Kenworthy, Marie Bryer, Susan Burk, Michelle Pridmore, Kathy Hunt, Patrick Beach, Rosalind Kilroy and Joshua Thornton for all their assistance during my time in the Department of Plant Science and Landscape Architecture.

My personal thanks to Piyumi Ranaweera, who made my final data collection possible, with all her hard work. I would also like to thank Sydney Wallace, Shaun Faulkner, Betty Morgavan, and Richelle Green for making my work at the University of Maryland research greenhouse complex as pleasant and productive as it was.

Sincere thanks to my friends, professors, and people back in Costa Rica, that also made their contribution in one way or another in encouraging me to keep trying and working hard to reach my dreams.

My most profound and special thanks to Karen Fiuza. She has been the person who has provided the most loving support of my work, and has giving me the joy of her companionship.

Table of Contents

Dedication.....	ii
Acknowledgements.....	iii
Table of Contents.....	iv
List of Tables.....	vi
List of Figures.....	viii
Chapter 1: Literature Review.....	1
Sensing Plant Available Water.....	1
Irrigation Scheduling.....	2
Which techniques are used to measure water in soil / soilless substrates?.....	5
Soil water potential.....	5
Soil water content.....	7
Capacitance Sensors.....	8
Factors Affecting the Measurement of Volumetric Water Content when utilizing Electromagnetic Sensors.....	13
Physical Properties of Soilless Substrates.....	16
Soilless substrates physical characteristics.....	17
Chemical Properties of Soilless Substrates.....	21
Chapter 2: Determination of Water Desorption and Sensor Calibration.....	28
Introduction.....	28
Materials and Methods.....	30
Soilless substrates.....	30
Moisture Sensors.....	30
Water Desorption Curve Generation.....	32
Sensor Calibration.....	36
Statistical Analysis.....	37
Results and Discussion.....	38
Volumetric Water Content vs. Matric potential.....	38
Estimation of Matric Potential.....	44
Integrating Volumetric Water Content and Matric Potential, for Precision Irrigation Scheduling.....	48
Chapter 3: Electrical Conductivity Calibration.....	53
Introduction.....	53
Brief Background.....	53
Study Objectives.....	55
Materials and Methods.....	55
Experimental Analysis.....	57
Data Collection.....	59
Models utilized.....	61
Greenhouse Study.....	65
Results and Discussion.....	66

Rhoades Model	66
Hilhorst (2000) model.....	71
Greenhouse Study.....	75
Chapter 4: Summary and Final Remarks.....	83
Volumetric Water content /Water matric potential.....	83
Pore water electrical conductivity.....	89
Appendices.....	92
Appendix A. 1.....	92
Appendix A. 2.....	94
Appendix A. 3.....	96
Appendix B.....	98
Appendix Fig. B1 a, b.....	98
Appendix Fig. B2 a, b.....	99
Appendix Fig. B3 a, b.....	100
Appendix Fig. B4 a, b.....	101
Appendix Fig. B5 a, b.....	102
Appendix Fig. B6 a, b.....	103
Appendix Fig. B7 a, b.....	104
Appendix Fig. B8 a, b.....	105
Appendix Fig. B9 a, b.....	106
Appendix Fig. B10 a, b.....	107
Appendix C. 1.....	108
Appendix C. 2.....	108
Glossary	109
Bibliography	110

List of Tables

<p>Table 2.1. Relationship of Volumetric Water Content (θ) and sensor output (mV) with increasing pressure is shown by the linear calibration regression equation with the corresponding correlation coefficient r^2 for each substrate in 5 cm and 20 cm columns. All regressions were highly significant ($P < 0.0001$).....</p>	42
<p>Table 2.2. Relationship of Volumetric Water Content (θ) and matric potential (Ψ_m) with increasing pressure is shown by the inverse second order equation with the corresponding correlation coefficient r^2 and data count (n) for each substrate in 5 cm and 20 cm columns. (Figs. 2.5a and 2.6a) All regressions were highly significant ($P < 0.0001$).....</p>	45
<p>Table 2.3. Physical properties and water distribution for different substrates in 5 cm tall columns with bulk density (BD), Container capacity (CC), total porosity (TP), air filled porosity (AFP), and water distribution as easily available water (EAW), water buffering capacity (WBC), and progressively unavailable water (PUW).....</p>	50
<p>Table 2.4. Physical properties and water distribution for different substrates in 20 cm tall columns with bulk density (BD), Container capacity (CC), and water distribution as easily available water (EAW), water buffering capacity (WBC), and progressively unavailable water (PUW).....</p>	51
<p>Table 3.1. Picture of the two EC sensors types (ECH₂O-TE and 5TE) illustrating their major physical design characteristics. Note that the 5TE version is the only version that is currently commercially available from Decagon Devices, Inc. (Pullman, WA).....</p>	58
<p>Table 3.2. Rhoades (1989) model variables descriptions and the equivalent determination of the variable in this experiment.....</p>	61
<p>Table 3.3. Regression equations for the ECH₂O-TE sensor depending on the different electrical conductivity solution utilized at each run (Fig. 3.2a) and regression equations for the actual bulk soilless electrical conductivity normalization (Fig. 3.2b), following Rhoades (1976) methodology.....</p>	69

Table 3.4. Regression equations for the 5TE sensor depending on the different EC solution utilized in each run (Fig. 3.3a) and regression equations for the actual bulk soilless electrical conductivity normalization (Fig. 3.3b), following Rhoades (1976) methodology.....	70
Table 3.5. Regression equations for the ECH ₂ O-TE (Fig. 3.4a) and 5TE (Fig. 3.4b) sensors, depending on the different electrical conductivity solution utilized in each run, following Hilhorst (2000) methodology....	74

List of Figures

Figure 1.1 Delivered yields estimates of total N and P from all sources in the Chesapeake Bay, Maryland (After Smith et al., 1997).....	2
Figure 1.2. A Schematic illustration of expected time-courses of leaf water potential (ψ_{leaf}) over a period of 3 days, following withholding of irrigation at time 0 (dashed lines) and for corresponding irrigated controls (continuous lines). (a) Typical diurnal trends of ψ_{leaf} smoothed by taking 3 h running means. In (b), the expected magnitude of instantaneous variation in ψ_{leaf} , as measured with a pressure chamber, is shown (based on data presented by Jones, 1990) (After Jones, 2007).....	4
Figure 1.3 Equivalent circuit diagram of a capacitance sensor where R is a resistor, C is the capacitance of the medium, Cs is the stray capacitance, G is the energy loss due to relaxation and ionic conductivity and V_{inp} and V_{out} are the supply and sensor reading voltage, respectively. (From Bogena et al., 2007).....	9
Figure 1.4 The charge and discharge curves of two capacitors with either high or low permittivity, using a repetitive square pulse with a pulse length Δt . (After Bogena et al., 2007).....	9
Figure 1.5. Decagon family sensors utilized in the present study. From top to bottom EC-20, EC-5, ECH ₂ O-TE, and 5TE.....	12
Figure 2.1. Custom desorption table with ten replicate pressure columns. This view shows, a 5-cm height column with a EC-5 sensor embedded in the top polycarbonate lid, inserted into the substrate and sealed by bolting the column and lid to the table. The columns were slowly pressurized utilizing compressed air, monitored with a digital pressure gauge and evenly distributed to all columns utilizing a manifold (center, front of table) and Teflon gas lines, attached with luer-lock fittings. Water desorbed was collected with graduated cylinders at each measured pressure increment. Sensors were attached to the multiplexer, CR10X datalogger and computer for logging and monitoring the column data, as noted in the text.....	33

Figure 2.2a, b, c, and d. Base polycarbonate plate (a), perforated with two hundred forty 1.0 mm diameter holes. Membrane (0.45 micron pore) (b), on top of each base plate. The red arrow on (c) is pointing out the seated O-ring gaskets in a 1mm groove milled at the top of the PVC columns. Base polycarbonate plate (d), holding in place the membrane and column.....	34
Figure 2.3 a, and b. Standard (a) moisture release curve for 5 cm height columns testing 80 peat : 20 perlite mix , with pressure applied in kilopascals, left hand ‘y’ axis as volumetric water content -- θ -- (VWC), right hand ‘y’ axis as actual water volume desorbed from the columns throughout the desorption run. Both regression lines are plotted to follow the trend for both axes. Correlation coefficient (r^2) is shown for VWC regression equation depending on matric potential (Ψ_m) and data point count (n). EC-5 sensor volumetric water content calibration (b) with sensor output as millivolt on the abscissa and VWC on the ordinate. Correlation coefficient (r^2) is shown for VWC sensor calibration equation and data point count (n).....	39
Figure 2.4 a, and b. Standard (a) moisture release curve for 5 cm height columns testing 100% perlite , with pressure applied in kilopascals, left hand ‘y’ axis as volumetric water content -- θ -- (VWC), right hand ‘y’ axis as actual water volume desorbed from the columns throughout the desorption run. Both regression lines are plotted to follow the trend for both axes. Correlation coefficient (r^2) is shown for VWC regression equation depending on matric potential (Ψ_m) and data point count (n). EC-5 sensor volumetric water content calibration (b) with sensor output as millivolt on the abscissa and VWC on the ordinate. Correlation coefficient (r^2) is shown for VWC sensor calibration equation and data point count (n).....	40
Figure 2.5 a, and b. Moisture release regression lines (a) for all five different substrates tested using 5 cm height columns with pressure applied in kilopascals, ‘y’ axis as volumetric water content -- θ -- (VWC). EC-5 sensor volumetric water content calibration regression lines (b) with sensor output as millivolt on the abscissa and volumetric water content on the ordinate.....	46
Figure 2.6 a, and b. Moisture release regression lines (a) for all five different substrates tested using 20 cm height columns with pressure applied in kilopascals, ‘y’ axis as volumetric water content -- θ -- (VWC). EC-20 sensor volumetric water content calibration regression lines (b) with sensor output as millivolt on the abscissa and volumetric water content on the ordinate.....	47
Figure 3.1. Raw data output values from the datalogger (in a MS Excel table), showing the values and the conversions to known outputs.....	60

Figure 3.2 a, and b. Normalization of bulk electrical conductivity by volumetric water content (a) with the ECH₂O-TE sensor. Bulk substrate electrical conductivity divided by leachate electrical conductivity, (σ_b / σ_w) vs. volumetric water content (θ) for 80 peat: 20 perlite mix substrate. Error bars indicated as standard error about the mean (SEM). (b) Bulk substrate electrical conductivity after normalization (σ_b) vs. leachate electrical conductivity (σ_w) for various fixed volumetric water content (θ). The average of intercepts with bulk substrate EC (σ_b) axis becomes the offset value (σ_s) according to Rhoades (1976) methodology.....	67
Figure 3.3 a, and b. Normalization of bulk electrical conductivity by volumetric water content (a) with the 5TE sensor. Bulk substrate electrical conductivity divided by leachate electrical conductivity (σ_b / σ_w) vs. volumetric water content (θ) for 80 peat: 20 perlite mix substrate. Error bars indicated as standard error about the mean (SEM). (b) Bulk substrate electrical conductivity after normalization (σ_b) vs. leachate electrical conductivity (σ_w) for various fixed volumetric water content (θ). The average of intercepts with bulk substrate EC (σ_b) axis becomes the offset value (σ_s) according to Rhoades (1976) methodology.....	68
Figure 3.4 a, and b. Offset value determination as outlined by Hilhorst (2000) for (a) ECH ₂ O-TE sensor and (b) 5TE sensor. Bulk soilless substrate electrical conductivity (σ_b) vs. bulk soilless substrate dielectric permittivity (ϵ'_b) for 80 peat: 20 perlite mix substrate. Error bars indicated as standard error about the mean (SEM). Intercepts (\bar{y}_0) as $\epsilon'_{\sigma_b=0}$ or offset values.....	73
Figure 3.5. Greenhouse experimental setup with 32 'New Guinea' <i>impatiens</i> planted in 15cm diameter x 10.5cm high containers. Four repetitions of each sensor (ECH ₂ O-TE and 5TE) were randomly assigned to different containers inside the experimental area with the remaining plants as guard rows.....	76

Figure 3.6. Pore water electrical conductivity estimation (σ_p) using ECH₂O-TE sensor with two different offset values (4.614 and 6) when fitting the Hilhorst (2000) model, and an offset value of -0.00205 when fitting Rhoades' (1989) model. Measurements made in Sunshine LC-1 substrate (80 peat : 20 perlite) over 11 days period of drying down and rehydration. Blue line in center of black (SEM) area is actual volumetric water content (θ). Matric potentials (Ψ_m) indicated with red arrows as kPa. Horizontal straight black line indicates the electrical conductivity of the solution applied (1 dS m⁻¹). Light blue line in center of black (SEM) area is Rhoades' σ_p estimate; similarly, the grey and light green colored areas surrounding each Hilhorst model estimate is the standard error about the mean (SEM; n=4 for each line)..... 77

Figure 3.7. Pore water electrical conductivity estimation (σ_p) using 5TE probe with offset value of 3.959 when fitting the Hilhorst (2000) model and an offset value of -0.00288 when fitting the Rhoades' (1989) model. Measurements made in Sunshine LC-1 substrate (80 peat : 20 perlite) over 11 days period of drying down and rehydration. Blue line in center of black (SEM) area is actual volumetric water content (θ). Matric potentials (Ψ_m) indicated with red arrows as kPa. Horizontal straight red line indicates the electrical conductivity of the solution applied (1 dS m⁻¹). Light blue line in center of black (SEM) area is Rhoades' σ_p estimate; similarly, the grey colored area surrounding the Hilhorst model estimate is the standard error about the mean (SEM; n=4 for each line)..... 78

Figure 3.8. Pore water electrical conductivity estimation (σ_p) using 5TE probe with offset value of 6 when fitting the Hilhorst (2000) model and an offset value of -0.00288 when fitting the Rhoades' (1989) model. Measurements made in Sunshine LC-1 substrate (80 peat : 20 perlite) over 11 days period of drying down and rehydration. Blue line in center of black (SEM) area is actual volumetric water content (θ). Matric potentials (Ψ_m) indicated with red arrows as kPa. Horizontal straight red line indicates the electrical conductivity of the solution applied (1 dS m⁻¹). Light blue line in center of black (SEM) area is Rhoades' σ_p estimate; similarly, light green colored area surrounding the Hilhorst model estimate is the standard error about the mean (SEM; n=4 for each line)..... 79

Appendix Fig. B1 a, b. Standard (a) moisture release curve for 5 cm height columns testing **100% pine bark** with pressure applied in kilopascals, left had ‘y’ axis as volumetric water content -- θ -- (VWC), right hand ‘y’ axis as actual water volume desorbed from the columns throughout the desorption run. Both regression lines are plotted to follow the trend for both axes. Correlation coefficient (r^2) is shown for VWC regression equation depending on matric potential (Ψ_m) and data point count (n). **EC-5** probe volumetric water content calibration (b) with probe output as millivolt on the abscissa and VWC on the ordinate. Correlation coefficient (r^2) is shown for VWC probe calibration equation and data point count (n)..... **98**

Appendix Fig. B2 a, b. Standard (a) moisture release curve for 5 cm height columns testing **100% coconut fiber (Coir)** with pressure applied in kilopascals, left had ‘y’ axis as volumetric water content -- θ -- (VWC), right hand ‘y’ axis as actual water volume desorbed from the columns throughout the desorption run. Both regression lines are plotted to follow the trend for both axes. Correlation coefficient (r^2) is shown for VWC regression equation depending on matric potential (Ψ_m) and data point count (n). **EC-5** probe volumetric water content calibration (b) with probe output as millivolt on the abscissa and VWC on the ordinate. Correlation coefficient (r^2) is shown for VWC probe calibration equation and data point count (n)..... **99**

Appendix Fig. B3 a, b. Standard (a) moisture release curve for 5 cm height columns testing **80 pine bark : 20 peat moss mix**, with pressure applied in kilopascals, left had ‘y’ axis as volumetric water content -- θ -- (VWC), right hand ‘y’ axis as actual water volume desorbed from the columns throughout the desorption run. Both regression lines are plotted to follow the trend for both axes. Correlation coefficient (r^2) is shown for VWC regression equation depending on matric potential (Ψ_m) and data point count (n). **EC-5** probe volumetric water content calibration (b) with probe output as millivolt on the abscissa and VWC on the ordinate. Correlation coefficient (r^2) is shown for VWC probe calibration equation and data point count (n)..... **100**

Appendix Fig. B4 a, b. Standard (a) moisture release curve for 20 cm height columns testing **100% pine bark**, with pressure applied in kilopascals, left had ‘y’ axis as volumetric water content -- θ -- (VWC), right hand ‘y’ axis as actual water volume desorbed from the columns throughout the desorption run. Both regression lines are plotted to follow the trend for both axes. Correlation coefficient (r^2) is shown for VWC regression equation depending on matric potential (Ψ_m) and data point count (n). **EC-20** probe volumetric water content calibration (b) with probe output as millivolt on the abscissa and VWC on the ordinate. Correlation coefficient (r^2) is shown for VWC probe calibration equation and data point count (n)..... **101**

Appendix Fig. B5 a, b. Standard (a) moisture release curve for 20 cm height columns testing **100% coconut fiber** (coir) with pressure applied in kilopascals, left had ‘y’ axis as volumetric water content -- θ -- (VWC), right hand ‘y’ axis as actual water volume desorbed from the columns throughout the desorption run. Both regression lines are plotted to follow the trend for both axes. Correlation coefficient (r^2) is shown for VWC regression equation depending on matric potential (Ψ_m) and data point count (n). **EC-20** probe volumetric water content calibration (b) with probe output as millivolt on the abscissa and VWC on the ordinate. Correlation coefficient (r^2) is shown for VWC probe calibration equation and data point count (n)..... **102**

Appendix Fig. B6 a, b. Standard (a) moisture release curve for 20 cm height columns testing **80 pine bark : 20 peat moss mix**, with pressure applied in kilopascals, left had ‘y’ axis as volumetric water content -- θ -- (VWC), right hand ‘y’ axis as actual water volume desorbed from the columns throughout the desorption run. Both regression lines are plotted to follow the trend for both axes. Correlation coefficient (r^2) is shown for VWC regression equation depending on matric potential (Ψ_m) and data point count (n). **EC-20** probe volumetric water content calibration (b) with probe output as millivolt on the abscissa and VWC on the ordinate. Correlation coefficient (r^2) is shown for VWC probe calibration equation and data point count (n)..... **103**

Appendix Fig. B7 a, b. Standard (a) moisture release curve for 20 cm height columns testing **80 peat moss : 20 perlite mix**, with pressure applied in kilopascals, left had ‘y’ axis as volumetric water content -- θ -- (VWC), right hand ‘y’ axis as actual water volume desorbed from the columns throughout the desorption run. Both regression lines are plotted to follow the trend for both axes. Correlation coefficient (r^2) is shown for VWC regression equation depending on matric potential (Ψ_m) and data point count (n). **EC-20** probe volumetric water content calibration (b) with probe output as millivolt on the abscissa and VWC on the ordinate. Correlation coefficient (r^2) is shown for VWC probe calibration equation and data point count (n)..... **104**

Appendix Fig. B8 a, b. Standard (a) moisture release curve for 20 cm height columns testing **100% perlite**, with pressure applied in kilopascals, left had ‘y’ axis as volumetric water content -- θ -- (VWC), right hand ‘y’ axis as actual water volume desorbed from the columns throughout the desorption run. Both regression lines are plotted to follow the trend for both axes. Correlation coefficient (r^2) is shown for VWC regression equation depending on matric potential (Ψ_m) and data point count (n). **EC-20** probe volumetric water content calibration (b) with probe output as millivolt on the abscissa and VWC on the ordinate. Correlation coefficient (r^2) is shown for VWC probe calibration equation and data point count (n)..... **105**

Appendix Fig. B9 a, b. Comparison of calibration constants for 80% peat : 20% perlite substrate when (a) calculated on a container capacity basis (517 mL) vs. (b) calculated on a total column volume basis (684.1 mL).....	106
Appendix Fig. B10 a, b. Comparison of calibration constants for 100% perlite when (a) calculated on a container capacity basis (349 mL) vs. (b) calculated on a total column volume basis (684.1 mL).....	107

Chapter 1: Literature Review

Sensing Plant Available Water

The Green Revolution brought a high yield production of many different crops which was thought would ameliorate the hunger around the world. We are presently living through what we could consider the 'Blue Revolution' (Zhang and Zhang, 2007) i.e. the struggle to improve the availability of fresh water and increasing efficiency of water use throughout the world. This is especially important as agriculture is still the predominant user of fresh water resources worldwide. Agricultural activities account for 70% of fresh water usage in the world (FAO, 2002). Poor water distribution, world climate change, and varying water use policies and regulations have led to a very complicated water situation not only in the US, but around the world. In the past few decades, potable water use has been scrutinized and is becoming more restricted, especially around high population areas (Beeson et al., 2004). Furthermore, the over-application of nutrients to cropped land for higher yield has had a significant environmental effect on lakes, rivers and groundwater). To illustrate Fig. 1 indicates the location and risk of nitrogen and phosphorus loading to the Chesapeake Bay, by subwatershed (Smith et al., 1997).

It is therefore obvious that agricultural water use efficiency (WUE) or the ability of plants to gain carbon (as total biomass or harvestable yield) per unit of water (transpired) is a key factor to conserve increasingly scarce water resources. Increasing the efficiency of water use depends mostly upon the type of irrigation system and the quantity of water actually delivered to the plant. Another critical efficiency factor is

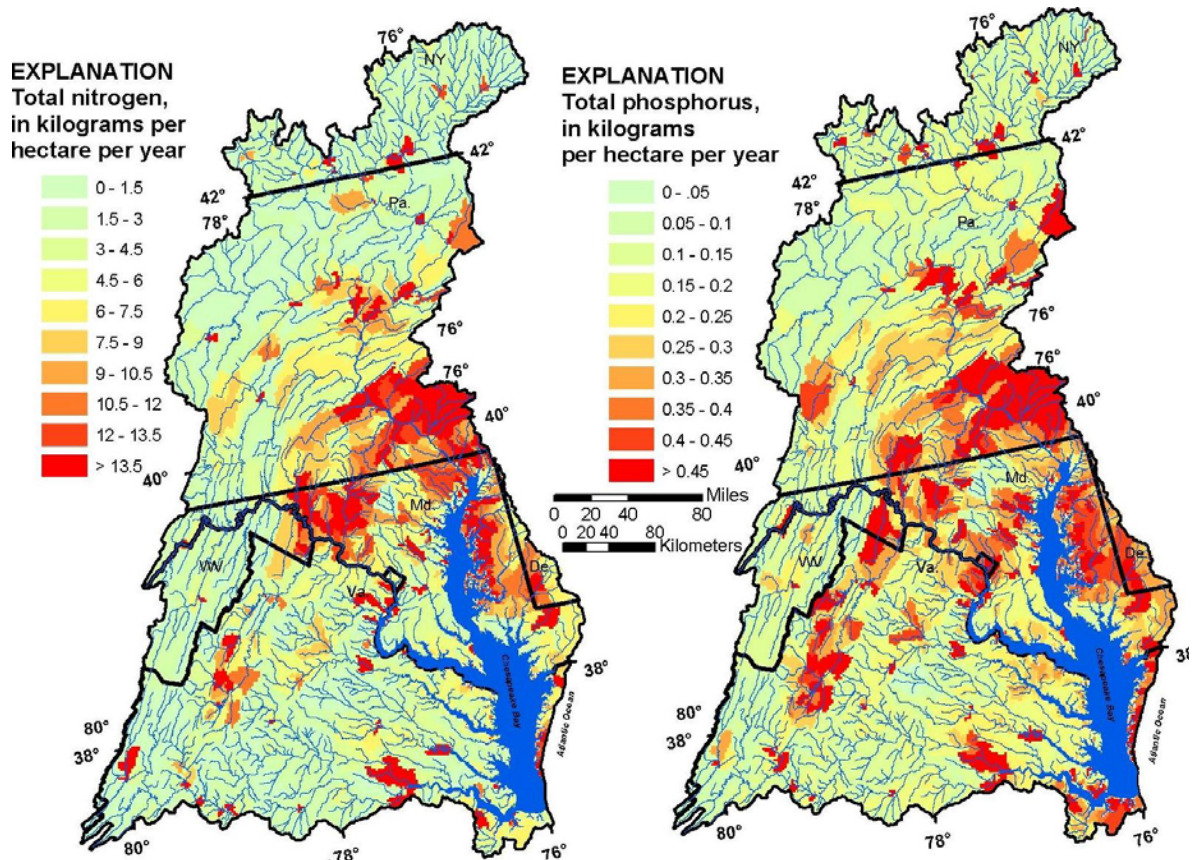


Figure 1.1 Delivered yields estimates of total N and P from all sources in the Chesapeake Bay, Maryland (After Smith et al., 1997).

scheduling irrigations at the correct time – which requires a considerable knowledge of the crop, and local conditions, on a daily basis.

Irrigation Scheduling

The importance of “on-time” irrigation is well understood by most growers, but precisely scheduling irrigations (both in terms of quantity and timing) is still extremely difficult for most agricultural growers, due to a lack of immediate information. Historically, there have been two main approaches: a plant-based approach and a soil-based approach. With plant-based scheduling, there are techniques that measure plant responses to water ‘stress’ such as leaf water status and physiological responses such as

stomatal conductance. Among these techniques are visual leaf wilting, pressure chamber, psychrometer, pressure probe, and xylem cavitation (Jones, 2004). Physiological response techniques include the use of porometers, thermal sensing, sap flow sensors, and measuring leaf growth rates (Jones, 2008). Most plant-based techniques are almost impossible to practically implement on a large scale; hence the low adoption of these technologies by commercial growers. Furthermore, most of these measurement techniques require sophisticated equipment and/or high level of technical skill; many techniques also give very variable data, because of environmental variation during the measurement period. Hence, there have been many questions about the unreliability of such data, over time.

One of the characteristics of living systems is the capability to adapt to changing environmental conditions, often very rapidly. Figure 1.2 illustrates the conundrum of scheduling irrigations based upon leaf water potential measurements with a fixed set point of around -2 MPa. By following the smoothed diurnal water potential measurements (Fig 1.2a) an irrigation scheduling decision appears easy, but when the actual measurements of leaf water potential are incorporated (Fig. 1.2b), we can see that the fluctuations in the data make the timing of this decision much more challenging. This is particularly evident by looking at the mid-day data during Day 1, when leaf water potential can change drastically about the ideal set point of -2 MPa within a matter of minutes. Those changes can be attributed to different environmental factors changes such as changing light levels, vapor pressure deficits (VPD), and leaf temperature. For further discussion about plant-based irrigation techniques, refer to Jones (2004; 2008).

Because of the difficulties associated with measuring plant-based parameters, our approach has been to utilize soil-based approaches that can either measure soil *water activity* (potential measurement), and/or *soil water quantity* (volumetric or gravimetric measurement). Since more than 60% of ornamental plants are now grown in containers in the United States (USDA, 2007) whose production utilize soilless substrates rather

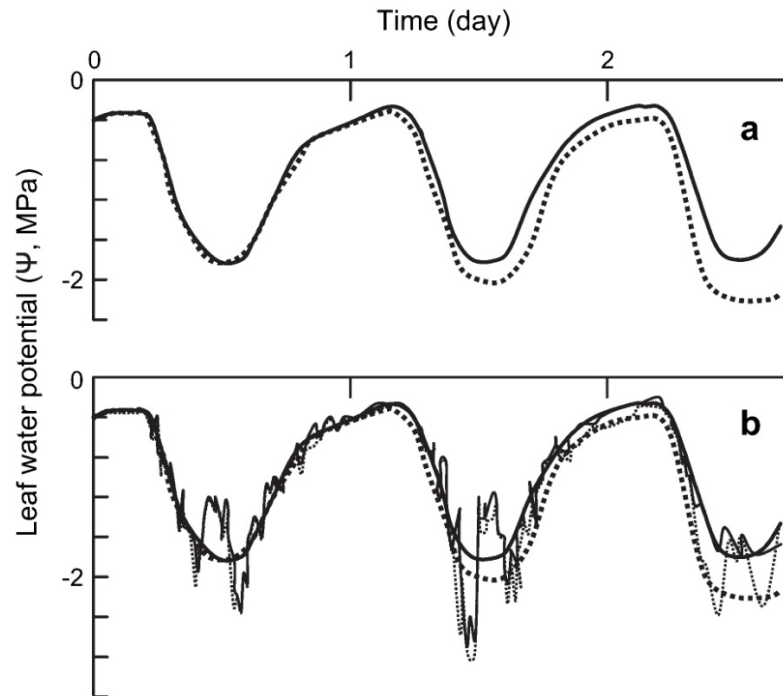


Figure 1.2. A Schematic illustration of expected time-courses of leaf water potential (Ψ_{leaf}) over a period of 3 days, following withholding of irrigation at time 0 (dashed lines) and for corresponding irrigated controls (continuous lines). (a) Typical diurnal trends of Ψ_{leaf} smoothed by taking 3 h running means. In (b), the expected magnitude of instantaneous variation in Ψ_{leaf} , as measured with a pressure chamber, is shown (based on data presented by Jones, 1990) (After Jones, 2007).

than soils, we will use soil and/or substrates as interchangeable terms when we discuss the measurement of water in the root zone of plants. The term substrate will be used to refer to the media that supplies a plant in a container with water, nutrients, and physical

anchoring (Raviv and Lieth, 2008). Soil or substrate water potential is defined as the amount of work per unit of pure water (i.e. $\text{cm}^3 \approx \text{mL}$ or m^3) that must be done by external forces (i.e. suction or pressure) to reversibly transfer a measurable amount of water from the standard state to the point under consideration, at constant temperature and pressure (Hopmans and Rottson, 2002). Total soil water potential can be described by the equation:

$$\Psi_t = \Psi_p + \Psi_z + \Psi_s + \Psi_a \quad [\text{Eq. 1.1}]$$

where Ψ_p , Ψ_z , Ψ_s , and Ψ_a are the pressure, gravitational, solute (osmotic) and air pressure potentials, respectively.

Since water in a substrate has various forces acting upon it, potential energy usually differs from point to point, and hence its potential energy is variable as well. It is important to note that two regions of substrates may hold different amounts of water at the same potential energy status and would not experience a flow of water between regions. Substrate water quantity (equivalent to soil water content) is defined as either the ratio of the mass of water present in the sample before drying, divided by the mass of the sample after it has been dried (gravimetric; $\text{kg} \cdot \text{kg}^{-1}$), or alternatively, as the volume of water present in a unit volume of soil or substrate (volumetric; $\text{cm}^3 \cdot \text{cm}^{-3}$).

Which techniques are used to measure water in soil / soilless substrates?

Soil water potential

The measurement of soil water has been studied by scientists and utilized by growers for many years. Tensiometers are devices that measure soil water potential, used

as early as 1908 by Livingston; more robust designs were later made for field applications by Richards in the early 1920's (Or, 2001). A tensiometer is simply a pipe filled with distilled water with a porous ceramic cup at the bottom end, with the top end attached to a measuring device, which is typically a gauge, or more recently, a type of transducer, since these offer multiple advantages. When inserted in soil, the ceramic cup equilibrates with the surrounding soil water, with water moving in or out of the ceramic cup, depending on the water status of the soil. If water moves from the tensiometer, a suction or negative potential is measured by the gauge or transducer that is connected to the water column. This device has good precision in most soil types, since it is not influenced by temperature or soil osmotic potential. However, the suction tension is often lost due to poor contact with the soil pore water, allowing air to enter the column, requiring frequent maintenance and loss of data.

There are many other soil-based techniques that are less precise or unsuitable for real-time measurements of water in substrates for instance gypsum blocks, watermark blocks (Hanson, et al., 2000) and Time domain reflectometry (TDR) sensors (Noborio, et al., 1999). De Boodt et al. (1972; 1974) proposed a method to measure water potential by utilizing pressure (or 'tempe') cells. A more refined method was developed by Topp and Zebchuk (1979), where soil cores were sampled from field and then pressurized to create moisture desorption curves, which is usually put in practice to visualize the relation of amount of water held by the soil at specific water potentials. However, none of these techniques have been used commercially due to the lack of versatility and the high maintenance (labor costs) of the technique. Most importantly, none of these water content measurement techniques have been utilized by the ornamental industry except for

analytic purposes, because of the high porosity of most soilless substrates. Low-tension tensiometers (Raviv et al., 1993) have been adapted for use in peat-based substrates, but the accuracy of tensiometers is poor, usually ± 5 kPa. Matric potentials in some substrates (e.g. rockwool) rarely exceed -3 kPa. Plant water availability also drops significantly when matric potential increases from 0 to -3 kPa, as a result of a sharp decline in the substrate hydraulic conductivity (Wallach et al., 1992). We therefore have issues with measuring precise amounts of water in many of these soilless substrates at very low tensions.

Soil water content

Soil water content can be determined by direct or by indirect methods. Direct methods involve the removal or separation of the soil or substrate matrix, with a direct measurement of the amount of water removed. This may be achieved by heating, extraction and replacement by a solvent or chemical reaction. The removal of water by heating is commonly referred to as the gravimetric method. Indirect methods measure some physical or chemical property of a soil or substrate which is correlated to the substrate water content. These techniques include time domain reflectometry (TDR), frequency domain reflectometry (FDR), time domain transmission (TDT), amplitude domain reflectometry (ADR), phase transmission and ground penetrating radar (GPR). They also include capacitance devices, radar scatterometry or active microwave, passive microwave, electromagnetic induction (EMI), neutron thermalization, nuclear magnetic resonance, and gamma ray attenuation (Dane and Topp, 2002). The drawback of TDR and GPR is the cost of the equipment and the level of skill needed to operate the equipment; most importantly, TDR, FDR, TDT sensors are typically not wireless, which

limits the range of deployment. The other methodologies mentioned are really only applicable to large-scale environments because of the cost of the technology. For this reason, we chose to focus our research on capacitance sensors, which are relatively cheap, rugged, portable and can be easily connected to newly develop dataloggers capable of transmitting data wirelessly from field sites, and solenoid actuation (Lea-Cox et al., 2008). Because of the range in size of these sensors, they are ideally suited to measuring substrate moisture in containers that are utilized by both nursery and greenhouse operations to grow ornamental plants.

Capacitance Sensors

The introduction of capacitance techniques into agriculture was made by Smith-Rose (1933; cited by Dane and Topp, 2002) and rapidly developed with the introduction of microelectronics. Simply defined, a capacitor is a device that stores electrical energy. Capacitance sensors include a certain volume of soil or substrate surrounding the sensor prongs as part of this capacitor, and measure the dielectric permittivity (ϵ') (i.e. how much energy is stored by the soil or substrate) of the surrounding medium as shown in Fig 1.3 (Bogena et al., 2007). A graphic representation from a capacitance sensor reading is shown in Fig. 1.4, where it can be seen how the water content alters the time of the pulse length ΔT with a fixed supply voltage V_t . Thus, with respect to a substrate, high water content will result in a longer pulse length time, because the sensor output is directly related to the average voltage over the period of change in pulse length time (Bogena et al., 2007).

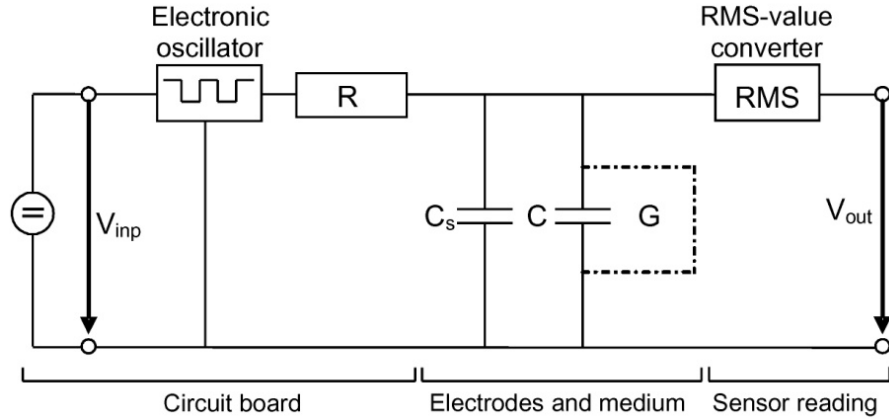


Figure 1.3 Equivalent circuit diagram of a capacitance sensor where R is a resistor, C is the capacitance of the medium, C_s is the stray capacitance, G is the energy loss due to relaxation and ionic conductivity and V_{inp} and V_{out} are the supply and sensor reading voltage, respectively. (From Bogena et al., 2007)

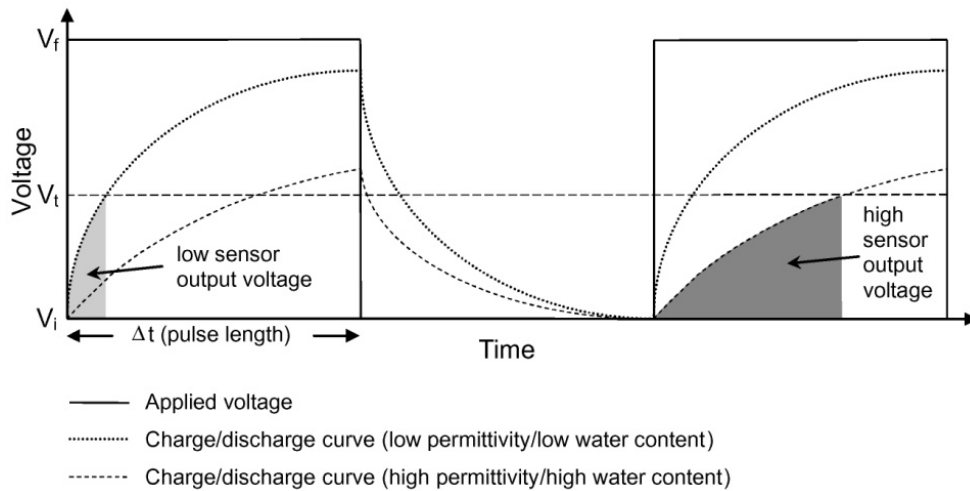


Figure 1.4 The charge and discharge curves of two capacitors with either high or low permittivity, using a repetitive square pulse with a pulse length Δt . (After Bogena et al., 2007)

Our interpretation of Fig. 1.4 is that a fixed voltage (V_f) is applied as an electromagnetic wave to the substrate (surrounding the sensor prongs); the time that it

takes for the applied voltage (V_f) to rise up to a threshold point (V_t) is short if there is low water content and it reaches V_t in a short period of time, correlating to low permittivity. If there is a larger amount of water, then it takes a longer time to rise up to the threshold point V_t , correlating with a higher permittivity value.

In an attempt to standardize the calibration methodology of electromagnetic water content sensors, Blomquist et al. (2005) set up an array of media mixtures or liquids of known properties, to compare among different sensor technologies. One of the sensors utilized for the trial was the ECH₂O EC-20, (see Fig. 1.5; Decagon Devices, Inc.; Pullman, WA). It was determined that the sensor showed minimal definition when reading permittivity values ranging from $\epsilon' \approx 40$ to $\epsilon' \approx 80$, with the consequent imprecision for predicting volumetric water content in soilless substrates that hold water in this permittivity range. It was also found that when the sensor was immersed in a solution with $\epsilon' = 40$ and the bulk electrical conductivity was increased from 0 to 2 dS \cdot m⁻¹, there was a drift of about -110 ϵ' units. It is therefore clear that the EC-20 sensor is susceptible to moderate salt concentration. Bandaranayake et al. (2007) also found a drift in output with the EC-20 under similar conditions (conductivity not specified) with an increase of about 200 mV in output. Nemali et al. (2007) found similar situation with the EC₂HO EC-10, where the sensor output increased by about 9% when the applied electrical conductivity of the solution was increased from 0 to 3 dS m⁻¹. With respect to temperature, the EC-20 had less drifting (about 3 ϵ' units), which was better than the higher frequency broadband sensors tested by Blomquist et al. (2005). The EC-10 tested by Nemali et al. (2007) also had an output increase with increasing temperature of about 1.88 mV °C⁻¹.

The substrate sample volume has a profound effect on sensor performance; large sampling volumes are therefore desirable. The distribution of the sampling substrate volume around the sensor is equally important, as uniform energy propagation through the substrate is the ideal. When energy is concentrated only at close proximity to the sensor (called a ‘skin effect’), this can cause a large variation in water content determination. In Blomquist et al. (2005) study, the EC-20 had the lowest sampling volume of about 1.99 cm³ and exhibited such a ‘skin effect’. On the other hand Bandaranayake et al. (2007) reported a sampling volume range for the same EC-20 sensor of 128 to 256 cm³.

When analyzing sensor response to supply voltage, Bogena et al. (2007) established a preferred supply voltage that minimizes the variation associated with the volumetric water content calibration equation. The two best fit voltages were 2.5 and 3.0 V with root mean squared error of 0.721 and 0.924 respectively. In contrast, the ECH₂O EC-5 exhibited a strong reduction in sensitivity when measuring higher permittivity. The EC-5 operates with a supply voltage frequency of 70 MHz, whereas the ECH₂O EC-10 and EC-20 sensors operate at 6 MHz, with the higher frequency conferring better tolerance in saline conditions to the EC-5 (Fig. 1.5). Bogena et al. (2007) concluded that the EC-5 has a maximum error of 6% with a bulk electrical conductivity equal to 1 dS • m⁻¹ and a permittivity of 40 (equivalent to $\theta = 0.5$). Parsons and Bandaranayake (2009) used the same methodology as Bandaranayake et al. (2007), but analyzed the performance of the EC-5. Overall, the EC-5 outperformed the EC-20 since volumetric water content readings were much more stable under saline conditions, although bulk density was found to have a large influence on the sensor readings. Kizito et al. (2008)



Figure 1.5. Decagon family sensors utilized in the present study. From top to bottom EC-20, EC-5, ECH₂O-TE, and 5TE.

carried out experiments with the EC-5 and ECH₂O-TE (subsequently replaced by the 5TE sensor in 2008), to examine interactions with sensor excitation frequency, temperature, and calibration. Their study on frequency showed how 66 MHz was high enough to minimize sensor volumetric water content variation, when utilized under increasing applied solution electrical conductivity. It is important to mention that this experimentation was done in rockwool substrate, which minimizes sensor interactions with the solid material because of a negligible interaction with the ions in solution. Some scatter was seen at higher volumetric water content, which could be similar for some soilless substrates where total porosity is about 80%. Kizito et al. (2008) concluded that there was no need for specific calibration equations for those soils tested during their experimentation; a universal equation was therefore fitted with linear parameterization.

The temperature effect on sensor readings was measured in air or water, being more variable in air and more consistent in water. Soils with large surface areas (e.g. high clay content) show evidence of water bonding effects, so the sensor was not able to distinguish such water due to the water molecular interaction with the particle surface.

Factors Affecting the Measurement of Volumetric Water Content when utilizing Electromagnetic Sensors.

Before we can discuss the measurement of soil moisture using electromagnetic (EM) sensors, it is necessary to understand a few key principles, specifically with regard to interferences with readings, and the potential for error in measurements. Firstly, it is well documented how increasing salt concentration – more widely referred as electrical conductivity (EC) – affects the measurement of volumetric water content in soils (Topp et al., 1980; Bandaranayake et al., 2007; Nemali et al., 2007). Thompson et al. (2007) reported a capacitance sensor (EnviroSCAN, Sentek sensor technologies, Stepney, SA, Australia) which works at > 100 MHz, as being sensitive to a soil solution EC > 1.8 dS m⁻¹. Hook et al. (2004) conclude that for most rigorous determinations of volumetric water content, sensor pulse rise times should be less than 6 ns, otherwise this could lead to questionable determinations. Kelleners et al. (2004) found that the combination of high volumetric water content and bulk EC caused a rejection of data. This was due to dielectric losses, which means that increasing concentrations of ions in solution dissipates the energy pulse and cannot be read back by the sensor; similar effects were reported by Plauborg et al. (2005), determined in drip irrigated sandy soils. Due to the variability of

electromagnetic sensors to increasingly saline conditions, Jones and Or (2004) proposed a model to extend TDR measurement to saline soils, which was also highly correlated to sensor design, since short TDR probes (10 – 15 cm length) reduce signal attenuation.

Temperature is another factor that significantly influences the measurement of volumetric water content. Polyakov et al. (2005) found that temperature changed volumetric water content readings at the rate of $0.001 \text{ cm}^3 \cdot \text{cm}^{-3} / ^\circ\text{C}$ and $0.0003 \text{ cm}^3 \cdot \text{cm}^{-3} / ^\circ\text{C}$ for soil and sand, respectively. This data is contrary to the findings of Persson and Berndtsson (1998), and also Seyfried and Murdock (2001) who observed negative temperature correlations using a TDR sensors working at 45 MHz. This contrasting evidence suggests that temperature effects may be different depending on specific substrates. So, ideally temperature measurements should be integrated into the computation of volumetric water content at the time of measurement. This is typically achieved by a small thermocouple in the sensor head, which provides a temperature correction. Burying the sensor head in the substrate is typically recommended by most manufacturers, to protect against the sensor head overheating. Robinson et al. (2004) concluded that their observation of a drift in data values was due to the sensor ‘overheating,’ due to sunlight exposure. Typically the temperature threshold value should not exceed 40°C or spurious volumetric water content measurements would occur as temperature rises.

The excitation frequency of the sensor is the last major variable to consider in the measurement of volumetric water content. Most capacitance sensors use excitation frequencies of 150 MHz or below, where the frequency dependence of the real part of permittivity (ϵ') cannot be ignored (Kelleners et al., 2005a). Seyfried and Murdock

(2004) also noticed that by supplying a voltage frequency of 50 MHz, temperature causes an overestimation of volumetric water content determinations and underestimation of volumetric water content in nearly saturated sand.

Some of the most cited research on electromagnetic (EM) water determination was done by Topp et al. (1980). Based upon this work, soil properties were recognized as having a significant influence on water content determination. The impact of the soil constituents on the real (ϵ') and imaginary (ϵ'') relative permittivity were described by Topp et al. (2000). Constituents such as dissolved salts and clay content play an important role in the measurement of volumetric water content, due to their negative influence on real permittivity determination. Thus it is not only water that has a unique effect on ϵ' values. This was exemplified by the study carried out by Hanson and Peters (2000) where several different EM sensors were evaluated in different soil type locations with default calibrations. From their regression coefficients, it was determined that all sensors had some degree of variation in readings, depending on the different soil types. Results varied from no correlation to highly correlated ($r^2 = 0.96$), with the lower correlations for silt type soils. Chandler et al. (2004) demonstrated that even when soil-specific calibrations were done, there were differences in θ determinations; consequently it was concluded that the effectiveness of the calibration depended on specific soil properties. Kelleners et al. (2005b) also found that calibration equations were dependant on soil type characteristics and their comparison between calculated ϵ' was good for sand, intermediate for sandy loam, and poor for two loam soils. The discrepancies between the sandy loam and the loam soils were attributed to ionic conduction (high bulk EC) and more importantly, they showed that the Topp et al. (1980) relationship between

apparent permittivity and volumetric water content should be only used in non-dispersive soils, which are soils with low bulk EC. Concurring with others, Kelleners et al. (2005a) suggested that by incrementing the excitation frequency to at least 175 MHz, the sensor will become insensitive to high bulk EC during volumetric water content determinations. Seyfried et al. (2005) concluded that signal attenuation may better explained by clay type and its characteristics such as surface area and cation exchange capacity (CEC). They also suggested that probe placement changes the accuracy of the calibration, especially when sensors are utilized at the surface of the soil or container. Logsdon (2005) made volumetric water content observations in soils with high surface area and found a significant correlation between average dielectric permittivity and soil surface specific area; he suggested that temperature correction for such materials is indispensable.

Physical Properties of Soilless Substrates

Introduction.

Water deficits and the consequently lowered substrate water potential/content are usually considered as one of the most important underlying stressors in crops, even at relatively small water deficits. Measuring the energy status and water content are therefore of greater value for providing a rigorous indication of water ‘availability’ to plants, with values that can allow for comparisons between any growing substrate (Jones, 2007).

Ornamental plant production has changed significantly over the past four decades, and is continuously evolving toward more efficient production systems (Raviv and Lieth,

2008). Nursery and greenhouse producers are using different materials and techniques that allow for higher productivity and profitability, per unit area. One significant improvement has been the adoption of containers for growing plants; however disease became a significant production issue when soils were initially used in containers, due to poor drainage (Handreck and Black, 2002). The success of using more porous soilless substrates of both organic and inorganic origin has driven the adoption of containers in the production of ornamental and vegetable transplants (Raviv and Lieth, 2008).

Soilless substrates physical characteristics

As part of any new development, soilless substrates were extensively characterized and scrutinized, to better understand their physical characteristics before they were utilized in large production systems. During the 1950's and 1960's, most of this research focused on particle size distribution and the characterization of water release (desorption) curves; this information was then related to additional variables such as bulk density and the amount of water that was readily-available to plants. One of the earliest researchers, (Bunt, 1961) began looking at different materials as "soil conditioners", focusing on total pore space, macro-pores and water distribution in containers. Bunt (1961) found that organic materials such as peat had a positive impact on soil mix physical properties, if the particle size distribution of that peat material had less than 10% of particle sizes of < 0.5 mm, and about 40% of particles $\geq 3-5$ mm.

De Boodt and Verdonck (1972) made a considerable contribution by establishing moisture release characteristics for several different soilless substrates, and by proposing specific plant available moisture parameters including easily available water (EAW; 0 to

-5 kPa), water buffering capacity (WBC; -5 to -10 kPa) and also by detailing instrumentation (De Boodt et al. 1974). More recently, Handreck and Black (2002) defined readily available water (RAW) as a parameter, which sums EAW and WBC (i.e. 0 to -10 kPa), also known as plant-available water (PAW).

Many other researchers (Goh and Maas, 1980; Fonteno et al., 1981; Bilderback et al., 1982; Verdonck, 1983; Verdonck et al., 1983; Brown et al., 1987; Fonteno, 1989; Cattivello, 1991; Gabriëls et al., 1991; Milks et al., 1989a; b; c) have tested various soilless substrates and techniques, quantifying their moisture retention characteristics and their effects on plant development (Karlovich et al., 1986; Tilt et al., 1987; Kiehl et al., 1992; Raviv et al. 2004). The major outcome of all this research has been to demonstrate that most soilless substrates retain a larger proportion of plant available water at very low matric potentials (i.e. less than -20 kPa).

Optimal plant growth is dependent on providing a balance of air and available water in the root zone, to maximize root growth and reduce the prevalence of disease (Argo, 1998b). Fonteno et al. (1995) stated that the four major factors which affect air and water dynamics in soilless substrates include not only substrate properties including particle size, component ratios and watering practices, but also the height and shape of the container (Bilderback and Fonteno, 1987; Tilt et al., 1987) and the substrate handling procedures when packing and transporting (Blom and Piott, 1992). Typically, soilless substrates are composed of one or more materials to ensure adequate aeration and drainage, since organic particles tend to break down over time (Allaire-Leung et al., 1999). Inorganic soilless substrate components, such as perlite and polystyrene, add volume to these mixes and help reduce poor aeration. The difference in results depends

largely on differences such as plant species, root/shoot ratio, root morphology, plant density, and container volume and geometry (Handreck and Black, 2002).

Of these factors, container height is important, as it affects not only the total air space in the substrate (as influenced by gravitational forces) but it also affects the total container volume, and hence the total water available to plant roots. Changes in air : water ratios are exacerbated in small containers, as illustrated by Fonteno et al. (1995), who showed a 3 to 4 times increase in air space in a number of substrates, merely by increasing plug height from 2.5 cm (1") to 5 cm (2").

Research has focused also on key parameters such as air : water : solid ratios (Handreck and Black, 2002). Frequently the air component is subdivided into total pore space (TPS); this refers to the total amount of pores filled either with air and/or water. The percentage of pores filled with air after irrigation and drainage is known as air filled porosity (AFP); the water-holding capacity (WHC) refers to the amount of water held by the substrate at container capacity (CC) (Waller and Harrison, 1991; Martinez et al., 1991; Brückner, 1997). All of these variables are affected by container height (gravitational potential) and the inherent physical properties of the substrate components in the mix. Container capacity describes the amount of water retained by the substrate after an irrigation event and after drainage. Easily available water (EAW) is the amount of water released by the substrate with a matric potential (pressure/suction) from 0 to -5 kPa, water buffering capacity (WBC) which is the amount of water released by the substrate with a matric potential from -5 kPa to -10 kPa, and unavailable water (UW) which is the proportion of water held by the substrate greater than -25 kPa. The point at which water becomes unavailable to the plant is probably dependent on the factors cited

by Handreck and Black (2002), and noted above. There is however, no doubt that the -1.5MPa value that is often quoted in the literature (Stevenson, 1982) as a “permanent wilting point” has little relevance to the measurement of incipient water stress in soilless substrates. It is likely that some mild water stress is experienced at matric potentials of about -15 kPa (Kiehl et al., 1992).

The solid component is generally analyzed by quantifying properties such as bulk density ($BD = g \cdot cm^{-3}$), particle size distribution and pore-size distribution. Bunt (1983) showed, by using different proportion combinations of peat and inorganic materials, that BD is inversely proportional to total pore space. It is well known that as the proportion of small particles increases, the WHC also increases, but TPS and capillary pore space decreases (Bunt, 1983; Tilt et al., 1987; Orozco, et al., 1997; Nkongolo and Caron, 1999). Pore-size distribution directly influences the hydraulic conductivity, tortuosity (a parameter that describes diffusion in porous media), and WHC, which in turn determines the water transport capabilities of each individual substrate (Drzal et al., 1999).

From the late 1980's until now, research has focused on additional variables, assessing new ways to understand soilless substrates dynamics. By taking advantage of new theoretical models and the development of electronic equipment, researchers have been able to analyze aspects of substrates to determine water desorption characteristics *in situ*, using time domain reflectometry (TDR; Paquet et al., 1993), measure saturated hydraulic conductivity in containers (Allaire et al., 1994), and quantify gas diffusion (Caron et al., 2005). From these studies, it is apparent that we still have much to learn about the intrinsic physical properties of soilless substrates.

Although desorption curves are generated by using either suction or applied pressure (pF; cm of water; cbar or kPa), most research has only been focused on the water release characteristics of substrates, without necessarily giving in depth attention to relating water desorption (volumetric water content) to substrate matric potential. Matric potential (Ψ_m) is more meaningful from a physiological point of view, and provides a variable that could normalize volumetric water content data from varying soilless substrates with very different physical properties, and hence water-holding capacities. For this reason, we chose to hybridize our research approach using various ECH₂O sensors, to understand the relationships between the volumetric water content and plant available water, measured as matric potential (kPa). We simultaneously measured both variables in a range of soilless substrates with contrasting particle size distributions and physical properties. Understanding these relationships in this fashion will expand our knowledge to determine when to or not irrigate, based on a physiologically meaningful parameter for plants. This would then provide a much more powerful tool for crop management purposes, where there is a need for repeatable control of irrigation scheduling.

Chemical Properties of Soilless Substrates

The chemical composition of substrates is highly influenced by particle size, surface physical characteristics and the inherent exchange capacity of the specific substrate. The total particle surface area and charge determines the ionic composition of the nutrient solution that equilibrates in the pore water (Rhoades et al., 1999). Ideally chemical substrate characteristics are quantified before the substrate is used in

production, as this has a large influence on plant nutrient availability. Nevertheless, it should be noted that substrate chemical characteristics can and will change as plant and microorganisms interact with the substrate.

One of the major factors influencing nutrient solubility in substrates is pH (i.e., how acid or basic is the pore water) of the substrate solution. Thus, under acidic conditions, certain elements can become more soluble and indeed more available for plant uptake, and vice versa (Handreck and Black, 2002). In most soilless substrates, phosphorus (P) does not precipitate at low pH, but does at high pH (Yeager and Barrett, 1985). Peterson (1981) concluded that the optimal pH for phosphate nutrition was 5.5 in media without soil, because above this pH, water-soluble phosphate concentrations began to decrease. In peat-based media, Stver and Koranski (1997) indicate a reduction in calcium (Ca) availability at low pH, contrary to Argo and Biernbaum (1996a) who concluded that low pH did not reduce Ca availability. Instead, low pH was an indication of a lack of calcium sources applied to the substrate. A more neutral pH can also affect plant uptake because of changes in the form of the nutrient in the soil solution. For example, at pH 4.5, the H_2PO_4^- form of water-soluble phosphorus is ten times more available to the plant than the HPO_4^{2-} form than at pH 7.2 (Bunt, 1988). Nitrogen uptake and pH dynamics are also influenced by the form of nitrogen, when ammonium (NH_4^+) and nitrate (NO_3^-) is supplied in varying amounts (Barker and Mills, 1980; Marschner, 1986; Lea-Cox et al., 1996), and also by microbiological activity or nitrification (the chemical conversion of NH_4^+ into nitrite (NO_2^-) and NO_3^- by microorganisms). The critical pH for the inhibition of nitrification in soilless media was found to be in a range from 5.4 to 5.7 (Argo and Biernbaum, 1997a; Lang and Elliott, 1991; Niemiera and

Wright, 1986). Argo and Biernbaum (1997a) and Niemiera and Wright (1986) found that above this critical pH range, minimal ammonium concentrations were measured in the medium, while below the critical pH range, ammonium began to accumulate in the medium.

The capacity of a substrate to exchange cations (positively charged ions) between the substrate surface (which is mostly negatively charged), and the soil solution is called cation exchange capacity (CEC; $\text{cmol} \cdot \text{kg}^{-1}$ or $\text{meq} \cdot 100\text{g}^{-1}$). This is a dynamic process where cations equilibrate with the pore water solution. Bunt (1988) reported that the CEC of peat moss substrate indicates the potential for divalent ion adsorption – primarily calcium (Ca) and magnesium (Mg), with most monovalent cations, i.e., NH_4^+ , potassium (K^+) and sodium (Na^+) remaining in solution. Rippy and Nelson (2007) found a variation of CEC from 108 to 162 $\text{cmol} \cdot \text{kg}^{-1}$ in Canadian peat moss and, that peat with high CEC had a greater buffering capacity than those with low CEC, resulting in less drastic pH changes. Materials such as perlite, polystyrene, or rockwool have minimal CEC and are typically included to increase aeration or water-holding capacity of other components of the substrate (Argo and Biernbaum, 1994; Nelson, 1991). Bark, calcined clay, coconut coir, and expanded vermiculite are added to soilless substrate for aeration and water-holding capacity, but each also has significant CEC (Argo and Biernbaum, 1997b; Bunt, 1988; Nelson, 1991).

For most organic materials utilized as soilless substrates, inherent acidity (low pH) is a common characteristic. Organic acids are released to the substrate matrix as natural decomposition occurs (Rippy and Nelson, 2007). Consequently, liming materials (materials with capacity of lowering the pH) are utilized by the industry to raise the pH to

a more tolerable range for roots. Some of the materials utilized are calcium carbonate, magnesium carbonate, calcium hydroxide, and magnesium hydroxide. The amount of liming material required to obtain an equilibrium pH of approximately pH 5.5 - 6.0 in the root environment depends not only on the components used to produce the medium, but also on the liming material's reactivity and particle size (Argo and Biernbaum, 1996b; Williams et al., 1988).

Organic substrates and more specifically peat-based substrates are not capable of supplying all the nutrients required to sustain optimal plant growth, so general recommendation and practices are to apply fertilizers to the substrate with both macro- (N, P, K, Ca, Mg and S) and micro-nutrients (B, Cu, Fe, Cl, Mn, Mo and Zn), before planting (Bunt, 1988; Nelson, 1991). However, since most organic substrates have negligible anion exchange capacity, anions, such as NO_3^- , PO_4^{2-} and SO_4^{2-} have to be supplied on a consistent basis (either through slow-release fertilizers or liquid feed), as the potential for anions leaching from containers is high, especially under irrigated conditions. The persistence of PO_4^{2-} incorporated in a peat-based root substrate before planting was tested by Yeager and Barrett (1985), who found that this substrate had a limited ability to retain PO_4^{2-} against leaching. Biernbaum et al. (1995) further demonstrated that all macronutrients supplied from one blended fertilizer leached very quickly from a peat-based substrate, under mist irrigation.

Several studies have been conducted to quantify the nutrient content of different sources of irrigation water in the United States. Based on 4300 samples, Argo et al. (1997a) found that the overall median water source in the United States had a mean pH of 7.1, a mean EC of 0.4 dS m^{-1} and a mean alkalinity of $130 \text{ mg CaCO}_3/\text{L}$. The suggested

range for irrigation water pH and alkalinity is from pH 5 - 7 and an alkalinity of 40 - 100 mg CaCO₃/L, respectively. Argo et al. (1997a) suggested that irrigation water having pH and alkalinity levels outside these ranges are not necessarily detrimental to plant growth, as long as the pH of the substrate is maintained within an acceptable range. Argo and Biernbaum (1996a) demonstrated that irrigation water alkalinity, not pH, is the primary factor influencing substrate pH management, as this greatly influences buffering capacity. Irrigation water containing large amounts of alkalinity (>250 mg CaCO₃/L) are commonly treated by adding acids into the irrigation water.

The type of water-soluble fertilizer applied to a root substrate affects pH and nutrient concentrations in two ways: directly, by nutrients applied to the root substrate, and indirectly, by acidification of the rhizosphere pH (i.e., the root / substrate interface) that is directly influenced by root secretions and associated soil microorganisms. Fertilization with NH₄⁺ causes the substrate pH to decrease, due to H⁺ secretion (maintenance of charge balance by the plant during root uptake) and also the nitrification of NH₄⁺ to NO₃⁻, which also releases H⁺. In contrast, fertilization with NO₃⁻ causes the substrate pH to increase because of OH⁻ or HCO₃⁻ secretion associated with counter-ion uptake for charge balance (Bunt, 1988; Nelson, 1991; Lea-Cox et al, 1996).

Understanding how these physical and chemical properties interact with nutrient supply and uptake, can help us better understand and optimize plant nutrient management. Changing one factor of a nutritional program typically requires a re-evaluation of other factors. For instance, a new water soluble N formulation may alter pH dynamics, affecting PO₄²⁻ or micronutrient availability. Fertilizer concentrations should be monitored consistently. Typically this is done by measuring the electrical

conductivity (EC) of the solution as an indicator of the total salts in solution. Ion-specific analyses of pore water (though substrate extraction) have to be performed by a laboratory, since reliable and precise ion-specific electrodes are still not available. Similarly, EC root-zone sensors for the *in situ* measurement of soil/substrate EC have not had the precision required for accurate and continuous monitoring in the root zone. This is because most EC sensors are designed to work in an aqueous environment, where the accurate measurement of EC is well characterized. Ensuring the precision and accuracy of EC sensors for use in *non-aqueous environments* will therefore have profound consequences for real-time nutrient management for nursery and greenhouse crop production. This capability will provide growers with an instantaneous indication of when fertilizer salts are either under the recommended value for a specific crop, or to know when salt concentrations are building up in the root zone, to levels that would compromising root function and nutrient uptake. The ability to measure EC in real time using a sensor will also be much more cost-effective than current labor-intensive methods, and allow growers to increase the frequency of measurements. Having the ability to plot these measurements and keep a long-term record of changes in EC will allow growers to gain much more insight into their fertilization programs than is currently possible.

Many soil/substrate EC sensors are available which are apparently capable of reading instantaneous EC in soilless substrates, but it should be noted that the measurement of non-aqueous EC in soil/substrate environments is not trivial. This is because most sensors measure the bulk EC (σ_b) of the substrate, which is the total electrical conductivity associated with the surface substrate ionic charge *plus* the

electrical conductivity of the ions in the pore water solution and air. As mentioned previously, soilless substrates are typically selected for a combination of good physical and chemical characteristics; as such, most soilless substrates have relative high CEC. This allows the equilibration of ions in the pore water with those on the exchange complex, within a period of time (Argo, 1998a). For that reason we are interested in solely predicting pore water EC (σ_p), which is the same as the EC of the liquid fraction extracted from the soilless substrate matrix by pressing or centrifuging. Obviously, the amount of water contained in the substrate at any one time has a profound effect on the concentration of salts in solution, and *vice versa* (Inoue et. al, 2008); however, temperature also has a profound effect on accurate bulk EC determination, requiring that sensors have a temperature compensation capability for precise measurement (Scoggins and van Iersel, 2006). Electrical conductivity sensors therefore need to simultaneously measure three variables – water content, temperature and σ_b – to provide a precise real-time measurement of *bulk* EC; however, to provide an accurate estimate of *pore water* EC, we need to go one step further and calculate a substrate-specific offset value, as such offsets eliminate the contribution of surface electrical conductivity (σ_s) and the permittivity of dry substrate $\varepsilon'_{\sigma_b=0}$ in the final estimation of pore water electrical conductivity. This has been well-described by Rhoades (1976, 1989) and Hilhorst (2000), who have spent many years refining their two models, respectively. Such models estimate pore water electrical conductivity (σ_p) by utilizing different physical parameters which are measured directly by the sensor, or estimated separately during laboratory experimentation. This methodology and detail is fully described in Chapter 3.

Chapter 2: Determination of Water Desorption and Sensor Calibration

Introduction

Ornamental plant production has changed significantly over the past four decades, and is continuously evolving toward more efficient production systems (Raviv and Lieth, 2008). One of the biggest changes was the adoption of containers for growing plants since this offered many benefits in handling and transportation; however disease became a significant production issue when soils were used in containers, due to poor drainage (Handreck and Black, 2002). The adoption and use of porous soilless substrates of both organic and inorganic origin has driven the widespread use of containers for the production of ornamental and vegetable transplants throughout the world (Raviv and Lieth, 2008).

Reductions in substrate water potential/content in the root zone beyond a certain level is one of the greatest plant growth limiting factors for normal plant development and yield. The ability to precisely measure the soil/substrate water content, and to assess the 'availability' of water to plants is therefore essential to maintain optimum plant growth rates. Since there are many techniques and units that can measure soil/substrate water content, we agree with Jones (2007), that a standardized metric should be used, that would allow for direct volumetric water content comparisons between various substrates with different physical and water-holding characteristics. Soilless substrates have been extensively characterized and scrutinized over the years, to better understand their physical characteristics. Bunt (1961) found that organic materials such as peat had a

positive impact on the physical properties of soil mixes. De Boodt and Verdonck (1972) established moisture release characteristics for several different soilless substrates, and proposed specific plant available moisture parameters including easily available water (EAW; 0 to -5 kPa) and water buffering capacity (WBC; -5 to -10 kPa) and detailing techniques (De Boodt et al. 1974). More recently, research has focused on the contribution of key parameters such as air : water : solid ratios to the availability of water in substrates (Handreck and Black, 2002). Additional research has focused on other variables, to assess and better understand substrate dynamics. For example, by taking advantage of new theoretical models and modern electronics, researchers have been able to analyze aspects of substrates to determine water desorption characteristics *in situ* using time domain reflectometry (TDR; Paquet et al., 1993), measure saturated hydraulic conductivity in containers (Allaire et al., 1994), and to quantify gas diffusion (Caron et al., 2005).

Although desorption curves can be generated by using either suction or applied pressure (pF, cm of water, cbar, kPa), most research has focused only on quantifying substrate water release characteristics, without relating water desorption (volumetric water content, VWC) to substrate matric potential (Ψ_m). The global objective of our research was to understand the relationships between measuring the volumetric water content (VWC) and plant available water (measured as matric potential; Ψ_m in kPa), using two types of ECH₂O sensors. We wanted to simultaneously quantify both variables in a range of soilless substrates, with contrasting particle size distributions and physical properties. By doing this, we wanted to better understand the relationships between

these variables and how they related to plant water availability, in order to make more objective decisions for scheduling irrigations in these substrates.

Materials and Methods

Soilless substrates

Five substrates were chosen for testing, based on their use in the greenhouse and container nursery industry, and their differing ability to hold and release water. The substrates were 100% Perlite (horticultural grade A-20; Pennsylvania Perlite Corp., Bethlehem, PA.), 100% coir (coconut fiber; Superior Growers Supply, MI), Sunshine Professional LC1 (80% peat : 20% perlite; Sun Gro[®] Horticulture Inc., Bellevue, WA), and two Maryland container-nursery substrates 80% pine bark : 20% sphagnum peat moss (Coastal Bark & Supply, Pendleton, SC), 100% pine bark (Chesapeake Nurseries, Salisbury, MD).

Moisture Sensors

Capacitance sensors were acquired from Decagon Devices Inc. (Decagon Devices, Pullman, WA). The sensors are manufactured with an electrode-printed circuit board that is extended into the sensor prongs, with the electronic circuitry covered by a plastic molding which protects it from moisture and elements in solution. There is an explicit recommendation from the manufacturer to not expose the head molding to direct sunlight, to avoid overheating and potential malfunction. A capacitor by simple definition is a device that stores electrical energy. Capacitance sensors incorporate the substrate surrounding the sensor prongs as part of this capacitor, to measure the dielectric

permittivity (i.e. how much energy is stored by the substrate) of the surrounding medium. The permanent dipoles of water in the substrate-water-air dielectric become polarized in response to the frequency of an imposed electric field. The volume of water in the portion of the substrate scanned by the sensor heavily influences the dielectric permittivity, because the permittivity of water ($\cong 80$) is much greater than the other constituents of substrate (e.g. mineral soil $\cong 3$; organic matter $\cong 4$; air $\cong 1$). Thus, when the amount of water changes in the substrate, the sensor measures a change in capacitance (from the change in permittivity) which can be directly correlated with the change in water content. Circuitry inside the sensor converts the capacitance measurement into a proportional millivolt (mV) output.

Each Decagon sensor has a standard 5 m cable with three wires as ground (bare), excitation (white), and sensor output (red). This provides an analog output for EC-20 and EC-5 sensors. The sensors used in each experiment were connected to a CR10X Campbell Scientific Instruments (Logan, UT) datalogger, in conjunction with an AM16/32 multiplexer (CSI, Logan, UT) thus enabling the simultaneous use of multiple sensors. Both the EC-20 and EC-5 (Fig. 1.5) were excited at 3V. Note that the output voltage produced by the sensor depends on the relative permittivity of the substrate surrounding the sensor; this output voltage ranges from 10 to 50% of the excitation voltage. The moisture calibration is therefore dependent on the excitation voltage used, which varies for the different sensors manufactured by Decagon Devices. The dielectric measurement frequency used by factory settings for the EC-20 and EC-5 analog sensors is 6 and 70 MHz respectively.

Water Desorption Curve Generation

Desorption curves were generated for each substrate, to specifically measure and test sensor performance in each substrate. We tested two ECH₂O capacitance sensors, EC-5 and EC-20 (Decagon Devices, Pullman, WA). A custom-built desorption table was constructed at the Department of Environmental Science and Technology, Project Development Center, University of Maryland (Fig 2.1). The tension table consists of ten individual pressure ('tempe' cells) or columns; each column was constructed of schedule 40 polyvinylchloride (PVC), with a fixed internal diameter of 12.7 cm and a column height of 5.2 cm for the EC-5 sensors, and a column height of 20.7 cm for the EC-20 sensor, respectively. The 20.7 cm (EC-20) column was packed by filling $\frac{1}{3}$ of the column with each specific substrate, saturating and draining the water; this procedure was repeated until the column was fully packed. A similar protocol was used to pack the substrate for EC-5 probes, except $\frac{1}{2}$ of the column was initially packed with substrate to ensure that a natural distribution of particles occurred.

The sensors were sealed into a (18 x 18 cm) polycarbonate lid using silicone seal (General Electric, Silicone I, Huntersville, NC). The sensor head molding was only slightly embedded (approximately 3mm) in the polycarbonate lid since all tests were conducted under laboratory conditions (no direct sunlight exposure and constant room temperature of approximately 24 °C \pm 1). This allowed the sensor prongs to be aligned with the base of the polycarbonate lid, and top of the substrate in the column (Fig. 2.1). When the columns were fully packed with a particular substrate, the polycarbonate lid with the embedded and sealed sensor was positioned centrally over the column and carefully inserted vertically down into the substrate, ensuring no air gaps were created

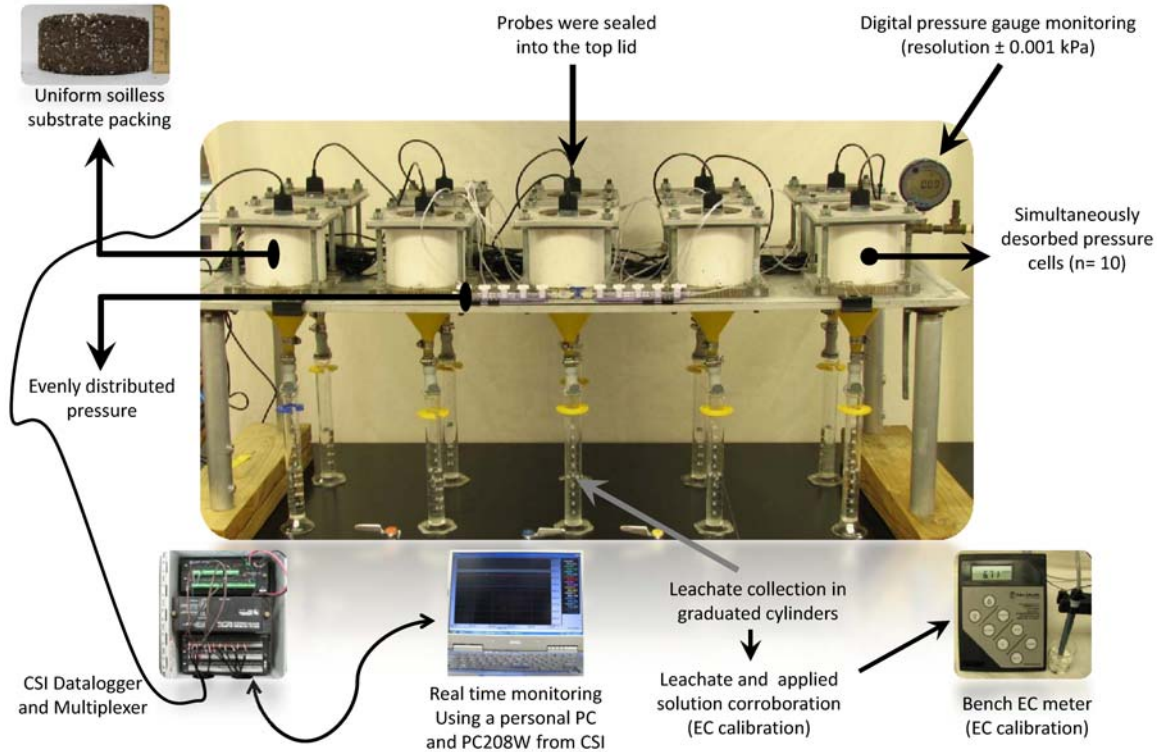


Figure 2.1. Custom desorption table with ten replicate pressure columns. This view shows, a 5-cm height column with a EC-5 sensor embedded in the top polycarbonate lid, inserted into the substrate and sealed by bolting the column and lid to the table. The columns were slowly pressurized utilizing compressed air, monitored with a digital pressure gauge and evenly distributed to all columns utilizing a manifold (center, front of table) and Teflon gas lines, attached with luer-lock fittings. Water desorbed was collected with graduated cylinders at each measured pressure increment. Sensors were attached to the multiplexer, CR10X datalogger and computer for logging and monitoring the column data, as noted in the text.

between the sensor and the substrate. The plate and sensor were then bolted down onto each column, to give a pressure-tight seal, using seated O-ring gaskets in a 1mm groove milled in the top and bottom of the PVC columns (Fig 2.2).

The base of each column was in direct contact with a polycarbonate plate, perforated with about two hundred forty 2.5 mm diameter holes (Fig 2.2a). The substrate

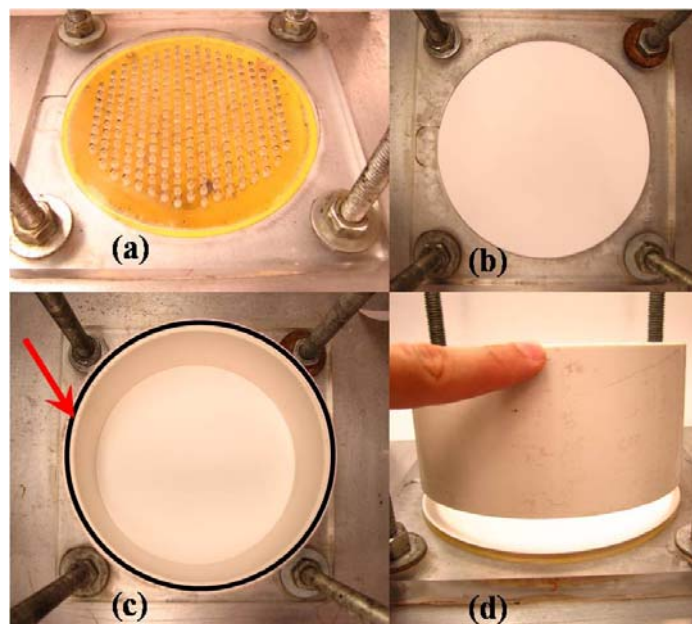


Figure 2.2a, b, c, and d. Base polycarbonate plate (a), perforated with two hundred forty 1.0 mm diameter holes. Membrane (0.45 micron pore) (b), on top of each base plate. The red arrow on (c) is pointing out the seated O-ring gaskets in a 1mm groove milled at the top of the PVC columns. Base polycarbonate plate (d), holding in place the membrane and column.

was separated from this plate by inserting a 0.45 micron membrane (Fig 2.2b) at the bottom of each column (GE Water & Process Technologies, Trevose, PA). New membranes were used for each substrate test. Vacuum grease was used to ensure the air tight seal of the O-ring gaskets between the column and the perforated polycarbonate base (Fig. 2.2c; d).

The columns were then slowly re-hydrated from the base of the column, to gradually force all interstitial air out from between the substrate particles, completely saturating the column. Air was allowed to escape from the sealed columns via a female luer thread (Cole-Parmer, Vernon Hills, IL) port in the top polycarbonate lid. This port was also used to pressurize each column. Substrate in each column was allowed to fully

saturate and establish equilibrium for at least 4 hours. Upon saturation, the ten replicate columns were allowed to drain freely overnight by gravity, thus reaching container capacity. Note that for 20-cm high columns, the gravitational pressure exerted by gravity at the top of the column is 2 kPa; for 5-cm columns this gravitational pressure is equal to 0.5 kPa, or 0.1 kPa for every centimeter of height (Milks et al., 1989c).

The volume of water expressed overnight was collected and measured for each column, providing the data for the later computation of total porosity (TP) and air filled porosity (AFP). During each run, positive gas pressure (compressed air) was applied and monitored with a digital pressure gauge (General Electric Druck Model DPI 104; TTI Instruments, Williston, VT; precision ± 0.001 kPa) and adjusted by a gas pressure regulator (Model E12 244D; Airgas East, Salem, NH). The following increments were applied to each substrate in the 20cm column: 2, 3, 5, 7, 9, 11, 21, 41, and 61 kPa. Pressure increments for 5 cm column were 1.25, 2.25, 4.25, 6.25, 8.25, 10.25, 15.25, 20.25, 40.25 and 60.25 kPa. Note that these values included the average gravitational potential of the column (= 1kPa and 0.25 kPa for 20-cm and 5-cm columns, respectively).

We collected the leachate volumes expressed from the columns at each pressure, using the following standardized protocol: Leachate volume readings were taken every 10 minutes throughout the run, using 100 ml graduated cylinders located under each column (directed by a funnel under each column under the table, see Fig. 2.1). When more than five of the columns did not change in volume by more than 1 mL during a 10 minute period, the subsequent pressure increment was applied. Runs generally took between 8 and 18 hours, depending upon the substrate and column height. At the end of each run, the volume of water leached during each pressure increment was totaled for

each replicate column. The sensor output (mV) data were continuously measured throughout each run using a AM16/32 multiplexer (Campbell Scientific, model) and CR10X datalogger (Campbell Scientific, Logan, UT) with scan ratio of 20 seconds and an average value logged every minute utilizing a modified datalogger program (*pers. comm.*, Colin Campbell, Decagon Devices; Appendix A1 and A2, for the EC-5 and EC-20 sensor, respectively).

Sensor Calibration

Capacitance sensors use the prongs as electrodes. Thus, when inserted into substrate this later works as a capacitor storing some of the energy applied by the sensor. Then, utilizing the time that takes for the substrate to store a threshold voltage is then correlated with relative permittivity, which is influenced the most part by water content (Dane and Topp, 2002). Capacitance sensors measure the average relative permittivity over the length of the sensor; hence also column volumes of equal height, as the sensor integrates the apparent dielectric constant gradient in the vertical plane when the sensor is placed vertically, as done in these experiments. Relative permittivity (or sensor output) measurements were taken simultaneously with the expressed water volumes during the desorption curve determinations. The simultaneous calibration of each capacitance sensor was therefore performed for two different variables, i.e., volumetric water content (θ) and matric potential (Ψ_m). Volumetric water content calibrations were made by measuring the leachate expressed at each pressure increment, and noting the time when equilibrium was reached; after each run, the sensor output at that specific time was retrieved from the datalogger file, to match water expressed over time. Two or three repeated runs were performed for each substrate and sensor combination (see statistical analysis section).

After each run, the substrate was carefully removed from each column and weighted, then oven-dried at 70°C for at least 96 hours, to estimate the water remaining in each substrate beyond the final pressure applied. By adding the expressed leachate volumes and the total remaining volume of water (1 g H₂O = 1 mL H₂O, at standard temperature and pressure) and dividing those volumes by the total volume of the column, it was therefore possible to calculate the actual volumetric water (θ) at each incremental (matric) pressure and the amount of water at container capacity (CC). By regression analysis, we can therefore predict θ , based on the specific sensor output. The matric potential (Ψ_m) can be used to characterize the water distribution that each substrate exhibits, which relates the specific volumetric water content of that substrate to a normalized ‘physiological’ value related to plant water availability (Jones, 2004, 2008).

Statistical Analysis

The volumetric water content calibration was made by analyzing the relationship between the matric potential (Ψ_m) applied as positive air pressure (kPa) with the sensor output (mV) and volumetric water content at each pressure increment. Identical runs were repeated three times. Each run was a completely randomized experiment with nine and ten pressure treatments (reached with smaller volumes) and ten replicates (column) per pressure for each run. Some column results were excluded from the analysis when membranes were occasionally pierced by the sensor prongs. Data were analyzed using SAS (SAS Institute Inc., Cary, NC, USA, 2002-2003), using the PROC MIXED model and the RANDOM statement, to ascertain whether there were interactions between runs at each pressure (i.e. run and run*kPa interactions). Since no significant interactions

were noted between runs (within substrates), all data were pooled to add strength to the regression analyses.

Results and Discussion

Volumetric Water Content vs. Matric potential

Moisture release curves were plotted for each substrate and sensor combination (Figs. 2.3a and 2.4a; Appendix Figs. B1 - B8). We will specifically contrast the results from the 80 peat : 20 perlite (Sunshine LC-1; Figs 2.3a, b) and the 100% perlite substrate (Figs. 2.4a, b). In general we can divide all tested substrates into two categories -mixes vs. non-mixes and high vs. low water holding capacity. All substrates showed a sharp decrease in water content with increasing pressure from 1.25 to 10.25 kPa (all Figures). Beyond 10.25 kPa, all water release curves became nearly asymptotic, indicating that the remaining water was more tightly bound to the substrate matrix, and hence 'progressively unavailable' for root uptake. This confirms data previously described by a number of authors, including Goh and Maas (1980), Fonteno et al. (1981), Bilderback et al. (1982); Verdonck (1983); Verdonck et al. (1983); Brown et al. (1987); Fonteno (1989); Cattivello (1991); Gabriëls et al. (1991) and Milks et al., (1989a; b and c). In most commercial production environments, the primary objective is to maintain a favorable environment for optimal plant development, without applying luxurious amounts of water or nutrients. Thus, having a reliable measure of plant available water would be required to determine whether PAW was at a $\Psi_m \leq 15$ kPa, maximizing plant-available water, yet minimizing the amount of water that could potentially leach from the container.

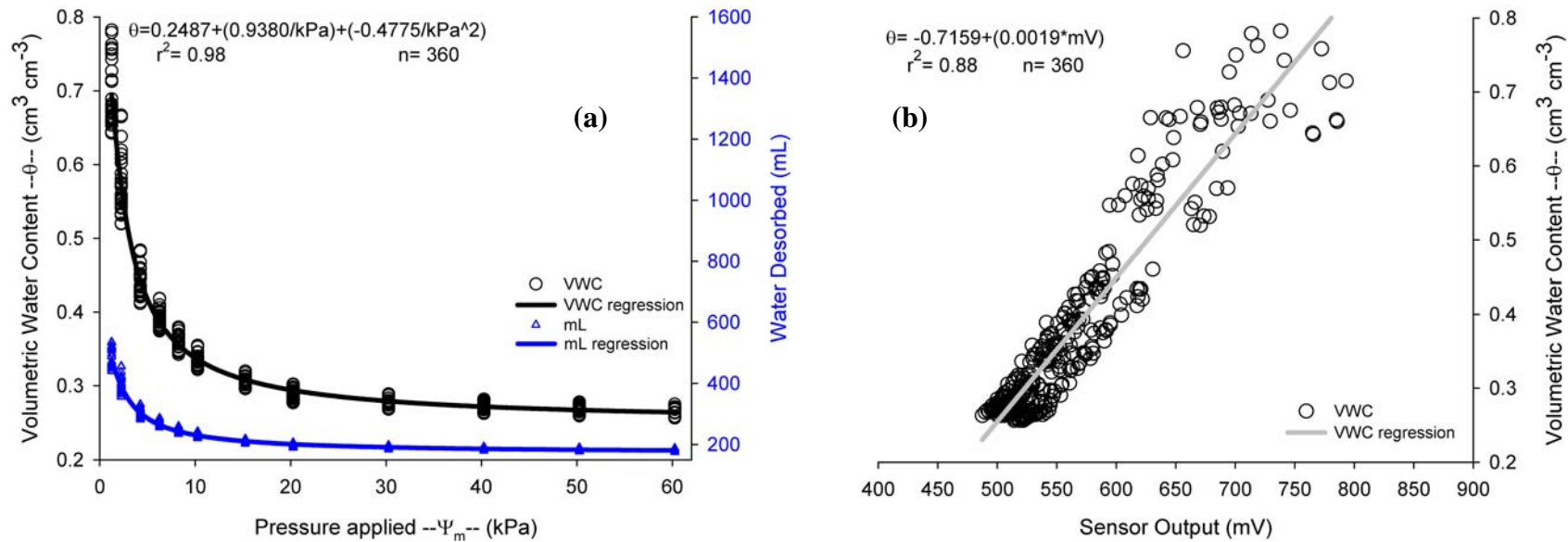


Figure 2.3 a, and b. Standard (a) moisture release curve for 5 cm height columns testing **80 peat : 20 perlite mix**, with pressure applied in kilopascals, left hand ‘y’ axis as volumetric water content -- θ -- (VWC), right hand ‘y’ axis as actual water volume desorbed from the columns throughout the desorption run. Both regression lines are plotted to follow the trend for both axes. Correlation coefficient (r^2) is shown for VWC regression equation depending on matric potential (Ψ_m) and data point count (n). **EC-5** sensor volumetric water content calibration (b) with sensor output as millivolt on the abscissa and VWC on the ordinate. Correlation coefficient (r^2) is shown for VWC sensor calibration equation and data point count (n).

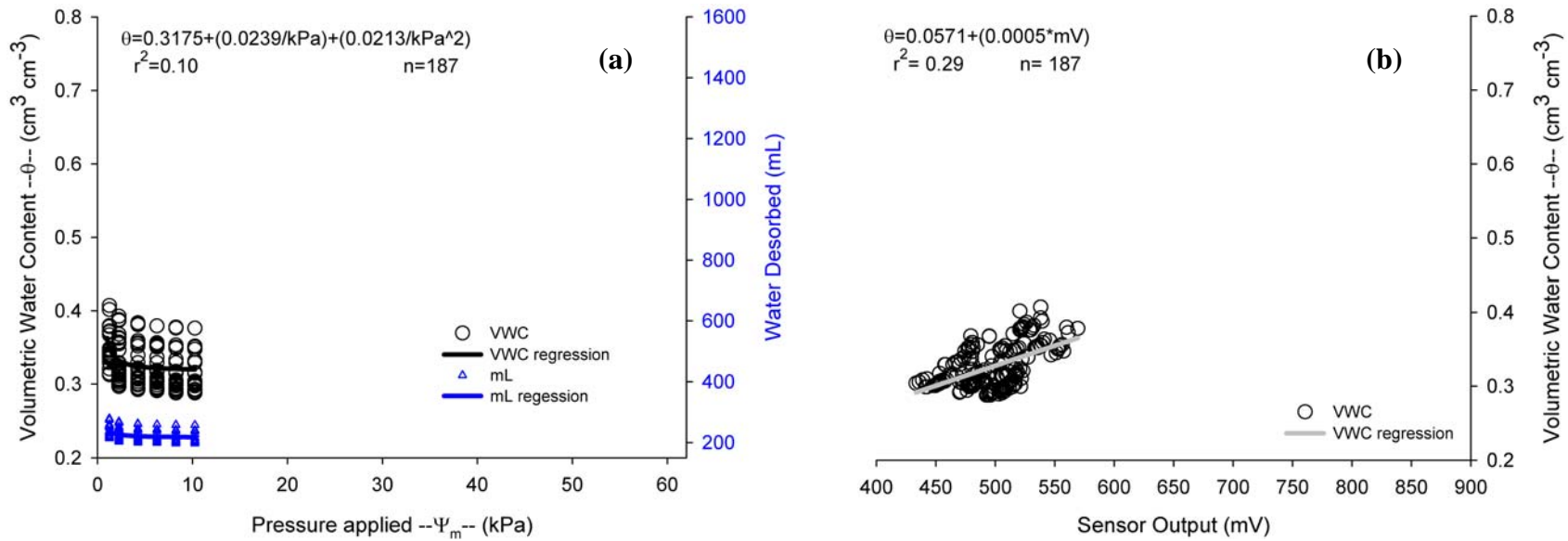


Figure 2.4 a, and b. Standard (a) moisture release curve for 5 cm height columns testing **100% perlite**, with pressure applied in kilopascals, left hand ‘y’ axis as volumetric water content -- θ -- (VWC), right hand ‘y’ axis as actual water volume desorbed from the columns throughout the desorption run. Both regression lines are plotted to follow the trend for both axes. Correlation coefficient (r^2) is shown for VWC regression equation depending on matric potential (Ψ_m) and data point count (n). **EC-5** sensor volumetric water content calibration (b) with sensor output as millivolt on the abscissa and VWC on the ordinate. Correlation coefficient (r^2) is shown for VWC sensor calibration equation and data point count (n).

Figures. 2.3a and 2.3b show the moisture release curve and sensor volumetric water content (θ) calibrations respectively, for the 80 peat : 20 perlite mix in 5cm high columns. Similar data is shown for the 100% perlite substrate in Figs. 2.4a and Fig. 2.4b.

When comparing Fig. 2.3a and 2.4a, we can quantify exactly how much water is present in each substrate from 1.25 kPa to 10.25 kPa for the 80 peat : 20 perlite mix (i.e. $\theta = 0.69$ to 0.33) which corresponds to a change of 36% volumetric water content. In contrast, there is a very small change in desorbed water in the 100% perlite (i.e. $\theta = 0.36$ to 0.31), from 1.25 to 10.25 kPa corresponding to only 5% change in volumetric water content, illustrating the very low water holding capacity of this substrate. The desorbed water (right hand 'y' axis, Figs. 2.3a and 2.4a) shows the actual volume of water desorbed from the columns at each pressure; the regression shows that desorbed water was closely related to sensor output (Figs. 2.3b and 2.4b; Table 2.1). Table 2.1 summarizes the descriptive statistics for volumetric water content (θ) vs. sensor output (mV) for all substrates and both column heights / sensor types. From this data it can be seen that both mixes that contain peat moss had the highest correlation coefficient for both sensors and column heights. It can be seen that substrates with larger pore diameters such as 100% pine bark, 100% coconut fiber, and 100% perlite had lower correlation coefficients. Notably, all r^2 relationships were highly significant, based on the number of replicate measurements (n), as indicated by the P values. This gives us confidence that these sensors can give reliable moisture readings in soilless substrates which have a wide range of air-filled porosity and water-holding capacities (Tables 2.2 and 2.3).

In general, the variation in the sensor readings increased with higher θ in all substrates tested (Figs. 2.3b, 2.4b; Appendix Figs. B1 - B8). The 80 peat : 20 perlite mix

Table 2.1. Relationship of Volumetric Water Content (θ) and sensor output (mV) with increasing pressure is shown by the linear calibration regression equation with the corresponding correlation coefficient r^2 for each substrate in 5 cm and 20 cm columns. All regressions were highly significant ($P < 0.0001$).

EC-5 Sensor (5 cm column Height)			
Substrate	Linear regression equation	Data points (n)*	Value (r^2)
100% Pine Bark	$\theta = -0.1165+(0.0010* \text{mV})$	168	0.43
100% Coconut fiber	$\theta = 0.2477+(0.0002*\text{mV})$	147	0.53
80 Pine bark : 20 Peat moss	$\theta = -0.6216+(0.0019*\text{mV})$	208	0.83
80 Peat moss : 20 Perlite	$\theta = -0.7159+(0.0019*\text{mV})$	360	0.88
100% Perlite	$\theta = 0.0571+(0.0005*\text{mV})$	187	0.29
EC-20 Sensor (20 cm column Height)			
100% Pine Bark	$\theta = 0.0432+(0.0006*\text{mV})$	198	0.76
100% Coconut fiber	$\theta = 0.2411+(0.0001*\text{mV})$	216	0.16
80 Pine bark : 20 Peat moss	$\theta = 0.0018+(0.0007*\text{mV})$	206	0.72
80 Peat moss : 20 Perlite	$\theta = -0.3110+(0.0012*\text{mV})$	180	0.79
100% Perlite	$\theta = 0.1031+(0.0019*\text{mV})$	240	0.47

* Varies depending on pressure treatments and valid replicates at the end of each desorption run.

had a higher r^2 value (0.88; $P < 0.0001$) than the 100% perlite ($r^2 = 0.29$, $P < 0.0001$) for the 5 cm height columns (Table 2.1). Typically, the more homogeneous and the smaller the particle size distribution of a substrate, the less variation would be expected in the sensor output (Kelleners et al., 2005a). Notably, although the perlite we used was a very homogeneous substrate, its micropore structure reveals some important details which explains some of the large variability observed in water-holding properties and volumetric water content sensor calibration. Perlite is a mined or volcanic silicate material (mainly SiO_2 and Al_2O_3 ; App. C1) that is expanded at high temperatures. Also has a specific surface area from 6 - 13 $\text{m}^2 \cdot \text{g}^{-1}$ and a very large internal surface area due to the expanded honeycomb shaped structure (App. C2). Note that soil matric potential is the sum of capillary forces and adsorptive forces which govern the retention of water in a substrate, due to surface charge. This dense honeycomb structure could therefore hold a large amount of water inside the micropores and ultramicropores (Drzal et al., 1999). This would explain the large amount of water held by perlite (Tables 2.2 and 2.3) beyond -10 kPa, with the practical consequences for most plants, since this water is likely to be progressively more unavailable at more negative (higher) matric potentials.

The low sensor correlation coefficients for substrates with high perlite contents could also possibly be explained by the fact that materials with a large surface area (in this case a large internal surface area) also exhibit strong dielectric relaxation (Logsdon, 2005). Dielectric relaxation is a direct reduction in the apparent energy storage (capacitance) of the substrate, which can be attributed to molecular rotation and ion migration (known as Maxwell-Wagner effect) (Jones et al., 2005). This reduction is more dramatic at frequencies below 500 MHz (Kelleners et al., 2005b).

Estimation of Matric Potential

Table 2.2 illustrates the relationship between volumetric water content (θ) and matric potential (Ψ_m) with increasing pressure, for all substrates and the two column heights. From these data, it can be seen that for most substrate and height combinations, the correlation coefficients are greater than 0.79, except for 100% pine bark and 100% perlite in the 5cm columns ($r^2 = 0.61$ and 0.10 , respectively). These data therefore proves that it is possible to equate θ with Ψ_m quite accurately by using these sensors in soilless substrates. This knowledge will have a profound impact on our ability to control irrigation schedules, based on a normalized physiological variable (i.e. Ψ_m), rather than θ , which obviously varies considerably with substrate physical properties. This has important considerations for understanding the thresholds to avoid plant water stress, since most container produced crops are C_3 plants with low water use efficiency (WUE). Even slight water stress can affect photosynthesis and consequently dry mass production (Flexas et al., 2004). Furthermore, there is evidence that leaf conductance (stomatal activity) responds at relatively moderate soil water contents (Jones, 1992), mediated by the plant regulator ABA which is released by dehydrating roots (Dodd, 2005). Evidence points out that photosynthesis of crops like tomato can be significantly reduced at very low ($\Psi_m = -2$ kPa) matric potentials (Caron et al., 2006; Pepin et al., 2008).

Figures 2.5a and 2.6a plot all moisture release regression lines, for all five different substrates for the EC-5 and EC-20 sensors (5cm and 20cm column heights). Similarly, Figs 2.5b and 2.6b plot θ calibration regression lines with sensor output (mV) for all five different substrates and column height. Figures 2.5 and 2.6 clearly illustrate the differences between substrates, sensor type and column height, on an equivalent

Table 2.2. Relationship of Volumetric Water Content (θ) and matric potential (Ψ_m) with increasing pressure is shown by the inverse second order equation with the corresponding correlation coefficient r^2 and data count (n) for each substrate in 5 cm and 20 cm columns. (Figs. 2.5a and 2.6a) All regressions were highly significant ($P < 0.0001$).

EC-5 Sensor (5 cm column Height)			
Substrate	Inverse second order Equation	Data points (n)*	Value (r^2)
100% Pine Bark	$\theta = 0.3819+(0.0841/kPa)+(0.0095/kPa^2)$	168	0.61
100% Coconut fiber	$\theta = 0.3190+(0.0756/kPa)+(-0.0373/kPa^2)$	147	0.83
80 Pine bark : 20 Peat moss	$\theta = 0.3721+(0.3885/kPa)+(-0.0625/kPa^2)$	208	0.97
80 Peat moss : 20 Perlite	$\theta = 0.2487+(0.9380/kPa)+(-0.4775/kPa^2)$	360	0.98
100% Perlite	$\theta = 0.3175+(0.0239/kPa)+(0.0213/kPa^2)$	187	0.10
EC-20 Sensor (20 cm column Height)			
100% Pine Bark	$\theta = 0.3698+(0.4020/kPa)+(-0.0833/kPa^2)$	198	0.79
100% Coconut fiber	$\theta = 0.3074+(0.0318/kPa)+(-0.0055/kPa^2)$	216	0.80
80 Pine bark : 20 Peat moss	$\theta = 0.4149+(0.1262/kPa)+(0.1457kPa^2)$	206	0.90
80 Peat moss : 20 Perlite	$\theta = 0.3519+(0.6669/kPa)+(-0.3839/kPa^2)$	180	0.98
100% Perlite	$\theta = 0.3166+(0.0518/kPa)+(-0.0078/kPa^2)$	240	0.79

* Varies depending on pressure treatments and valid replicates at the end of each desorption run.

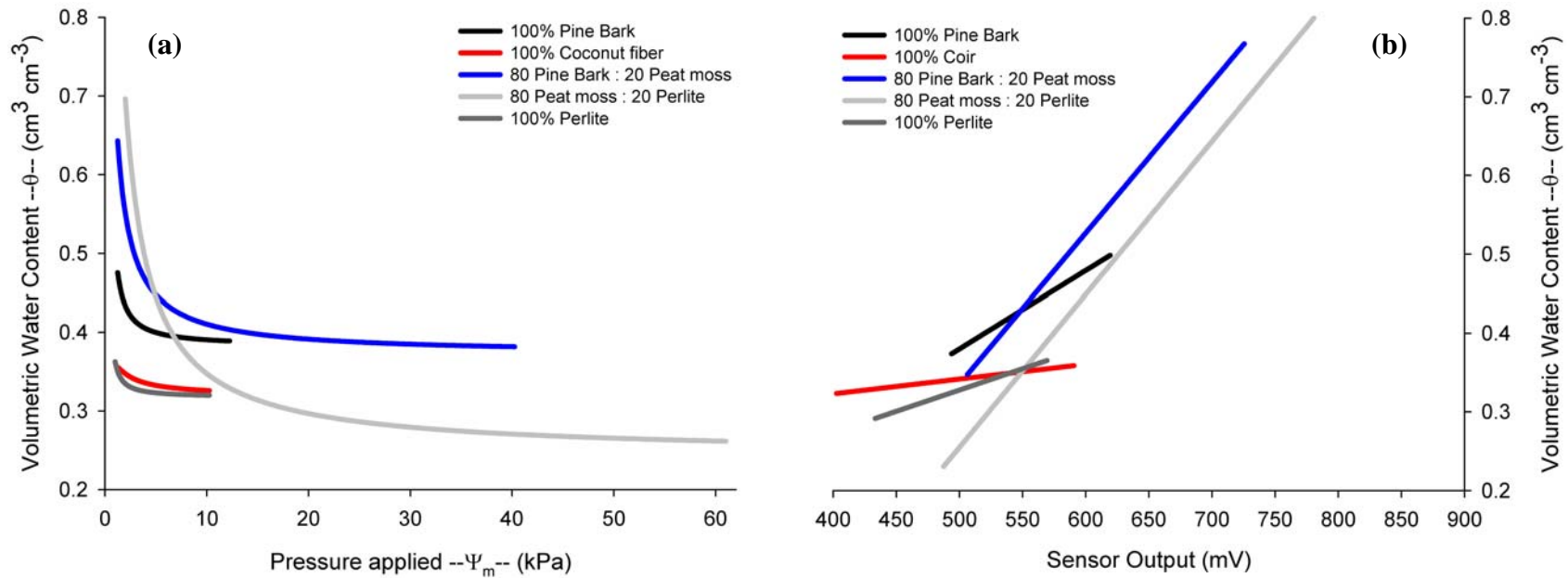


Figure 2.5 a, and b. Moisture release regression lines (a) for all five different substrates tested using 5 cm height columns with pressure applied in kilopascals, 'y' axis as volumetric water content θ (VWC). EC-5 sensor volumetric water content calibration regression lines (b) with sensor output as millivolt on the abscissa and volumetric water content on the ordinate.

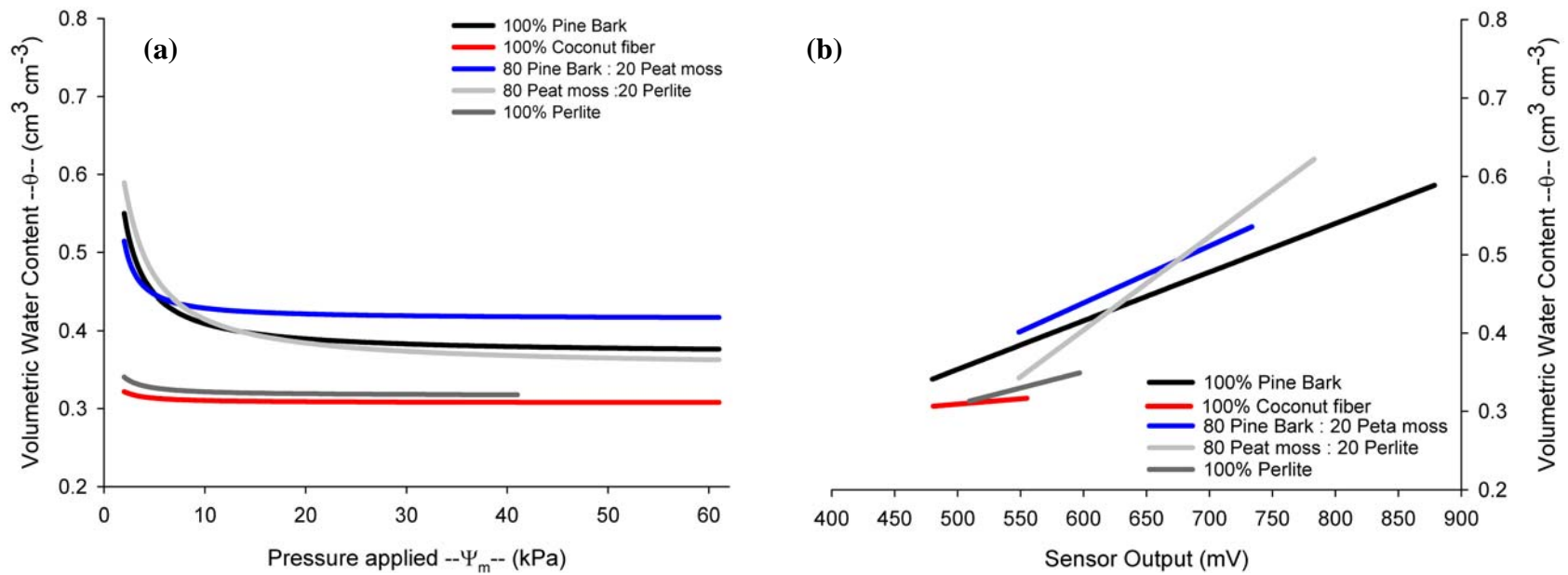


Figure 2.6 a, and b. Moisture release regression lines **(a)** for all five different substrates tested using **20 cm** height columns with pressure applied in kilopascals, 'y' axis as volumetric water content θ (VWC). **EC-20** sensor volumetric water content calibration regression lines **(b)** with sensor output as millivolt on the abscissa and volumetric water content on the ordinate.

basis. It is evident that some water was still being expressed from the 20 cm columns at 60 kPa (Fig. 2.6a), in contrast to the same substrates in the 5cm column (Fig. 2.5a).

However, it is also evident that most substrates released the majority of water between 1 to 10 kPa of applied pressure, irrespective of column height. This has important ramifications on the total water available to plants, which is obviously more limited in smaller containers than in larger containers (both height and volume). It is interesting to note that both the 100% coconut fiber and 100% perlite desorption curves leveled off at a θ of about 0.3, independent of column height, illustrating the proportion of bound water. The 80 peat : 20 perlite mix had the highest water holding capacity in both 5 cm and 20 cm columns.

From Figs 2.5b and 2.6b, it can be seen that the regressions (Table 2.1) are clearly different for the EC-5 and the EC-20 sensors. Even though some regressions have equivalent slopes, it is important to recognize that the substrate water-holding capacity extends beyond range of other sensor output, e.g. comparing 80 pine bark : 20 peat and 80 peat : 20 perlite data (Fig. 2.5b; Table 2.1). For this reason, we conclude that sensors should be calibrated for individual substrates if the user requires higher precision. However, it is likely that the calibration equations given in Table 2.1 would be adequate for use in similar types of substrates and container heights, for most production uses (e.g. scheduling irrigation events).

Integrating Volumetric Water Content and Matric Potential, for Precision Irrigation Scheduling

Tables 2.3 and 2.4 show the water distribution into readily available water (RAW, from 0 to -10 kPa) which in turn is typically subdivided into easy-available water (EAW,

0 to -5kPa) and water buffering capacity (WBC, -5 to -10 kPa). The remainder of the water is progressively-unavailable water (PUW, greater than -10 kPa). It is important to note that water distribution (Tables 2.3 and 2.4) is computed by definition based on the amount of water released within these matric potential ranges, and then normalized dividing by container capacity (CC). This is different from the volumetric water content (θ) calculation, where the volume of water released is normalized dividing by the *total volume of the column*. The VWC data in Figs. 2.4, 2.5, 2.6 and 2.7, was calculated in this manner, as per convention. However, if we calculate θ based on container capacity, this clearly changes the calibration constants. We have illustrated this difference for 80% peat : 20% perlite and 100% perlite, respectively (Appendix Figs. B9; B10). For the 80% peat : 20% perlite substrate (Appendix Fig. B9), the difference in volumes (684 vs. 517 mL; 24% less) makes little difference, but for the 100% perlite substrate (Appendix Fig. B10), the difference in volume (684 vs. 349 mL; 49% less) was significant. Note that the calculation using CC brings the data in line with the water retained by the perlite substrate as PUW (Tables 2.3 and 2.4). It is therefore apparent that we should revisit how we calculate volumetric water content in substrates that either have very low water holding capacities, or unusual physical properties.

The percentage of progressively-unavailable water (PUW) was surprisingly high for all substrates and combinations tested. For perlite, this proportion equaled 62.8% and 80.0% in the 5-cm and a 20-cm column, respectively. As discussed in Chapter 1, a proportion of this water at tensions greater than -10 kPa may in fact, be available for uptake by roots, although, Keihl et al. (1992) showed that the growth of *Chrysanthemum* [*Dendranthema grandiflorum* (Ramat.) cv. Kitamura], in soilless substrates was reduced

Table 2.3. Physical properties and water distribution for different substrates in **5 cm** tall columns with bulk density (BD), Container capacity (CC), total porosity (TP), air filled porosity (AFP), and water distribution as easily available water (EAW), water buffering capacity (WBC), and progressively unavailable water (PUW).

		100% Perlite	80 Pine Bark : 20 Peat	100% Coir	100% Pine Bark	80 Peat: 20 Perlite
BD	(g • cm⁻³)	0.114	0.204	0.086	0.218	0.106
CC[†]	(mL)	349	517	341	419	534
TP	(%)	62.2	77.6	88.5	71.5	80.0
AFP	(%)	11.7	2.1	38.6	10.2	2.6
	Pressure (kPa)	Water Distribution (%)				
EAW	(1.25 to 5.25)	36.0	40.0	32.6	34.6	43.7
WBC	(5.25 to 10.25)	1.2	7.0	2.1	2.2	13.1
PUW	(>10.25)	62.8	53.0	65.3	63.2	43.2

[†] Total volume of the 5-cm column = 684.1 mL. Note that CC (%) = TP - AFP. Use CC values to interconvert data.

Table 2.4. Physical properties and water distribution for different substrates in **20 cm** tall columns with bulk density (BD), Container capacity (CC), and water distribution as easily available water (EAW), water buffering capacity (WBC), and progressively unavailable water (PUW)

		100% Perlite	80 Pine Bark : 20 Peat	100% Coir	100% Pine Bark	80 Peat: 20 Perlite
BD	(g • cm⁻³)	0.103	0.151	0.072	0.166	0.100
CC †	(mL)	1014.7	1474.4	1099.8	1475.0	1605.9
TP	(%)	75.4	85.0	94.1	86.3	90.1
AFP	(%)	35.4	26.8	50.7	28.1	26.7
Pressure (kPa)		Water Distribution (%)				
EAW	(2 to 5)	18.3	23.2	27.6	20.1	27.8
WBC	(6 to 11)	1.7	3.4	1	10.1	11.0
PUW	(>11)	80.0	73.4	71.4	69.8	61.2

† Total volume of the 20-cm column = 2533.5 mL. Note that CC (%) = TP - AFP. Use CC values to interconvert data.

at water tensions as low as -16 kPa. For this reason, we think that set-points for scheduling irrigations using these sensors should ideally be between -1 and -10 kPa, to avoid plant water stress utilizing most substrates. This should of course be confirmed by empirical determinations once the sensors are in place in the container, and giving stable readings in the root zone.

In summary, from these results, it is clear that container height and substrate water retention properties have significant effect on the precision and accuracy of Decagon capacitance sensors in these soilless substrates. Cumulatively, these data give proves that is possible to equate θ quite accurately with Ψ_m . Being able to precisely measure plant available water is essential to schedule irrigations in different substrates, maintain Ψ_m in the range of plant-available water, and minimize the leaching of water and nutrients from the container.

Chapter 3: Electrical Conductivity Calibration

Introduction

Electrical conductivity (EC) sensors have not had the precision required for accurate monitoring of salt concentrations in soilless substrates until now, since most EC sensors are designed to work in aqueous environments, where the accurate measurement of EC is well characterized. Ensuring the precision and accuracy of EC sensors for use in a non-aqueous environments (e.g. in soilless substrates) will have profound consequences for real-time nutrient management for nursery and greenhouse crop production. This capability will provide growers with an instantaneous indication of when fertilizer salts are either under the recommended value for specific crops or when salts are building up in the root zone, perhaps compromising plant growth. The ability to measure EC in real time using a sensor will also be much more cost-effective than the current labor-intensive methods used to monitor EC, and will also allow growers to increase the frequency of measurements. Having the ability to plot these measurements and keep a long-term record of changes in EC will give us much more insight into managing fertilization programs than is currently possible.

Brief Background

Many sensors are available that are apparently capable of reading instantaneous EC in soilless substrates, but the measurement of electrical conductivity (EC) in non-aqueous environments is not trivial. This is because most sensors measure the bulk EC (σ_b) of the substrate, which is the total electrical conductivity associated with the surface

substrate ionic charge *plus* the electrical conductivity of the ions in the pore water solution (σ_p) and air. Soilless substrates are typically selected for a combination of good physical and chemical characteristics; as such, most soilless media have relative high cation exchange capacity, associated with the negative charge on substrate particles. This allows the equilibration of ions in the pore water with those on the exchange complex, within a period of time (Argo, 1998a). For that reason we are interested in predicting pore water EC (σ_p), rather than bulk EC (σ_b), equated to the liquid fraction extracted from the soilless substrate matrix, by direct extraction (pressing or centrifugation). Obviously, the amount of water contained in the substrate at any one time has a profound effect on the concentration of salts in solution, and *vice versa* (Inoue et. al, 2008); temperature also has a significant effect on accurate bulk EC determination, requiring that sensors have a temperature compensation capability for precise measurement (Scoggins and van Iersel, 2006). Electrical conductivity sensors therefore need to simultaneously measure three variables – water content, temperature and σ_b – to provide a precise real-time measurement of *bulk* EC. However, to provide an accurate estimate of *pore water* EC, we need to go one step further and calculate a substrate specific offset value. This offset eliminates the contribution of surface electrical conductivity (σ_s) and permittivity of dry substrate ($\epsilon'_{\sigma_b=0}$) in the final estimation of pore water electrical conductivity, as described by the Rhoades (1976, 1989) and Hilhorst (2000) models, respectively. Such models estimate pore water electrical conductivity (σ_p) by utilizing different physical parameters read directly by the sensor or estimated separately during laboratory experimentation (further details in the model section, below).

Study Objectives

This study had three primary objectives: (1) to calibrate and compare the performance of two types of EC sensors in a commercial Sunshine Professional LC1 substrate (80 peat: 20 perlite; Sun Gro® Horticulture Inc., Bellevue, WA) with a range of electrical conductivities from 0.22 to 8.0 dS m⁻¹; (2) Since both sensors measure bulk EC (σ_b), the second objective of this study was to derive an offset value that would ensure the accurate prediction of pore water EC (σ_p) from the measurement of σ_b ; and (3) compare the precision of these offset values with two alternative models, namely from Rhoades (1976, 1989) and Hilhorst (2000). It should be noted that Decagon Devices, Inc., who produce both sensors, currently uses the Hilhorst model to predict σ_p using an offset value of 6.0 with both sensors.

Materials and Methods

We previously described a method to measure the desorption of water using a modified tension table (Chapter two). In order to measure the model's input variables required for the measurement of pore and bulk EC, we had to modify the desorption protocol that was previously described. The soilless substrate used in these EC studies was a commercial Sunshine Professional LC1 (80 peat: 20 perlite; Sun Gro® Horticulture Inc., Bellevue, WA) media. Calibration runs were repeated twice for every salt concentration, testing the response of two types of EC sensors (ECH₂O-TE and 5TE, Decagon Devices, Inc; n=5 each) at increasing salt concentrations of 0.22, 1.0, 2.0, 4.0, 6.0, and 8.0 dS • m⁻¹. Columns were repacked between each run with new substrate, saturated with a differing salt concentration.

The bulk density of this substrate was normalized for all runs at $0.12 \text{ g} \cdot \text{cm}^{-3}$ as a standard bulk density, according to nine different laboratories throughout Europe (Gabriëls et al., 1991). This was a standard procedure for all columns and all repeated runs, using the desorption table (Fig. 2.1). This refinement in methodology was made to reduce the variation due to different air-filled porosities, and allowed for a direct comparison to typical bulk densities found in commercial production. Bulk density normalization was done by first determining the total weight of substrate needed to have the desired bulk density on a dry basis and adding the adjusted weight, based in the substrate moisture content. This is because peat moss substrates are typically sold with added moisture, to reduce shrinkage and rewetting issues. Half of the substrate for each individual column ($n=10$ in total; $n=5$ for each sensor type) was weighed and placed in individual 1 L beakers, for each column. Initial salt residues in the substrate were leached by adding 600 mL of deionized water, vigorously stirring and pouring off the supernatant three times. Potassium chloride (KCl) was used to make up the salt solution for each run (Rhoades, 1976) and independently measured with a Traceable[®] Bench (Conductivity Control Company, Friendswood, TX) Model 4163 EC meter. The substrate for each column was equilibrated with the desired electrical conductivity solution for each run (i.e. 0.22, 1.0, 2.0, 4.0, 6.0 and 8.0 dS m^{-1}), by allowing the solution to stabilize for one day between flushes. A new batch of substrate (from the same bag) was used for each successive run. Five-centimeter deep columns were packed, as previously described in Chapter 2, except that columns were re-hydrated with the chosen salt solution. Desorption runs were then done at incremental pressures of 1.25, 2.25, 4.25, 6.25, 8.25, 10.25, 15.25, 20.25, 40.25 and 60.25 kPa, as previously described. Two

repeated runs were made with each electrical conductivity solution, to ensure adequate replication for each sensor type and EC.

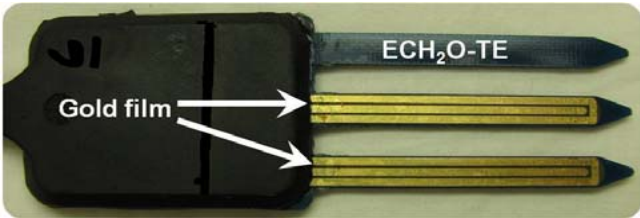
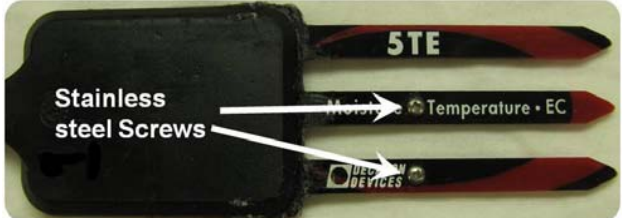
Every repeated run using the desorption table had five replicate columns for each sensor type (ECH₂O-TE and 5TE). Both sensors are illustrated in Table 3.1 with their specific characteristics noted. Sensors were randomly assigned to different columns for each run. The expressed pore water from each column was collected at the end of every incremental pressure; the expressed leachate volume and leachate conductivity (σ_w) was recorded for each fraction expressed at each pressure (Fig 2.1). The EC of the expressed leachate at each pressure increment was independently measured using the Traceable[®] Bench Model 4163 EC meter.

Substrates were removed from the columns after each EC run, and oven-dried at 70°C for at least 96 hours, to estimate the water that remained in each substrate beyond the pressure applied end point to calculate ‘unavailable’ volumetric water content θ_{ws} (previously described in Ch. 2 as progressively unavailable water, PUW). By adding the expressed leachate and oven-dried volumes, it was therefore possible to calculate actual volumetric water content at each specific pressure increment (θ_w) (Table 3.2).

Experimental Analysis

Identically designed runs were performed twice for each experiment. Each run was a completely randomized experiment with ten pressure treatments and five replicates (column) per pressure for each run. Data were analyzed using SAS (SAS Institute Inc., Cary, NC, USA, 2002-2003), using the PROC MIXED model and the RANDOM statement, to ascertain whether there were interactions between runs at each pressure for

Table 3.1. Picture of the two EC sensors types (ECH₂O-TE and 5TE) illustrating their major physical design characteristics. Note that the 5TE version is the only version that is currently commercially available from Decagon Devices, Inc. (Pullman, WA).

Variable	Sensor	
	ECH ₂ O-TE	5TE
		
Sensing area (cm ²)	2.162	0.062
Sensing area made of	gold	stainless steel
Sensing area toughness	regular	better
Calibration	two point	five point

every variable measured (i.e. ϵ'_p , ϵ'_b , σ_b , θ). No significant interactions were found between runs; consequently all data were pooled to add strength of representing evidence from independent replicates of the two runs made.

Data Collection

The ECH₂O-TE and 5TE (digital) sensors were excited at 12V; a single resistor of 220 ohm was used between the datalogger and multiplexer to minimize noise from the output signal. Both the ECH₂O-TE and 5TE sensors utilize a 70 MHz oscillating frequency.

A data-stream of three numbers was stored and retrieved from a Campbell Scientific CR10X datalogger for each sensor, at 1-minute intervals. Sensors were attached to the datalogger using a Campbell Scientific AM16/32 model multiplexer. Fig. 3.1 illustrates the raw data outputs in an Excel spreadsheet, with the conversions to known outputs. The first output number is the raw dielectric output for the 5TE sensor, or raw counts for the ECH₂O-TE. The equations used to transform this raw data to bulk dielectric permittivity (ϵ'_b) differs for each sensor, as noted in Fig. 3.1. For the 5TE sensor, ϵ'_b is calculated by dividing the raw dielectric output by 50. For the TE sensor, we applied the equation to the raw counts provided by the manufacturer (Decagon Devices, 2008).

The raw EC data (second column, labeled EC; Fig. 3.1) and raw temperature data (third column) were similar for each type of sensor, and the conversion procedures for bulk electrical conductivity (σ_b) and dielectric permittivity of soil's pore water (ϵ_p) from the raw data are equivalent for both sensors, as shown in Fig. 3.1. The raw electrical

conductivity data was divided by 100 to obtain σ_b in dS m^{-1} . Temperature is converted from the raw data by subtracting four hundred and dividing by ten, to obtain degrees Celsius ($^{\circ}\text{C}$). This measurement of temperature is utilized to obtain the dielectric permittivity of the pore water (ϵ_p) by the sensor, i.e.,

$$\epsilon_p = 80.3 - [0.37 * (T_{\text{soil}} - 20)] \quad [\text{Eq. 3.1}]$$

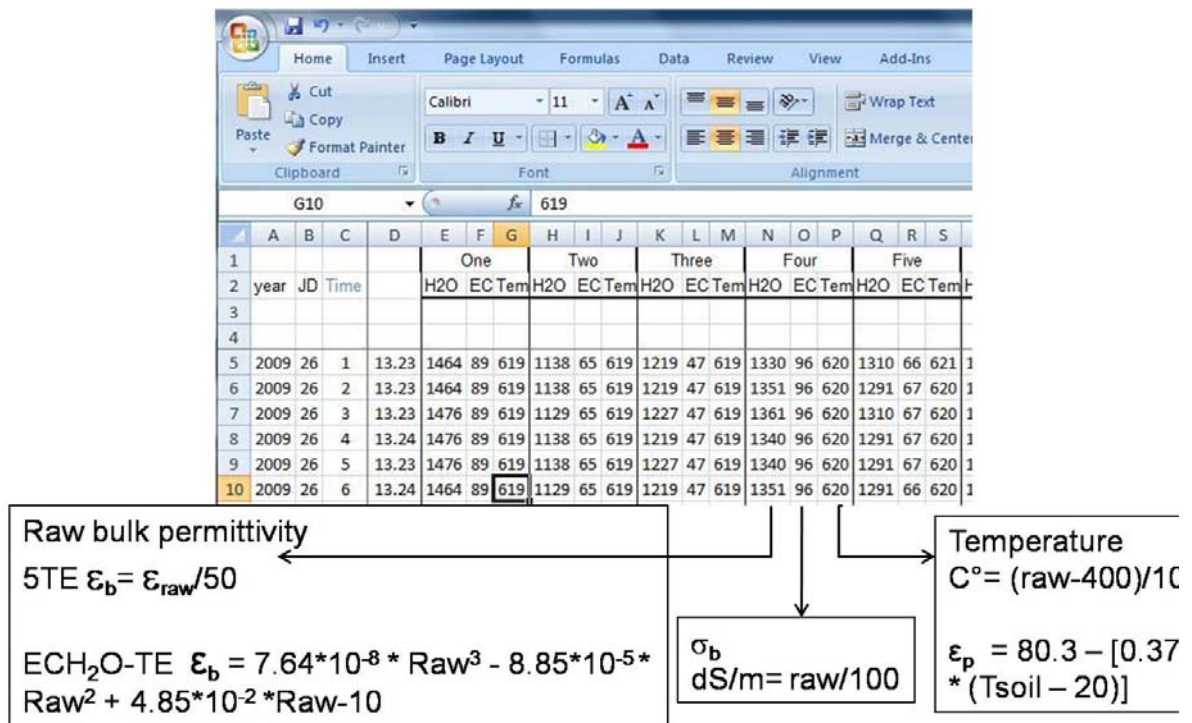


Figure 3.1. Raw data output values from the datalogger (in a MS Excel table), showing the values and the conversions to known outputs.

Models utilized

Rhoades (1976, 1989) states the necessity for an offset value or estimation of surface electrical conductivity (σ_s), in order to estimate pore water electrical conductivity

Table 3.2. Rhoades (1989) model variables descriptions and the equivalent determination of the variable in this experiment.

Variable	Variable as explained by the model	Variable as measured in this experiment
σ_p	Pore water electrical conductivity	—
θ_w	Volumetric water content	$\theta_w = [\text{expressed leachate (mL) at every incremental pressure} + \text{oven-dried (mL)}] / \text{total column volume (mL)} \{1\text{mL}=1\text{cm}^{-3}\}$
θ_s	is equal to the ratio of substrate bulk density (ρ_b) and substrate particle density (ρ_s),	$\theta_s = \rho_b / \rho_s$ $\rho_b = \text{Dry mass (g)} / \text{Total column Volume (cm}^3\text{)}$ $\rho_s = \rho_b / (1 - \text{Total porosity})$ Total porosity = Total water / Cylinder volume
θ_{ws}	volumetric water content in the series-coupled pathway (small pores) or “immobile water”	$\theta_{ws} = \text{oven-dried (mL)}$; As previously described, as progressively unavailable water (PUW)
θ_{wc}	volumetric water content in the continuous liquid pathway (large pores) or “mobile water”	Expressed water after each pressure increment with the tension table
σ_{ws}	Specific electrical conductivity of the soil water that are in series-coupled with the solid particles	—
σ_{wc}	Specific electrical conductivity of the soil water in the continuous conductance element	—
σ_s	Substrate specific surface electrical conductivity	Normalization of σ_b as $(\sigma_b / \sigma_w, \theta)$ and plotted as (σ_b, σ_w) with resulting ‘ y_0 ’ intercepts as σ_s
σ_b	Substrate specific bulk electrical conductivity	Measured directly by the sensor

(σ_p). This offset is likely to be substrate-specific. The exact value of this offset for soilless substrates needs to be determined since all the research published to date has been done using inorganic soils, not soilless substrates. This offset value (σ_s) is calculated by plotting the bulk conductivity (σ_b) vs. the solution electrical conductivity (σ_w). However, before that can be done, the σ_b data must be normalized using volumetric water contents (θ). Symbol descriptions can be found in Table 3.2.

By using the θ data generated with the tension table and values of σ_b and σ_w measured at the various measured water contents, it is possible to plot σ_b/σ_w vs. θ as seen in the results section (Figs. 3.2a and 3.3a). Utilizing the regression equations derived from (σ_b/σ_w , θ) (Experimental results section; Tables 3.3 and 3.4), it is then possible to accurately estimate the ratio σ_b/σ_w at specific combinations of volumetric water content (i.e. 0.3, 0.4, 0.5, 0.6, 0.7, 0.8 cm³ cm⁻³) for every solution applied (i.e. 0.22, 1, 2, 4, 6, 8 dS m⁻¹) guided by the intersections of the vertical broken lines and regression curves (Figs. 3.2a and 3.3a). It is therefore possible to estimate σ_b since we have known values of ‘ratio’ and fixed values of σ_w , and we can solve for σ_b in equation 3.2, using equation 3.3.

$$\sigma_b/\sigma_w = \text{Ratio} \quad [\text{Eq. 3.2}]$$

$$\sigma_b = \text{Ratio} * \sigma_w \quad [\text{Eq. 3.3}]$$

When this procedure is repeated for every θ selected (every intersection of the broken lines with the solution applied regression lines in Figs. 3.2a and 3.3a) the process

yields a new (estimated) σ_b , data essentially independent of volumetric water content. This is plotted again as (σ_w, σ_b) , as seen in Figs. 3.2b and 3.3b. The offset value is the resulting average of the intersections from the regression lines on the y-axis at zero σ_w (Tables 3.3 and 3.4).

The model proposed by Rhoades et al (1989) was intended to assess soil salinity as bulk electrical conductivity (σ_b) as seen in equation [3.4].

$$\sigma_b = \left[\frac{(\theta_s + \theta_{ws})^2 \sigma_{ws} \sigma_s}{(\theta_s) \sigma_{ws} + (\theta_{ws}) \sigma_s} \right] + (\theta_w - \theta_{ws}) \sigma_{wc} \quad [\text{Eq. 3.4}]$$

Equation [3.4] can be solved for σ_p with the assumption that $\sigma_{ws} \approx \sigma_{wc}$. Although, σ_{ws} might not be the same in composition as σ_{wc} the diffusion processes will cause σ_{ws} and σ_{wc} to reach equilibrium at some point. Note that inputs (irrigation, rain) and outputs (drainage, evapotranspiration) of water will disturb this equilibrium until equilibrium is once again reached (See Table 3.2).

Equation [3.4] can be re-arranged as a quadratic equation, and solved for its positive root as:

$$\sigma_p = \frac{-B + \sqrt{B^2 - 4AC}}{2A} \quad [\text{Eq. 3.5}]$$

Where: $A = [(\theta_s) (\theta_w - \theta_{ws})]$

$B = [(\theta_s + \theta_{ws})^2 (\sigma_s) + (\theta_w - \theta_{ws}) * (\theta_{ws} \sigma_s) - (\theta_s \sigma_b)]$

$C = -[\theta_{ws} \sigma_s \sigma_b]$

Hilhorst (2000) also recognized the necessity of an offset value ($\varepsilon'_{\sigma_b=0}$) or permittivity for nearly dry substrates ($\theta \geq 0.10$), due the fact that dry materials are still polarizable; therefore, $\varepsilon'_{\sigma_b=0} \neq 0$ is used to estimate pore water electrical conductivity (σ_p), by utilizing this model. There are very few published references that measure this offset value for soilless substrates; there are only two references that we are aware of – Balendonck et al. (2005), who mention the determination of such a substrate offset value (equal to 6.2) and follow-up research by Incrocci et al. (2009) that utilized the same offset value determined by Balendonck et al., (2005). The results from Balendonck et al., (2005) were reached only after performing multiple mathematical iterations aimed at achieving a higher correlation coefficient. This offset value ($\varepsilon'_{\sigma_b=0}$) is calculated by plotting the real part of the permittivity (ε'_b) vs. the bulk electrical conductivity (σ_b), with the resulting $y=0$ as the offset, and with no further intermediate steps needed. Again, this is explained in more detail in the experimental results section (see below; Fig. 3.4). Hilhorst (2000) calculated several offset values ranging from 1.9 to 7.6 and suggested using an average value of 4.1 with, and only when $\theta > 0.10$. On the other hand, Decagon Devices Inc. indicates that according to their research with various agricultural soils, organic and inorganic growth substrates, $\varepsilon'_{\sigma_b=0} = 6$ yielded better estimations of pore water EC (Decagon Devices, 2008). Note that $\varepsilon'_{\sigma_b=0}$ is a unitless number since permittivity has no units. The Hilhorst (2000) model is therefore:

$$\sigma_p = \frac{\varepsilon'_p * \sigma_b}{\varepsilon'_b - \varepsilon'_{\sigma b=0}} \quad [\text{Eq. 3.6}]$$

Where:

ε'_p is the dielectric permittivity of substrate pore water (unitless),

σ_b is the bulk electrical conductivity (dS m^{-1}),

ε'_b is the real portion of the bulk dielectric permittivity (unitless), and

$\varepsilon'_{\sigma b=0}$ is an offset value for ε'_b .

Three of these four variables are simultaneously read by both the ECH₂O-TE or 5TE sensors, as shown in Fig. 3.1.

Greenhouse Study

A greenhouse study was conducted to provide an empirical dataset, to apply each model and test the derived offset values from the laboratory determinations. Actual bulk EC, bulk permittivity, and pore water permittivity values were recorded by each sensor type (n=4) during a gradual water content dry-down within the root zone of an *Impatiens* ‘New Guinea’ greenhouse crop. This 41-day greenhouse study was performed during fall 2008 at the University of Maryland (College Park, MD) greenhouse complex. Thirty-two plants were transplanted into 15cm diameter x 10.5cm high containers, using the same 80 peat: 20 perlite greenhouse substrate (Sunshine LC-1). Plants were sub-irrigated daily with a solution made from Peters Professional 20-10-20 (Scotts Company, Columbus, OH) at 1.0 dS m^{-1} for the first three weeks of the study. There were two dry-down periods (to wilt) with no watering given between days 16-27 and days 32-40 (the two dry-down periods). Plants were completely rehydrated between these two periods by daily sub-

irrigations using 20-10-20 at 1.0 dS m^{-1} , as before. The plant material was organized in a single block with offset rows of 4 x 3 plants, with guard row plants surrounding the block. Only inner plants had EC sensors embedded in the root zone, inserted half-way down the container, through the sidewall of the container (Fig. 3.5). Four replicate containers with one sensor (ECH₂O-TE or 5TE) per container (n=8) were randomly assigned to different containers. Data were continuously logged at 1-minute intervals using two EM50 dataloggers (Decagon Devices Inc).

Results and Discussion

Rhoades Model

Applying the Rhoades (1976, 1989) model, values of σ_b/σ_w at the various measured water contents were plotted for the ECH₂O-TE (Fig. 3.2a) and the 5TE sensors (Fig. 3.3a). A greater variation in σ_b/σ_w at higher volumetric water contents can be seen, especially with the 5TE sensor (Fig 3.3a), although the goodness of fit of the regression lines (r^2) are equal or greater than 0.945 ($P>0.0001$) for both sensors (Tables 3.3 and 3.4). The procedure utilized to normalize the bulk electrical conductivity (σ_b) that was described on page 62 (Fig. 3.2b; Fig. 3.3b), was initially described by Rhoades et al., (1976) and followed by Nadler (1982) and Amente et al., (2000), among others. In this instance, offset values are equated to the particle surface electrical conductivity (σ_s) the average of which was found to be -0.00205 and -0.00288 for the ECH₂O-TE and 5TE sensors, respectively with standard error of the mean equal to 0.00531 and 0.00464 respectively (Tables 3.3 and 3.4).

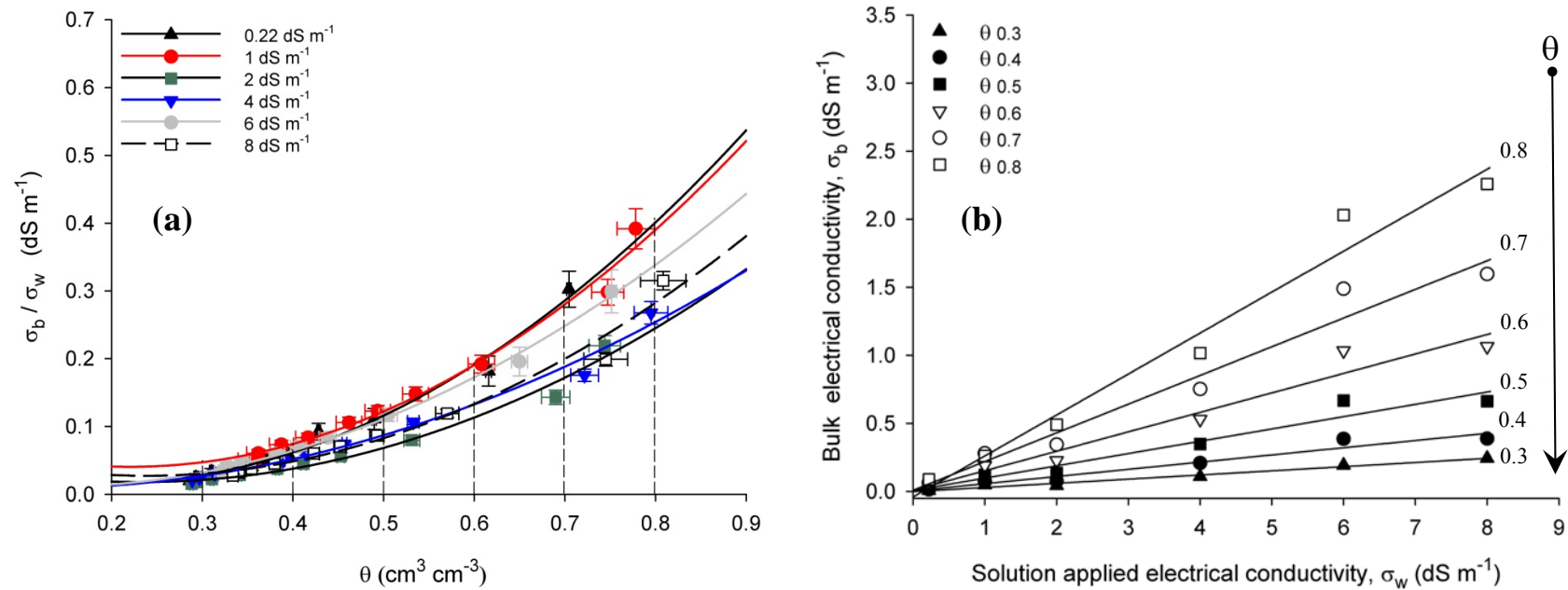


Figure 3.2 a, and b. Normalization of bulk electrical conductivity by volumetric water content **(a)** with the **ECH₂O-TE** sensor. Bulk substrate electrical conductivity divided by leachate electrical conductivity, (σ_b / σ_w) vs. volumetric water content (θ) for 80 peat: 20 perlite mix substrate. Error bars indicated as standard error about the mean (SEM). **(b)** Bulk substrate electrical conductivity after normalization (σ_b) vs. leachate electrical conductivity (σ_w) for various fixed volumetric water content (θ). The average of intercepts with bulk substrate EC (σ_b) axis becomes the offset value (σ_s) according to Rhoades (1976) methodology.

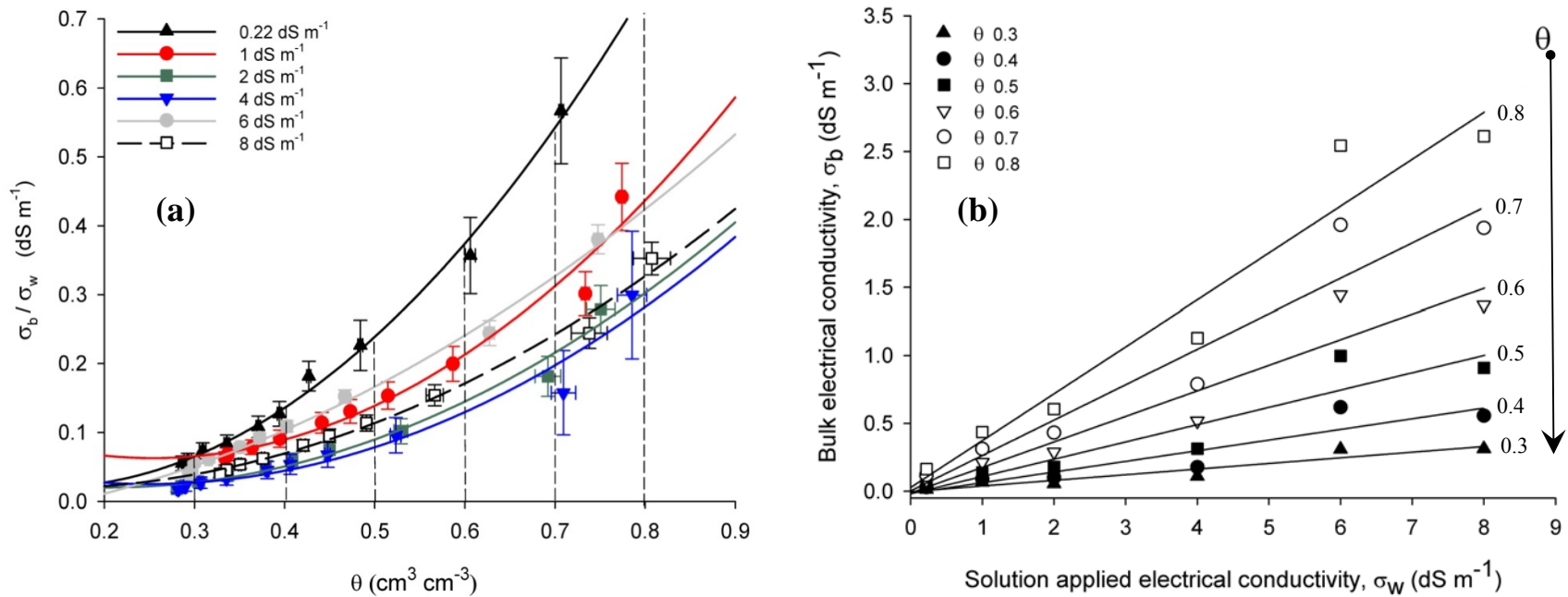


Figure 3.3 a, and b. Normalization of bulk electrical conductivity by volumetric water content (a) with the 5TE sensor. Bulk substrate electrical conductivity divided by leachate electrical conductivity (σ_b / σ_w) vs. volumetric water content (θ) for 80 peat: 20 perlite mix substrate. Error bars indicated as standard error about the mean (SEM). (b) Bulk substrate electrical conductivity after normalization (σ_b) vs. leachate electrical conductivity (σ_w) for various fixed volumetric water content (θ). The average of intercepts with bulk substrate EC (σ_b) axis becomes the offset value (σ_s) according to Rhoades (1976) methodology.

Table 3.3. Regression equations for the ECH₂O-TE sensor depending on the different electrical conductivity solution utilized at each run (Fig. 3.2a) and regression equations for the actual bulk soilless electrical conductivity normalization (Fig. 3.2b), following Rhoades (1976) methodology.

ECH₂O-TE Sensor		
Figure 3.2a		
Solution applied σ_w (dS/m ⁻¹)	Regression equation	r^2
0.22	$\sigma_b/\sigma_w=0.0486+(-0.3745*\theta)+[1.0191*(\theta^2)]$	0.99
1	$\sigma_b/\sigma_w=0.0907+(-0.4566*\theta)+[1.0388*(\theta^2)]$	0.98
2	$\sigma_b/\sigma_w=0.0563+(-0.3287*\theta)+[0.7058*(\theta^2)]$	0.98
4	$\sigma_b/\sigma_w=0.0146+(-0.1121*\theta)+[0.5144*(\theta^2)]$	0.98
6	$\sigma_b/\sigma_w=0.0266+(-0.1860*\theta)+[0.7261*(\theta^2)]$	0.99
8	$\sigma_b/\sigma_w=0.0728+(-0.3833*\theta)+[0.8065*(\theta^2)]$	0.97
Figure 3.2b		
Volumetric water content θ	Regression equation (\bar{y}_0 = offset value)	r^2
0.3	$\sigma_b=(-0.0013)+(0.0306*\sigma_w)$	0.98
0.4	$\sigma_b=(0.0041)+(0.0528*\sigma_w)$	0.95
0.5	$\sigma_b=(0.0076)+(0.0903*\sigma_w)$	0.94
0.6	$\sigma_b=(0.0091)+(0.1430*\sigma_w)$	0.95
0.7	$\sigma_b=(0.0087)+(0.2108*\sigma_w)$	0.96
0.8	$\sigma_b=(-0.0405)+(0.3010*\sigma_w)$	0.97

Table 3.4. Regression equations for the 5TE sensor depending on the different EC solution utilized in each run (Fig. 3.3a) and regression equations for the actual bulk soilless electrical conductivity normalization (Fig. 3.3b), following Rhoades (1976) methodology.

5TE Sensor		
Figure 3.3a		
Solution applied σ_w (dS/m ⁻¹)	Regression equation	r^2
0.22	$\sigma_b/\sigma_w = 0.0489 + (-0.433*\theta) + [1.626*(\theta^2)]$	0.99
1	$\sigma_b/\sigma_w = 0.1436 + (-0.637*\theta) + [1.254*(\theta^2)]$	0.97
2	$\sigma_b/\sigma_w = 0.0532 + (-0.324*\theta) + [0.794*(\theta^2)]$	0.99
4	$\sigma_b/\sigma_w = 0.0775 + (-0.421*\theta) + [0.846*(\theta^2)]$	0.95
6	$\sigma_b/\sigma_w = -0.0351 + (0.118*\theta) + [0.570*(\theta^2)]$	0.99
8	$\sigma_b/\sigma_w = 0.0285 + (-0.167*\theta) + [0.675*(\theta^2)]$	0.99
Figure 3.3b		
Volumetric water content θ	Regression equation (\bar{y}_0 = offset value)	r^2
0.3	$\sigma_b = (-0.0025) + (0.0415*\sigma_w)$	0.90
0.4	$\sigma_b = (-0.0152) + (0.0785*\sigma_w)$	0.86
0.5	$\sigma_b = (-0.0184) + (0.1274*\sigma_w)$	0.87
0.6	$\sigma_b = (-0.0123) + (0.1881*\sigma_w)$	0.90
0.7	$\sigma_b = (0.0031) + (0.2606*\sigma_w)$	0.92
0.8	$\sigma_b = (0.0280) + (0.3450*\sigma_w)$	0.94

Substrate moisture contents (θ) are shown at the right of Figs. 3.2b and 3.3b. From these data, it can be seen that the relationship (σ_b , σ_w) changes as θ changes, so it is important that the model can integrate this variable into the estimation of σ_p . This has an important practical implication as noted by Scoggins and van Iersel (2006). They found that with other EC sensors, an increased inaccuracy when water content measurements fell below a volumetric water content of approximately 35% ($\theta = 0.35$). However, we should note that this volumetric water content equates to a matric potential of -10kPa in this specific substrate (Figs. 3.6, 3.7 and 3.8), which is approximately the upper matric potential threshold for readily-available water in most soilless substrates. It will be necessary to conduct more studies with different soilless substrates to further determine whether these offset values are applicable to other commercial soilless substrates for the real-time measurement of electrical conductivity (Lea-Cox et al., 2008).

Hilhorst (2000) model

Values of ε'_b at the various measured bulk electrical conductivities are shown for the ECH₂O-TE (Fig. 3.4a) and the 5TE sensors (Fig. 3.4b). A greater variation in σ_b at 4 dS m⁻¹ can be seen, especially with the 5TE sensor; this may be related to the much smaller sensing area (= 0.062cm²) of the 5TE sensor screws compared to the surface area of the ECHO-TE sensor (= 2.162 cm²; see Table 3.1). It could also be related to a deficient rinsing of the substrate during preparation of the 4 dS m⁻¹ run. There is an interesting difference between regression lines as shown in Fig. 3.4b where the lower electrical conductivities of the solution applied 0.22, 1, 2, and 4 dS m⁻¹ (σ_w) exhibit an

exponential regression line, in contrast to the linear regression exhibited at 6 and 8 dS m⁻¹. (Nadler, 1981; Nadler and Frenkel, 1980).

Furthermore, it should be noted that the differences in the intercepts (Table 3.5) are considerable, with a range of about 7 ε'_b units for the 5TE sensor. In contrast, the ECH₂O-TE sensor exhibits all linear regressions (Fig. 3.4a), with less variation about the mean with much closer intercepts (Table 3.5) and a difference in range of about 1.7 ε'_b units. The average offset values for $\varepsilon'_{\sigma b=0}$ are 4.614 for the ECH₂O-TE sensor, and 3.959 for 5TE sensor with standard error of the mean equal to 0.288 and 1.230, respectively. These two offsets values deviate slightly from each other, which could be explained in part by the differences between the sensors, with regard to the differences in sensing area and how the two sensors are calibrated (Table 3.1).

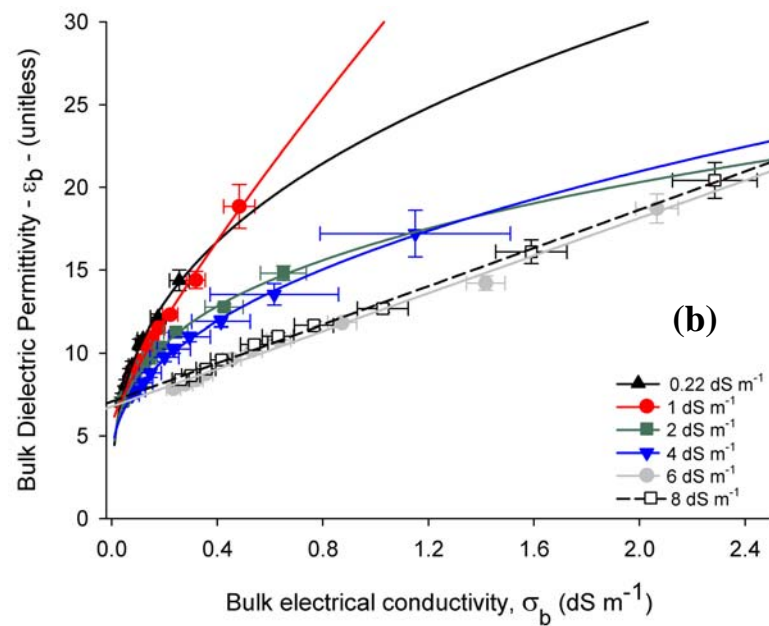
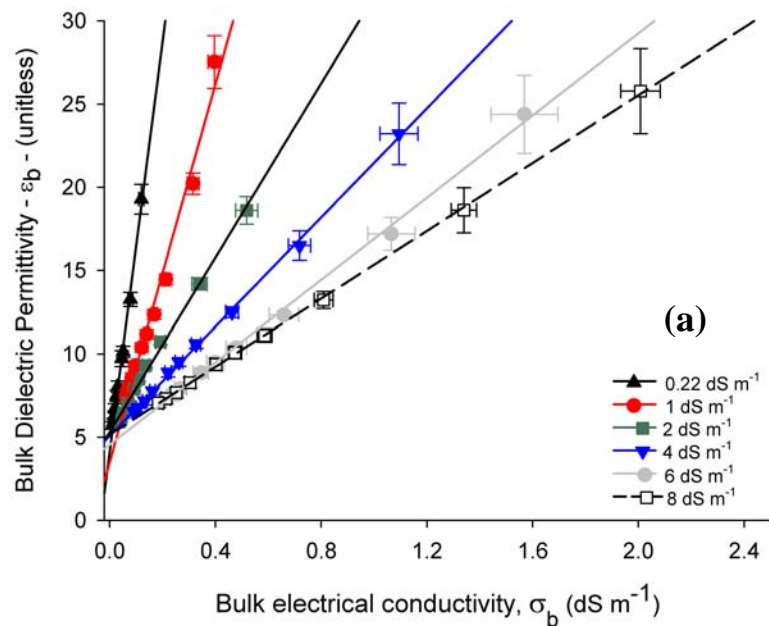


Figure 3.4 a, and b. Offset value determination as outlined by Hilhorst (2000) for **(a)** ECH₂O-TE sensor and **(b)** 5TE sensor. Bulk soilless substrate electrical conductivity (σ_b) vs. bulk soilless substrate dielectric permittivity (ϵ'_b) for 80 peat: 20 perlite mix substrate. Error bars indicated as standard error about the mean (SEM). Intercepts (\bar{y}_0) as $\epsilon'_{\sigma_b=0}$ or offset values.

Table 3.5. Regression equations for the ECH₂O-TE (Fig. 3.4a) and 5TE (Fig. 3.4b) sensors, depending on the different electrical conductivity solution utilized in each run, following Hilhorst (2000) methodology.

ECH2O-TE Sensor		
Figure 3.4a		
Solution applied σ_w (dS/m ⁻¹)	Regression equation ($\bar{y}_0 = \text{offset value}$)	r^2
0.22	$\varepsilon'_b = 4.1166 + [123.174 * (\sigma_b)]$	0.99
1	$\varepsilon'_b = 3.4916 + [56.776 * (\sigma_b)]$	0.98
2	$\varepsilon'_b = 5.3048 + [26.341 * (\sigma_b)]$	0.99
4	$\varepsilon'_b = 5.0764 + [16.394 * (\sigma_b)]$	0.99
6	$\varepsilon'_b = 4.5459 + [12.359 * (\sigma_b)]$	0.99
8	$\varepsilon'_b = 5.1507 + [10.196 * (\sigma_b)]$	0.99

5TE Sensor		
Figure 3.4b		
Solution applied σ_w (dS/m ⁻¹)	Regression equation ($\bar{y}_0 = \text{offset value}$)	r^2
0.22	$\varepsilon'_b = 0.114 + [23.130 * (\sigma_b^{0.362})]$	0.99
1	$\varepsilon'_b = 5.662 + [23.716 * (\sigma_b^{0.828})]$	0.99
2	$\varepsilon'_b = 0.865 + [15.760 * (\sigma_b^{0.303})]$	0.99
4	$\varepsilon'_b = 3.257 + [13.013 * (\sigma_b^{0.444})]$	0.99
6	$\varepsilon'_b = 6.775 + [5.685 * (\sigma_b)]$	0.99
8	$\varepsilon'_b = 7.080 + [5.789 * (\sigma_b)]$	0.99

Greenhouse Study

The estimated pore water electrical conductivities were plotted using the average raw data values recorded by each sensor (ECH₂O-TE and 5TE; n=4) over the dry down period experienced by the *Impatiens* plants. The two models were applied to the raw data, applying the previously calculated offset values for each sensor type (Tables 3.3, 3.4, and 3.5). An offset value of 6 was also plotted for comparison, since this is the offset value recommended by Decagon Devices. Readers should note that the plotted lines in Figs. 3.6, 3.7, and 3.8 are data points taken every minute, which create a solid line. Time is shown on the x-axis as the date when data was recorded. Two y-axes are displayed with the left hand y-axis showing the estimated pore water EC (σ_p) in $\text{dS} \cdot \text{m}^{-1}$ and the right y-axis showing the volumetric water content (θ) in $\text{cm}^3 \cdot \text{cm}^{-3}$. Plots show two sequential dry-down events. The water depletion in the first period from 9/21/08 to 9/25/08 was faster than during the second dry-down period (9/25/08 to 10/02/08). This is explained by higher light and vapor pressure deficits during the first period (data not shown).

From Fig. 3.6, it can be seen how the Hilhorst model greatly overestimates σ_p (using both offset values 4.614 and 6) from saturation (where volumetric water content = 1.00; right hand axis). This pore water electrical conductivity overestimation is even more evident with the 5TE sensor data (Fig. 3.7; offset = 3.959 and Fig. 3.8; offset = 6). The overestimation at saturation was as much as one unit during the first period and somewhat less during the second period. It can also be seen from Figure 3.6 how the Hilhorst model, with either offset value, rises faster than the Rhoades model as the substrate loses moisture. This is explained in part by the differences between the models

and how each model relies on different physical parameters to estimate σ_p . The Hilhorst model relies heavily only on bulk permittivity, bulk electrical conductivity, and permittivity of nearly dry soil (offset, $\varepsilon'_{\sigma_b=0}$).

On the other hand, the Rhoades model takes into account variables such as particle density, bulk density, mobile water, immobile water, surface electrical conductivity (offset, σ_s), and finally bulk electrical conductivity (σ_b), which both models share as a common factor.



Figure 3.5. Greenhouse experimental setup with 32 ‘New Guinea’ *impatiens* planted in 15cm diameter x 10.5cm high containers. Four repetitions of each sensor (ECH₂0-TE and 5TE) were randomly assigned to different containers inside the experimental area with the remaining plants as guard rows

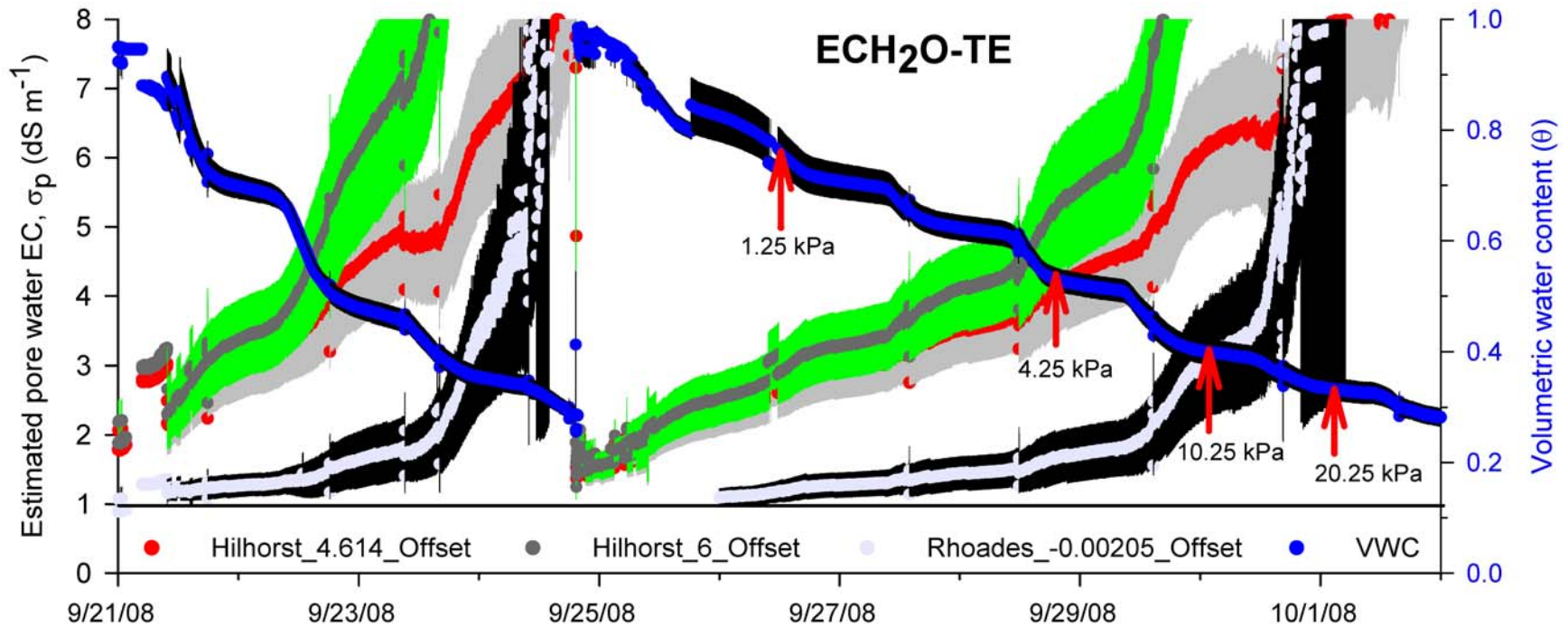


Figure 3.6. Pore water electrical conductivity estimation (σ_p) using ECH₂O-TE sensor with two different offset values (4.614 and 6) when fitting the Hilhorst (2000) model, and an offset value of -0.00205 when fitting Rhoades' (1989) model. Measurements made in Sunshine LC-1 substrate (80 peat : 20 perlite) over 11 days period of drying down and rehydration. Blue line in center of black (SEM) area is actual volumetric water content (θ). Matric potentials (Ψ_m) indicated with red arrows as kPa. Horizontal straight black line indicates the electrical conductivity of the solution applied (1 dS m⁻¹). Light blue line in center of black (SEM) area is Rhoades' σ_p estimate; similarly, the grey and light green colored areas surrounding each Hilhorst model estimate is the standard error about the mean (SEM; n=4 for each line).

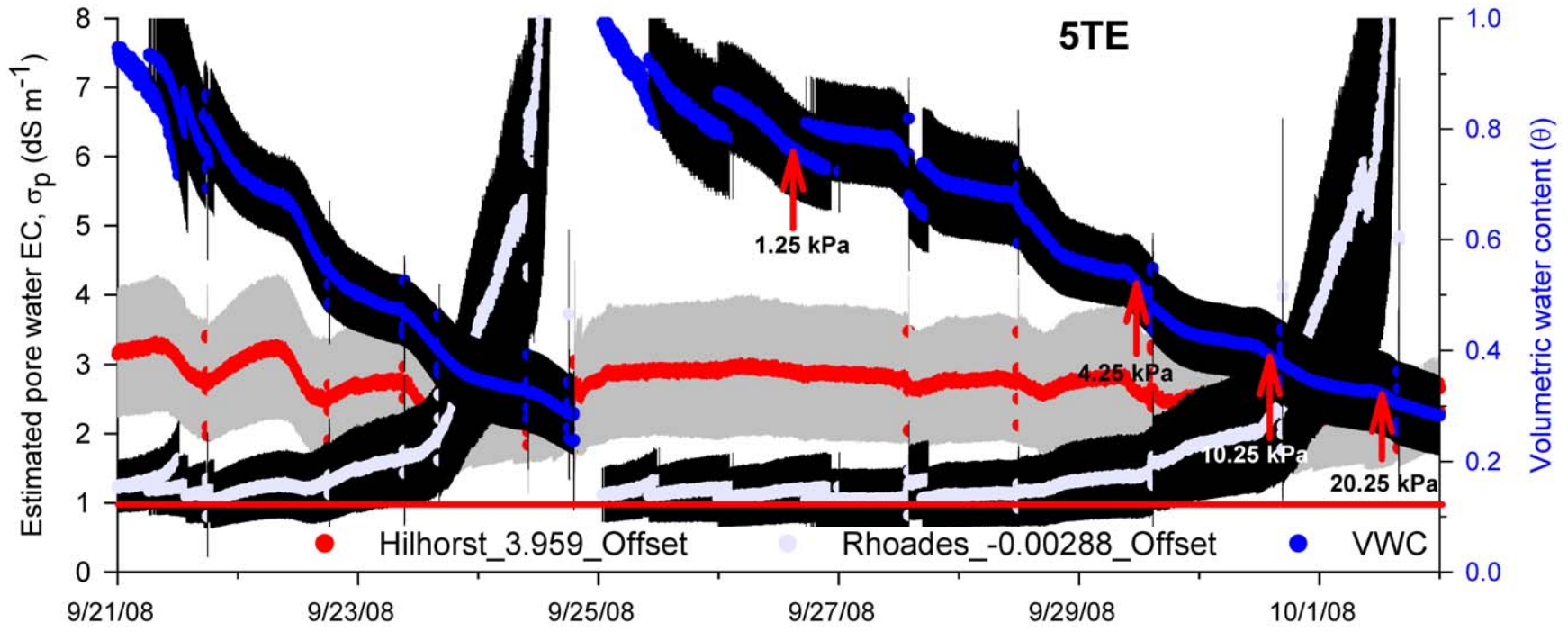


Figure 3.7. Pore water electrical conductivity estimation (σ_p) using 5TE probe with offset value of 3.959 when fitting the Hilhorst (2000) model and an offset value of -0.00288 when fitting the Rhoades' (1989) model. Measurements made in Sunshine LC-1 substrate (80 peat : 20 perlite) over 11 days period of drying down and rehydration. Blue line in center of black (SEM) area is actual volumetric water content (θ). Matric potentials (Ψ_m) indicated with red arrows as kPa. Horizontal straight red line indicates the electrical conductivity of the solution applied (1 dS m^{-1}). Light blue line in center of black (SEM) area is Rhoades' σ_p estimate; similarly, the grey colored area surrounding the Hilhorst model estimate is the standard error about the mean (SEM; $n=4$ for each line).

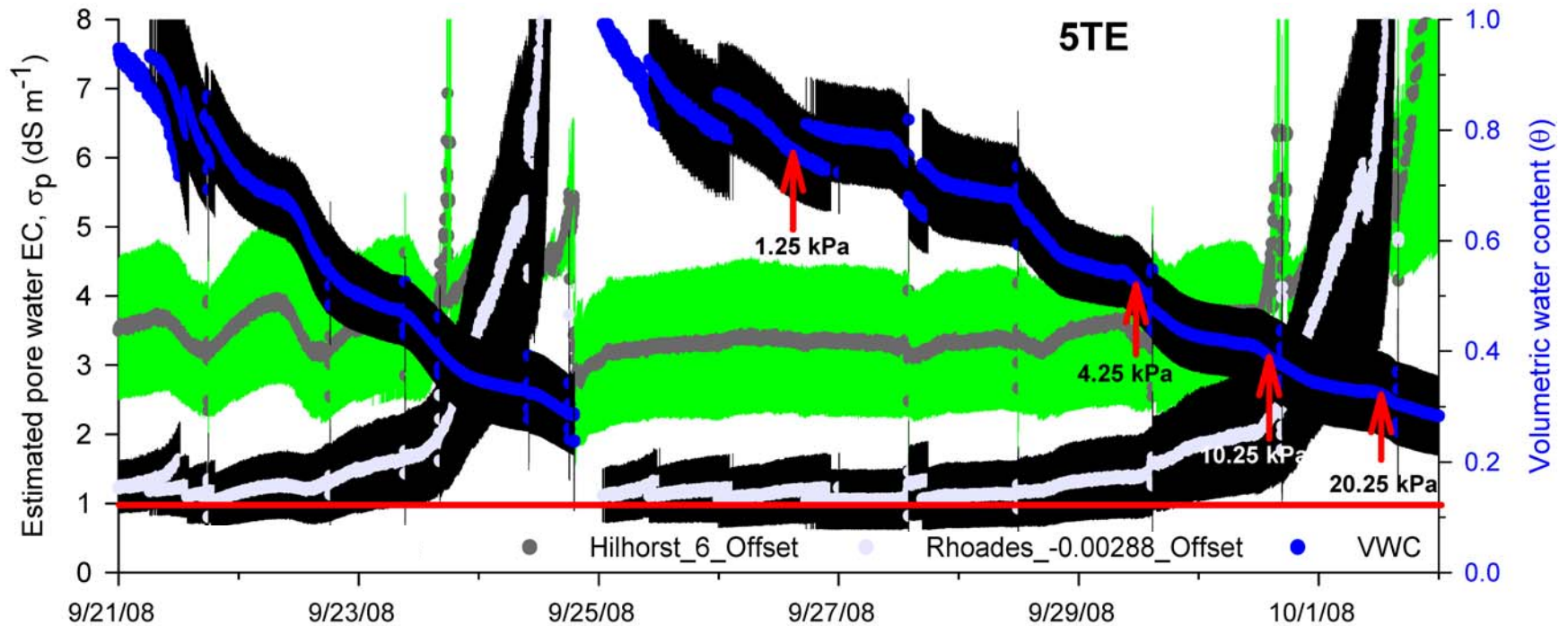


Figure 3.8. Pore water electrical conductivity estimation (σ_p) using 5TE probe with offset value of 6 when fitting the Hilhorst (2000) model and an offset value of -0.00288 when fitting the Rhoades' (1989) model. Measurements made in Sunshine LC-1 substrate (80 peat : 20 perlite) over 11 days period of drying down and rehydration. Blue line in center of black (SEM) area is actual volumetric water content (θ). Matric potentials (Ψ_m) indicated with red arrows as kPa. Horizontal straight red line indicates the electrical conductivity of the solution applied (1 dS m^{-1}). Light blue line in center of black (SEM) area is Rhoades' σ_p estimate; similarly, light green colored area surrounding the Hilhorst model estimate is the standard error about the mean (SEM; $n=4$ for each line).

Examining the Rhoades' model fitted to the ECH₂O-TE data more closely (light blue line surrounded by the black area; Fig.3.6) we can see that this model better approximates the actual value of the σ_w of the applied salt solution ($1 \text{ dS} \cdot \text{m}^{-1}$) over the first 3-4 days of the drawdown period, where the Ψ_m went from 0 to 4.25 kPa (θ from 0 to 0.5). Both models rose very fast after a certain point, as approximated by the data. With the Rhoades model, when θ_w approaches the value of θ_{ws} , the estimated σ_p rises; in the case of the Hilhorst model, when ε'_b approaches the value of $\varepsilon'_{\sigma_b=0}$, the estimated σ_p again rises rapidly.

It is clear after comparing both Hilhorst predicted σ_p values with the ECHO-TE sensor (Fig. 3.6), depending on the offset value used, the predicted σ_p value does not rise as rapidly with the lower offset (4.614) as it does with the higher offset (6). This is explained by examining the model. Since the denominator is essentially the bulk permittivity minus the offset, the larger the offset the smaller the denominator (Eq. 5). This has the result of inflating the data beyond a certain point.

This effect can also be explained by the decreasing change in substrate water content. As the substrate moisture decreases, the bulk permittivity also decreases, becoming smaller and closer to the offset value. We therefore decided to filter the bulk permittivity data, and only use data which was larger than the sum of the calculated offset, plus the standard error about the mean (Cobos, D. 2009; *pers. comm.*). With the ECHO-TE sensor (Fig. 3.6) the offset value of 4.614 determined by this experimentation seemed to yield an estimate that does not go out of scale as fast as the factory recommended value of 6. Finally if we compare standard error values (colored areas

surrounding both model lines), we can see that the Rhoades model has much less variation, i.e., higher precision.

For the 5-TE sensor data, we plotted the Hilhorst σ_p data from the two offset values separately, since the data overlapped on the same scale (Fig. 3.7; offset = 3.959 and Fig 3.8; offset = 6). In Fig. 3.7, the predicted σ_p values remained relatively stable even after θ values had decreased below 0.3. However, we know that the volume of water was reduced by 70% due to evapotranspiration, so it is reasonable to assume that the salts in solution were now more concentrated in the remaining pore water, which makes the predicted σ_p values nonsensical. In contrast, using the 6 offset value (Fig. 3.8) caused an increase of σ_p at low values of θ , as expected. However, this increase was only noticeable after reaching θ values equivalent or greater than -10.25 kPa, in contrast to the expected gradual increase in σ_p as water is depleted. When we compare both Hilhorst plots in Figures 3.7 and 3.8, it is evident that the predicted σ_p stays very stable around 3.5 dS m⁻¹, overestimating the expected initial value of 1 dS • m⁻¹ by over 2.5 times, at least initially.

With the Rhoades data (Fig. 3.6), the predicted σ_p values show much lower variation, in comparison to the high variability of the Hilhorst data (represented by the grey and green colored areas surrounding the estimated σ_p lines). Comparing the ECH₂O-TE data (Fig. 3.6) to the 5-TE data (Figs. 3.7 and 3.8), we can see how this error is reduced, indicating better precision. We hypothesize that this precision is by and large due to the larger sensing surface area of the ECH₂O-TE sensor, compared to the much smaller

sensing surface area of the 5TE sensor, as previously discussed. Consequently, when the 5TE sensor is used in more porous soilless substrates, the small screws might be in or close to an air-filled space in the substrate, which could increase the variability of the data even more than in this dense, peat-based substrate. Note also that this variation might also be offset, in part, by the better (5-point) calibration of the 5-TE sensor, in contrast to the two-point calibration of the ECH₂O-TE sensor (Table 3.1).

Both sensors are subject to the same limitation when bulk EC is close to or lower than 0.01 dS • m⁻¹, due to the low accuracy at the low end of measurements (both sensors have bulk EC resolution equal to 0.01 dS • m⁻¹ from 0 to 7 dS • m⁻¹), thus negatively affecting an accurate estimation of σ_p . A low bulk EC in this range could be affected by low substrate water contents, and/or large substrate particles that would increase the tortuosity of the electrical path. i.e., the conductivity of electricity is reduced by the increasing path-length.

In summary, it appears from these results that the Rhoades model provides a much better estimation of pore water EC (σ_p) with both sensor types. The Hilhorst model did not provide a good estimate of σ_p with either sensor. We believe that the larger surface area of the ECH₂O-TE contributes to better precision, although we speculate that the 5-point calibration of the 5-TE sensor may have contributed to the precision of those results in this study. It will be necessary to conduct further studies for different soilless substrates to determine whether these models and offset values are applicable to other soilless substrates, for the real-time measurement of non-aqueous EC using wireless sensor networks (Lea-Cox et al., 2008). It is evident from this study that

an ideal sensor should combine positive attributes from both tested sensors, which should increase the accuracy and precision of the sensor.

Chapter 4: Summary and Final Remarks

Volumetric Water content /Water matric potential

Although determining desorption (moisture release) curves was originally a soil-based technique, it is also a useful technique to determine the availability of water in soilless substrates. This is because desorption curves provide us with fundamental information about the water-holding characteristics of different substrates. In these studies, we have also established the relationship between substrate volumetric water content (θ) and substrate water potential (Ψ_m). Illustrating the relationship between these two variables gives us insight into plant-available water using an easily related physiological measurement (i.e., Ψ_m), than just a purely physical measurement (i.e., θ) of substrate water content. Furthermore, by utilizing Ψ_m , we can normalize substrate-specific water availability that cannot be achieved by substrate water content, since this availability is due to inherent substrate properties. This has been well illustrated by the calibration results that we have shown for the five substrates that we test. The availability of water at say $\theta = 0.3$ is not the same for 100% pine bark as it is for peat-based substrates. However, a $\Psi_m = 5$ kPa directly relates the amount of water at that tension, between substrates. In addition, we have shown how these two measurements are clearly different in various substrates, since the majority of water in many substrates is beyond what is accepted by many researchers as “easily-available water.” In doing so, we

have calibrated two types of capacitance sensors in the range of substrates with differing physical properties, and have clearly illustrated how these sensors operate in significantly different ranges than in most soils.

The results from Chapter 2 also demonstrate the differences in water holding capacity (WHC) among substrates and container height. In this particular study, substrate mixes containing some amount of peat moss showed the highest WHC, although, with very low levels of air filled porosity (AFP). On the other hand, substrates with low WHC typically had a good AFP. These characteristics can't be assumed as being negative. Different horticultural applications may call for substrates having completely opposite characteristics of WHC and AFP. For example, orchid production requires substrates with higher AFP's, whereas most plug and cutting production requires a substrate mix with high WHC to keep the young roots from desiccating.

We have demonstrated that WHC does not necessarily reflect an exact measure of water availability in these diverse substrates, and clearly illustrated the differences between water distribution (EAW, WBC and PUW). These fractions delineate plant-available water into significant subdivisions, depending on how tightly that water is bound to the substrate matrix, expressed as matric potential (Ψ_m). We found that much of the water can be tightly bound to the substrate as in the case of 100% perlite. This substrate has a low container capacity, but also the highest percentage PUW in containers of 20-cm height. In practice, if we don't have tools to accurately measure plant-available water, then we cannot hope to achieve more precise irrigation scheduling. The consequence of this is that growers can easily over- or under-irrigate crops when merely estimating the water content of a container by more subjective methods. Our studies

have calibrated the response of these sensors to these very small changes in available water for five specific substrates. From our results, we are confident that capacitance sensors provide accurate and precise data that can be utilized to schedule irrigations at these very low tensions (i.e. EAW = 0 to -5 kPa), where water is most freely available to the plant.

It is important to note that with the methodology applied in this experiment, we were able to determine water content differently from the standard computational method. The conventional method for estimating water quantity is to use volumetric water content (θ ; VWC), which is done by dividing the volume of water present in the sample by the total volume of the container holding the sample. This standard procedure yields a volumetric unit of measurement (i.e. $\text{cm}^3 \cdot \text{cm}^{-3}$ or $\text{m}^3 \cdot \text{m}^{-3}$). In contrast, since we measured the container capacity (CC) of each substrate, we calculated VWC using this variable. We directly compared the differences between these two measurements in one substrate, and considered the implications of using CC values to normalize the data as an alternative to total container volume (App. Figs. B9a and B10a). With substrates with high WHC (e.g. 80% peat : 20% perlite; App. B9), the calibration constants changed slightly, but not significantly. In contrast, substrates with very low WHC (such as 100% perlite; App. Fig. B10), the calibration constants were significantly different, resulting in better precision of the fitted data ($r^2 = 0.29$ vs. 0.38). We feel this issue needs further scrutiny and analysis, since this could well explain some of the known anomalies in VWC with substrates such as perlite.

Soil moisture sensors are not a recent invention, but few perform well enough to give accurate real-time estimates of plant-available water and electrical conductivity. The

nursery and greenhouse industry utilize many different substrates to grow plants, and component materials are chosen based on particular chemical and physical parameters. One of those physical parameters that has previously limited the effectiveness of soil moisture sensors such as tensiometers is substrate particle size and pore size. Since excessive water can be retained when utilizing small particle-size substrates, the addition of components with larger particle sizes create larger-sized macropores; consequently these substrates are well drained and better adapted for use in container production. Substrate porosity is the main reason why most soil moisture sensors have failed when used in soilless substrates.

We have demonstrated that Decagon capacitance high frequency root-zone sensors have good precision in a range of soilless substrates, which will enable us to make significant progress in accurately scheduling irrigation events, in comparison to the more subjective methods that are typically used by most growers. Precision irrigation scheduling is the most effective way to reduce excessive irrigation applications, and nutrient leaching and runoff. Scheduling precise irrigation applications may sound very simple, but due to the lack of a reliable measure of plant-available water, that simple goal has not been possible in container production, until now.

Our work has also confirmed some of the limitations of these capacitance sensors. The interaction of substrate sampling volume, sensor length and sensor operational frequency has an interesting effect on performance. The larger sensor EC-20 (20 cm) tested gave good performance in laboratory measurements of volumetric water content despite its small sampling volume on either side of the blade, due to its low frequency. This small lateral sampling volume was compensated by a much larger integrated area

along the sensor blade, which increased the precision of substrate water measurements. However, since it has a low operational frequency (6 MHz), the sensor readings are known to be less reliable even in low salinity ($> 1 \text{ dS} \cdot \text{m}^{-1}$). This makes the EC-20 less suitable for most container-production situations, since slow-release fertilizers are often used. This is why we are now testing the new Decagon 10-HS sensor, which operates at a higher frequency. The short EC-5 (5cm) sensors we tested also have a higher operational frequency (70MHz), which makes them less sensitive to increasing EC, apparently up to $8 \cdot \text{dS} \cdot \text{m}^{-1}$. This makes it better suited to container-production environments, with the added advantage that they can be used in relatively small containers (e.g. in greenhouse production), where larger sensors may not fit.

One subject that needs to be addressed by further experimentation is sensor placement. It is highly likely that sensor placement could greatly increase sensor data repeatability and accuracy under field conditions. There are many variables to consider, including sensor placement inside the container (i.e. sensing the top, middle or bottom sections of the container) for best repeatability over time. A related issue at a larger scale, is sensor placement within a production block or in very large containers (e.g. directly under an overhead sprinkler, spray emitter, or dripper or where known dry-edge effects occur). Thus, laboratory sensor calibration is an essential step towards fine tuning a sensor, but placement of that sensor will depend on individual characteristics of production systems, which need to be better defined.

Another possible interaction which could bias sensor readings is the proximity of the sensor to roots and the root density in the container. Capacitance sensors likely sense the water contained within roots, as well as external to roots. The water of interest is the

available water outside the root, so the presence or absence of roots may have a significant effect over time on how sensor readings accurately measure available water in the substrate. Since the sensor does not discriminate between water inside or outside the root, which could lead to crops being under-irrigated. We also know that substrate bulk density is also a factor, which interacts with water determinations (data not shown). Briefly, this interaction can be described as a shift of the data to the right or left had on the x-axis of (mV , θ) calibration plots (Figs. 2.3b, 2.4b; App. Figs. B1b to B8b). In summary, the shape or distribution of the curve is not changed, but merely moves to either the right (sample with higher bulk density) or left (sample with lower bulk density). This has a practical effect on sensor calibrations. During calibration, homogeneously packed substrates between columns would increase the repeatability of water content determination, as we showed. Thus, the more similar the substrate bulk density is between laboratory calibration conditions and those within the containers in the nursery, the more accurate the calibrations, and *vice versa*. So, further experimentation should perform a sensitivity analysis of the calibration equations under varying bulk density conditions. To better understand all these interactions, further research should focus on analyzing placement inside a container, which can be combined with modeling the water movement through the container depending on irrigation method, substrate porosity and bulk density, container size and/or shape and increasing plant root density, over time.

Pore water electrical conductivity

After irrigation, fertilization is the major cultural practice that maximizes plant growth rates. Irrigation water and nutrients are supplied by several methods by nursery and greenhouse operations. Providing enough water to plants without leaching nutrients is a challenge. Accurately measuring nutrient availability is time-consuming and high cost operation for many growers. One of the first recommended “best management practice” (BMP) techniques was the Virginia Tech pour-through technique (Wright, 1983 and 1986). This technique provides a measure of total salt concentration in the substrate pore water solution, by measuring EC. This is done by saturating the substrate (i.e. by irrigation) and then collecting a leachate sample after the contained nutrient salts equilibrate for an hour or two. In practice, this technique is time consuming and very laborious which is why it is no often practiced by growers. Also, not all the elements equilibrate uniformly with the pore water. This means that the EC inside the substrate could be different from what is leached. For this reason it would be more preferable to estimate pore water EC using an *in situ* measurement (σ_p), rather than using a leachate fraction EC (σ_w).

Our interest is in using non aqueous (substrate) EC sensors, since these tools offer a more versatile and very efficient way to measure EC concentrations in the root-zone. We calibrated two different sensors ECH₂O-TE (no longer in commercial production) and the 5TE, again using the desorption table, and saturating the substrate with increasing EC solutions between test runs. This process was used to obtain the data needed for two

different models to predict pore water electrical conductivity (σ_p). It is important to keep in mind that both models were originally developed for use in soils.

We found that the Rhoades' model (1989) provided a more accurate measure of EC over a large range of substrate moisture availability when fitted to an empirical greenhouse dataset, in contrast to the Hilhorst model, which effectively gave inaccurate results with both sensors. We showed that the Rhoades model estimated σ_p very well. The offset used with this model was determined by this experimentation, with good results. The Rhoades model takes into account a wider range of variables that influence σ_p . It should be said that from the six parameters (ρ_b , ρ_s , θ_w , θ_{ws} , σ_s , σ_b) needed to apply the Rhoades' model, two are measured (σ_b) or estimated (θ_w) through calibration, making them readily available. Another two (ρ_b , ρ_s) are easily determined in the field or in the laboratory, and the last two (θ_{ws} , σ_s) can be determined by estimations described and summarized by Rhoades et al. (1999). Most importantly, all of this information could be easily integrated into the sensor firmware and/or the data management software, similar to what Decagon Devices currently allows, with specific calibration inputs in their DataTrac™ software. Specific offsets could be inputted by the user, and the software output would automatically integrate the two variables read by the EC sensor, to give the estimated pore water EC as an output, based on the set parameters.

We observed a large variation in the Hilhorst model data with both sensors, (expressed by the standard error about the mean; Figs. 3.7 and 3.8). The ECH₂O-TE sensor response showed that the predicted pore water EC was initially close to the EC of the supplied solution, but then rose very quickly after a specific point. In contrast, the

response of the 5TE sensor showed a more stable predicted pore water EC value using the Hilhorst model, paralleling the EC of the supplied solution until the bulk permittivity was much reduced. At this point, the predicted pore water EC rose quickly, as bulk permittivity decreased due to low water content. The positive aspect of the Hilhorst model is that it does not require many variables. The only substrate-specific variable is the offset value; the other inputs are all measured by the sensor. For this reason, the Hilhorst model is more easily applied, in practice.

Our work on calibrating the substrate EC root-zone sensors illustrates good progress towards providing a solution to the dilemma of trying to monitor real-time EC in non-aqueous environments. However, further work needs to be done, both on improving the performance of the sensor, and perhaps by applying the Rhoades model. Once a sensor is available that can reliably measure EC within a wider range of substrate moisture contents, our ability to measure this important production metric will enable the industry to better understand daily and seasonal nutrient dynamics. Multiple sensors can cover a large area when combined with datalogger and wireless communication devices, which would greatly enhance our daily nutrient management decisions. This capability will enhance production efficiency, by increasing the efficiency of irrigation and fertilizer applications, which in turn would increase profitability, by reducing our use of resources and the impact of nursery and greenhouse on the environment.

Appendices

Appendix A. 1

CR10X Campbell Scientific Datalogger Program used with the EC-5 sensor

* This is an example of program used for the calibration EC-5 sensor. It is not intended to be an absolute guide. Note the excitation voltage was adjusted to 3 volts with multiplier equal to one, and an offset adjusted to zero in order to obtain raw output values.

```
};CR10X
;EC-5_Program.DLD
;Created by Short Cut (2.6)
;$
;:BattV      :ProgSig  :VW_1
;VW_2        :VW_3
;:VW_4        :VW_5      :VW_6
;VW_7        :VW_8
;:VW_9        :VW_10
;$
;
;:Final Storage Label File
for: EC-5_Program.SCW
;Date: 10/7/2009
;Time: 21:10:46
;
;101 Output_Table 1.00 Min
;1 101 L
;2 Year_RTM L
;3 Day_RTM L
;4 Hour_Minute_RTM L
;5 BattV_AVG L
;
;102 Output_Table 1440.00 Min
;1 102 L
;2 Year_RTM L
;3 Day_RTM L
;4 Hour_Minute_RTM L
;5 BattV_MIN L
;6 ProgSig L
;
;Estimated final storage
locations used per day:
7206
;%
```

MODE 1
SCAN RATE 10.0000
1:P10
1:1
2:P92
1:0
2:1440
3:30
3:P19
1:2
4:P95
5:P86
1:42
6:P22
1:1
2:0
3:15
4:0
7:P87
1:0
2:3
8:P90
1:3
9:P86
1:71
10:P22
1:1

2:0	
3:1	
4:0	
11:P4	
1:3	
2:5	
3:1	
4:1	
5:1	
6:3000	
7:3--	
8:1	
9:0	
12:P95	
13:P86	
1:71	
14:P22	
1:1	
2:0	
3:1	
4:0	
15:P4	
1:1	
2:5	
3:1	
4:1	
5:1	
6:3000	
7:12	
8:1	
9:0	
16:P86	
1:52	
17:P22	
1:1	
2:0	
3:15	
4:0	
18:P92	
1:0	
2:1	
3:10	
	19:P80
	1:1
	2:101
	20:P77
	1:1220
	21:P71
	1:1
	2:1
	22:P92
	1:0
	2:1440
	3:10
	23:P80
	1:1
	2:102
	24:P77
	1:1220
	25:P74
	1:1
	2:0
	3:1
	26:P70
	1:1
	2:2
	MODE 2
	SCAN RATE 10.0000
	1:P96
	1:71
	MODE 3
	MODE 10
	1:28
	2:107
	3:0
	MODE 12
	1:0000
	2:0000
	3:0000

Appendix A. 2

CR10X Campbell Scientific Datalogger Program used with the EC-20 sensor

* This is an example of program used for the calibration EC-20 sensor. It is not intended to be an absolute guide. Note the excitation voltage was adjusted to 3 volts with multiplier equal to one, and an offset adjusted to zero in order to obtain raw output values.

```
};CR10X
;EC-20_Program.DLD                2:P92
;Created by Short Cut (2.6)        1:0
;                                  2:1440
;:BattV      :ProgSig  :VW_1      3:30
;VW_2        :VW_3
;:VW_4        :VW_5      :VW_6      3:P19
;VW_7        :VW_8      1:2
;:VW_9        :VW_10
;                                  4:P95

;%                                  5:P86
;Final Storage Label File         1:42
for: EC-20_Program.SCW
;Date: 10/7/2009                  6:P22
;Time: 21:26:13                   1:1
;                                  2:0
;101 Output_Table 1.00 Min         3:15
;1 101 L                           4:0
;2 Year_RTM L
;3 Day_RTM L                        7:P87
;4 Hour_Minute_RTM L              1:0
;5 BattV_AVG L                    2:3
;
;102 Output_Table 1440.00 Min      8:P90
;1 102 L                           1:3
;2 Year_RTM L
;3 Day_RTM L                        9:P86
;4 Hour_Minute_RTM L              1:71
;5 BattV_MIN L
;6 ProgSig L                      10:P22
;                                  1:1
;Estimated final storage          2:0
locations used per day:           3:1
7206                             4:0
;%                                  11:P4

MODE 1                            1:3
SCAN RATE 10.0000                 2:5
                                   3:1
1:P10                              4:1
1:1                                5:1
```

6:3000
7:3--
8:1
9:0

12:P95

13:P86
1:71

14:P22
1:1
2:0
3:1
4:0

15:P4
1:1
2:5
3:1
4:1
5:1
6:3000
7:12
8:1
9:0

16:P86
1:52

17:P22
1:1
2:0
3:15
4:0

18:P92
1:0
2:1
3:10

19:P80
1:1
2:101

20:P77
1:1220

21:P71
1:1
2:1

22:P92
1:0
2:1440
3:10

23:P80
1:1
2:102

24:P77
1:1220

25:P74
1:1
2:0
3:1

26:P70
1:1
2:2

MODE 2
SCAN RATE 10.0000
1:P96
1:71

MODE 3

MODE 10
1:28
2:107
3:0

MODE 12
1:0000
2:0000
3:0000

Appendix A. 3

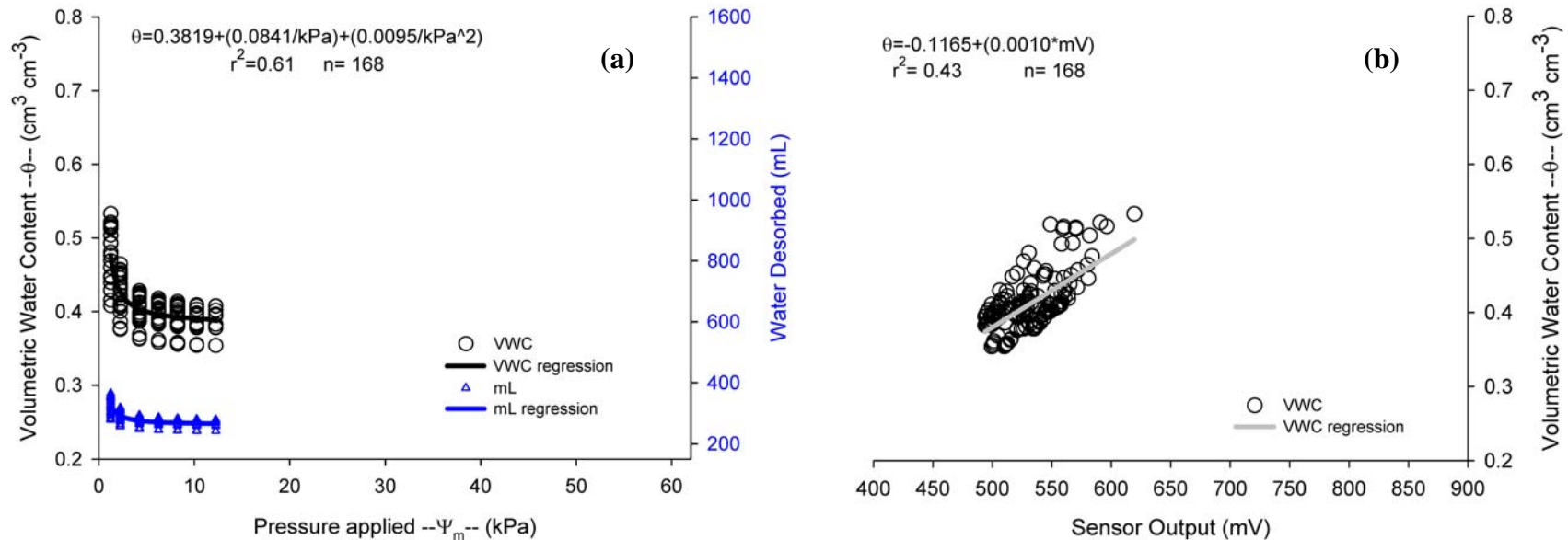
CR10X Campbell Scientific Datalogger Program used with the ECH2O-TE and 5TE sensors

* This is an example of program used for the calibration ECH2O-TE and 5TE sensors. It is not intended to be an absolute guide. Note the excitation voltage was adjusted to 12 volts with multiplier equal to one, and an offset adjusted to zero in order to obtain raw output values.

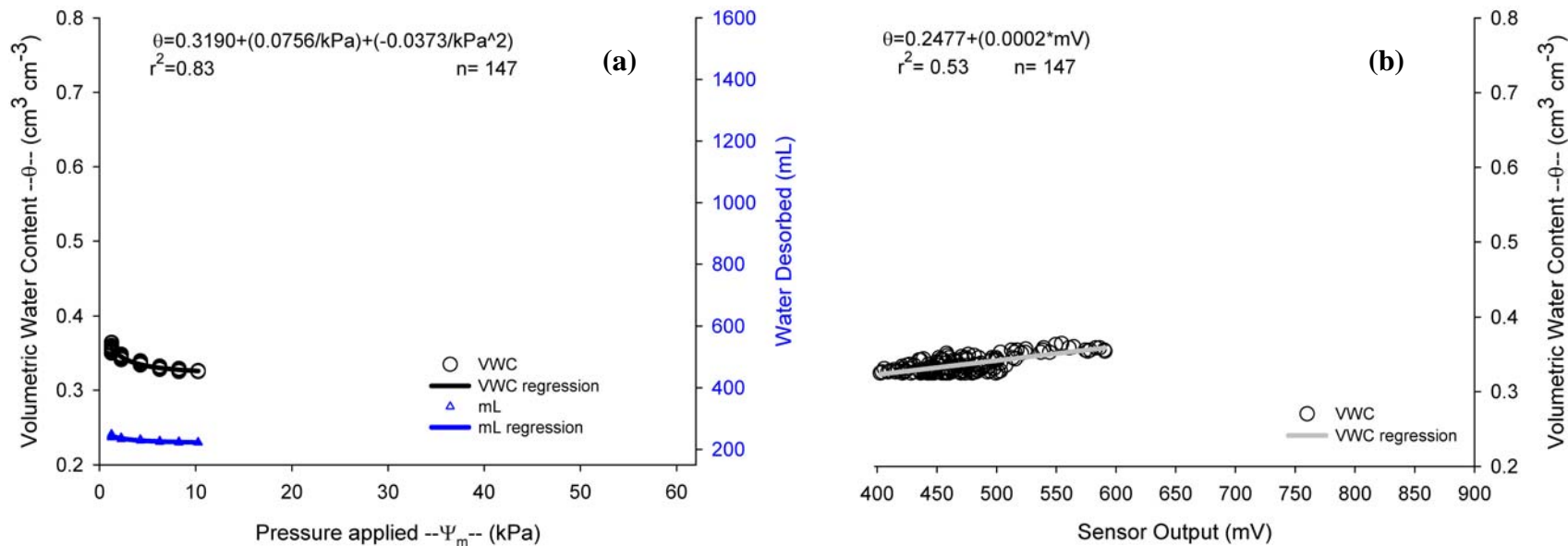
};CR10X	8:50
MODE 1	9:50
SCAN RATE 20	10:3--
1:P10	11:1
1:1	12:0
2:P92	11:P86
1:0	1:53
2:1440	
3:30	12:P95
3:P19	13:P86
1:2	1:51
4:P95	14:P92
	1:0
5:P86	2:1
1:41	3:10
6:P87	15:P80
1:0	1:1
2:10	2:101
7:P86	16:P77
1:72	1:1220
8:P90	17:P71
1:3	1:1
	2:1
9:P86	18:P70
1:43	1:32
10:P15	2:3
1:1	
2:0	19:P86
3:0	1:20
4:40	
5:3	20:P92
6:0	1:0
7:13	2:1440

3:10	5:2048
21:P80	MODE 12
1:1	1:0
2:102	1:0
	1:0
22:P77	
1:1220	MODE 13
	13:8
23:P74	8:0
1:1	
2:0	MODE 13
3:1	13:9
	9:0
24:P86	
1:20	MODE 13
	13:10
25:P0	10:0
MODE 2	MODE 13
SCAN RATE 10	13:13
1:P96	13:0
1:71	
	MODE 11
2:P0	1:59082
	2:9893
MODE 3	3:256
1:P0	4:0
	5:0
MODE 10	6:9801
1:32	7:21
2:64	8:3.0726
3:0	9:99
4:62272	10:0
11:0	

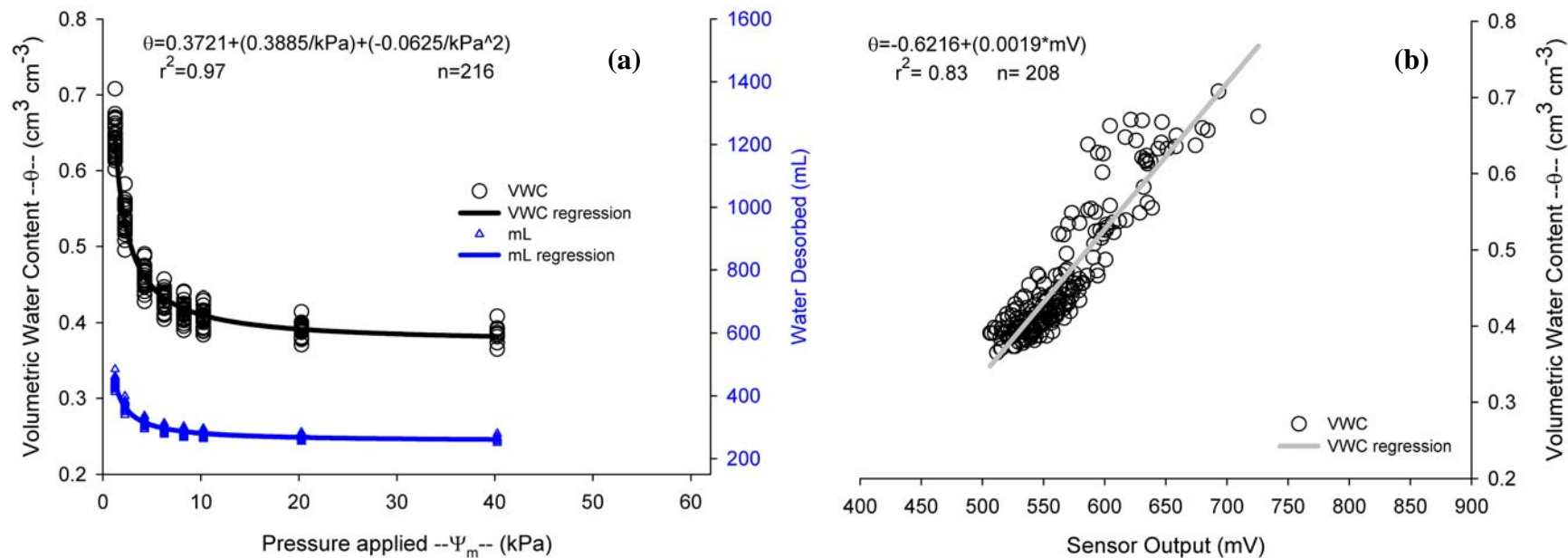
Appendix B



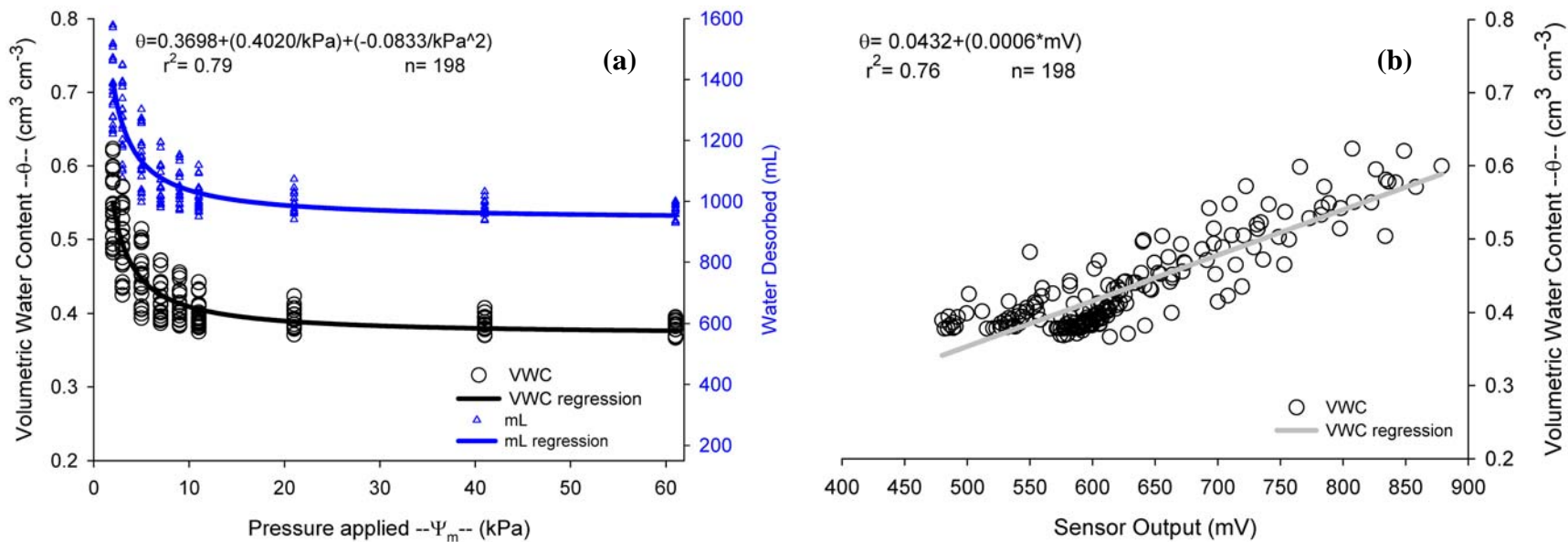
Appendix Fig. B1 a, b. Standard (a) moisture release curve for 5 cm height columns testing **100% pine bark** with pressure applied in kilopascals, left hand 'y' axis as volumetric water content θ (VWC), right hand 'y' axis as actual water volume desorbed from the columns throughout the desorption run. Both regression lines are plotted to follow the trend for both axes. Correlation coefficient (r^2) is shown for VWC regression equation depending on matric potential (Ψ_m) and data point count (n). **EC-5** probe volumetric water content calibration (b) with probe output as millivolt on the abscissa and VWC on the ordinate. Correlation coefficient (r^2) is shown for VWC probe calibration equation and data point count (n).



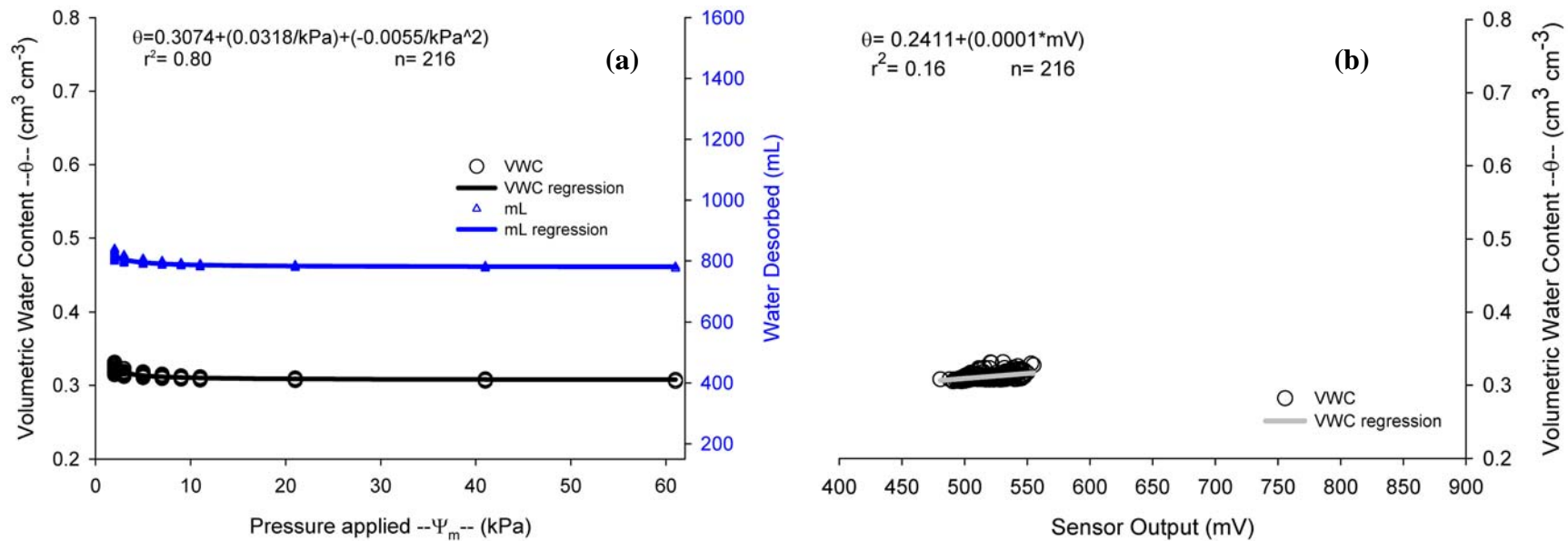
Appendix Fig. B2 a, b. Standard (a) moisture release curve for 5 cm height columns testing **100% coconut fiber (Coir)** with pressure applied in kilopascals, left had 'y' axis as volumetric water content -- θ -- (VWC), right hand 'y' axis as actual water volume desorbed from the columns throughout the desorption run. Both regression lines are plotted to follow the trend for both axes. Correlation coefficient (r^2) is shown for VWC regression equation depending on matric potential (Ψ_m) and data point count (n). **EC-5** probe volumetric water content calibration (b) with probe output as millivolt on the abscissa and VWC on the ordinate. Correlation coefficient (r^2) is shown for VWC probe calibration equation and data point count (n).



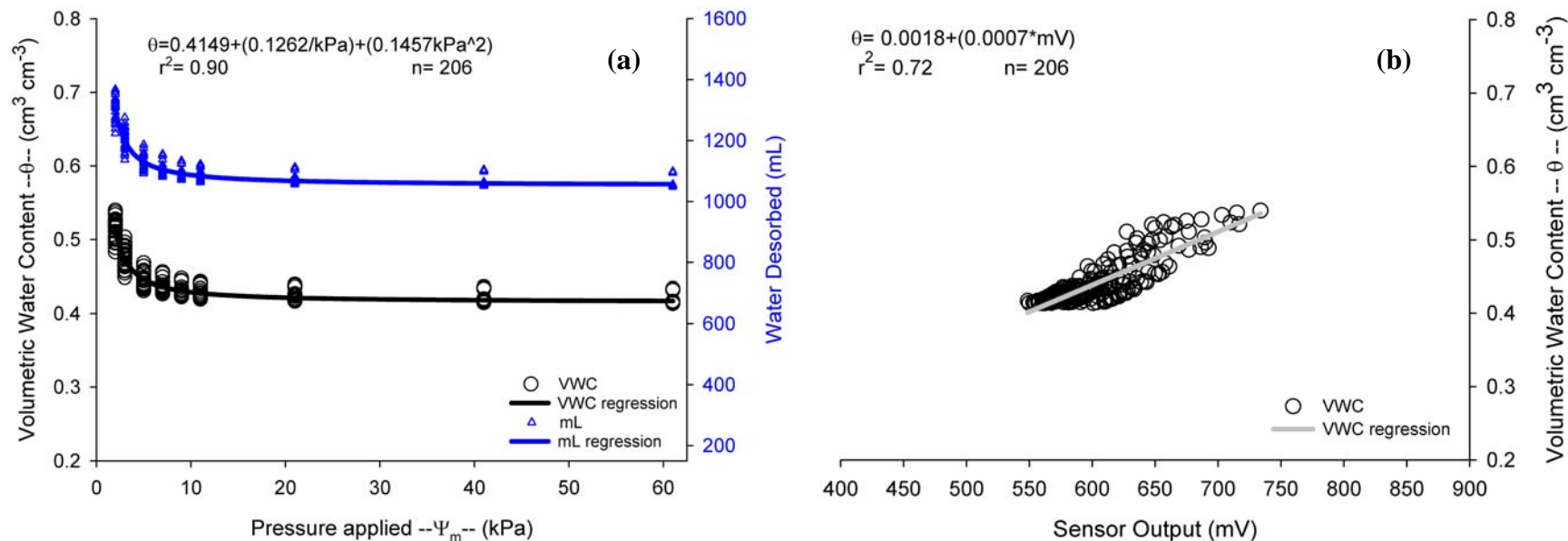
Appendix Fig. B3 a, b. Standard (a) moisture release curve for 5 cm height columns testing **80 pine bark : 20 peat moss mix**, with pressure applied in kilopascals, left had ‘y’ axis as volumetric water content θ (VWC), right hand ‘y’ axis as actual water volume desorbed from the columns throughout the desorption run. Both regression lines are plotted to follow the trend for both axes. Correlation coefficient (r^2) is shown for VWC regression equation depending on matric potential (Ψ_m) and data point count (n). **EC-5** probe volumetric water content calibration (b) with probe output as millivolt on the abscissa and VWC on the ordinate. Correlation coefficient (r^2) is shown for VWC probe calibration equation and data point count (n).



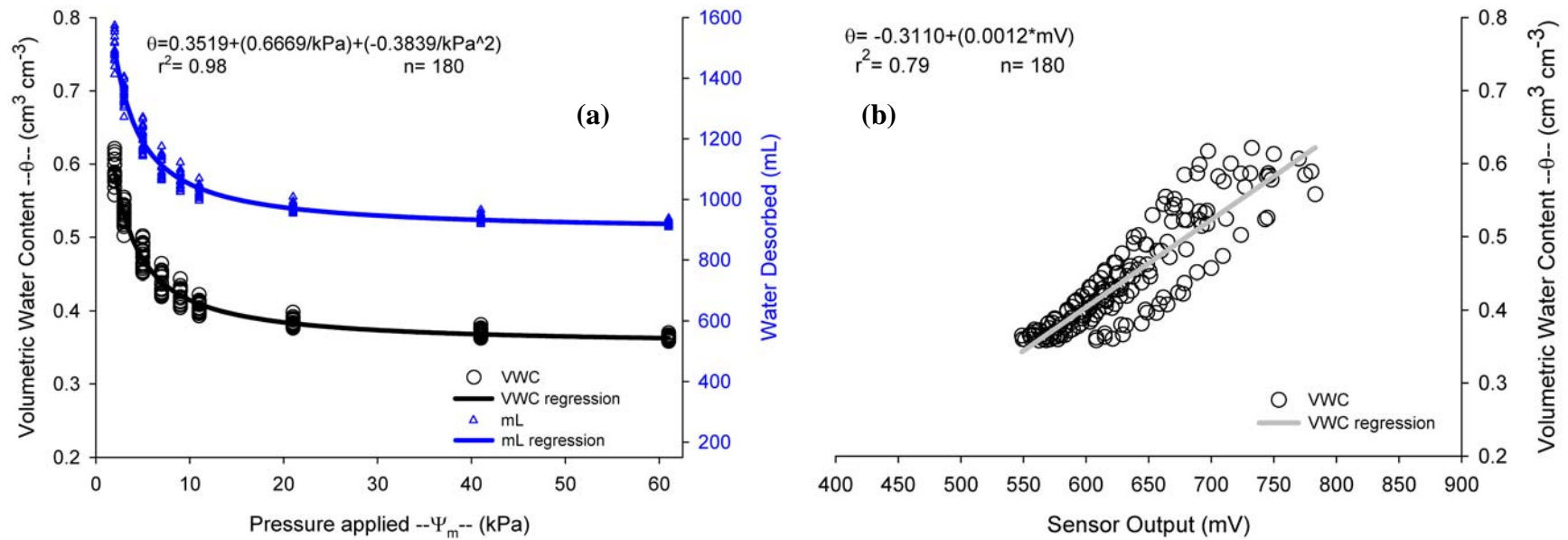
Appendix Fig. B4 a, b. Standard (a) moisture release curve for 20 cm height columns testing **100% pine bark**, with pressure applied in kilopascals, left hand ‘y’ axis as volumetric water content -- θ -- (VWC), right hand ‘y’ axis as actual water volume desorbed from the columns throughout the desorption run. Both regression lines are plotted to follow the trend for both axes. Correlation coefficient (r^2) is shown for VWC regression equation depending on matric potential (Ψ_m) and data point count (n). **EC-20** probe volumetric water content calibration (b) with probe output as millivolt on the abscissa and VWC on the ordinate. Correlation coefficient (r^2) is shown for VWC probe calibration equation and data point count (n).



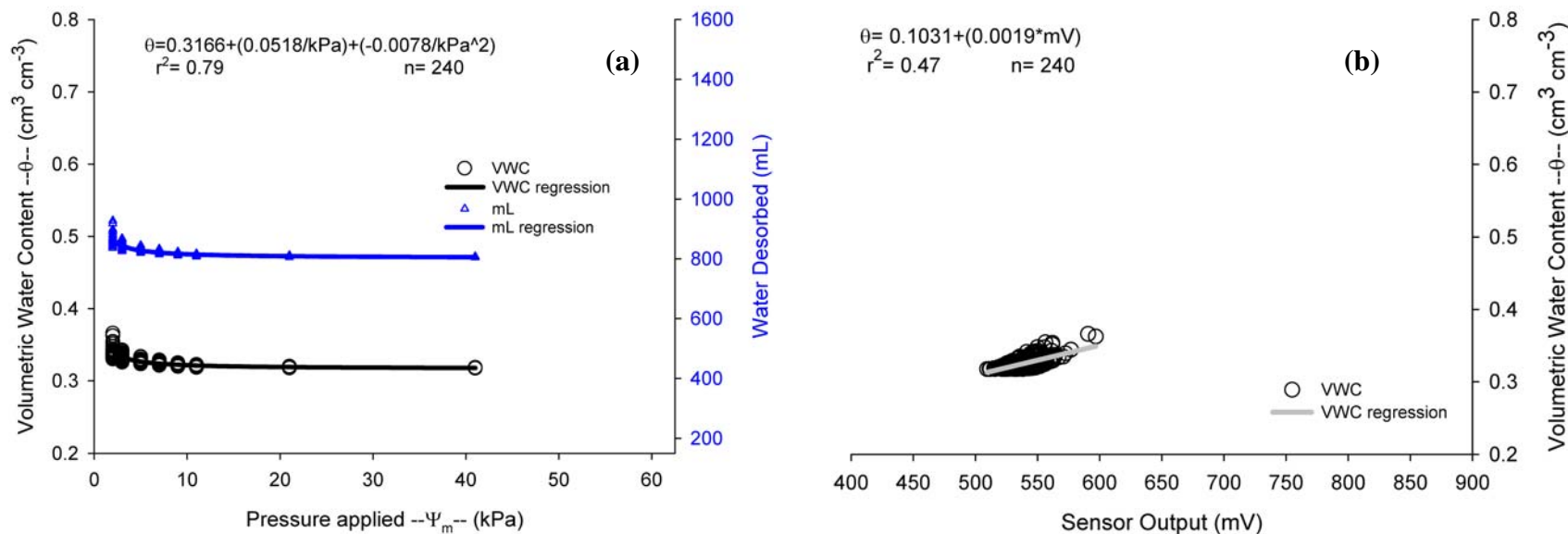
Appendix Fig. B5 a, b. Standard (a) moisture release curve for 20 cm height columns testing **100% coconut fiber** (coir) with pressure applied in kilopascals, left had 'y' axis as volumetric water content -- θ -- (VWC), right hand 'y' axis as actual water volume desorbed from the columns throughout the desorption run. Both regression lines are plotted to follow the trend for both axes. Correlation coefficient (r^2) is shown for VWC regression equation depending on matric potential (Ψ_m) and data point count (n). **EC-20** probe volumetric water content calibration (b) with probe output as millivolt on the abscissa and VWC on the ordinate. Correlation coefficient (r^2) is shown for VWC probe calibration equation and data point count (n).



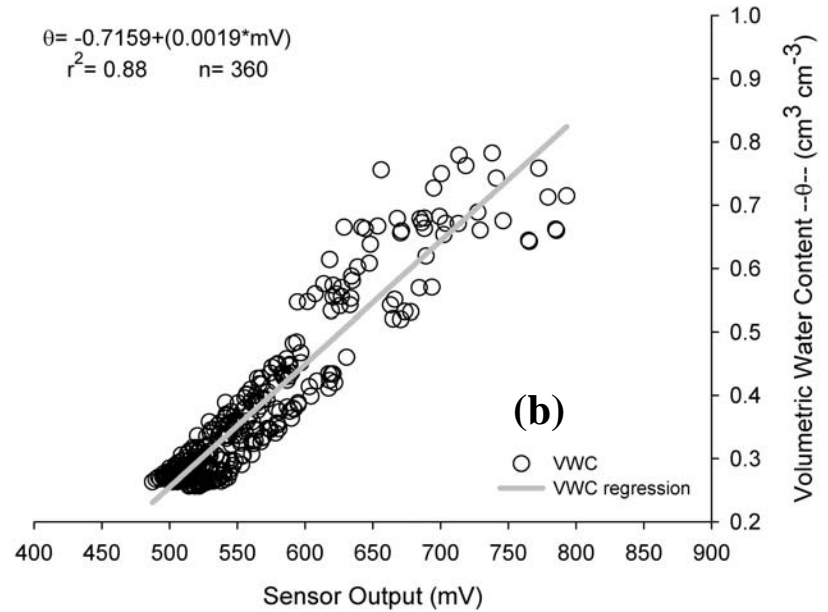
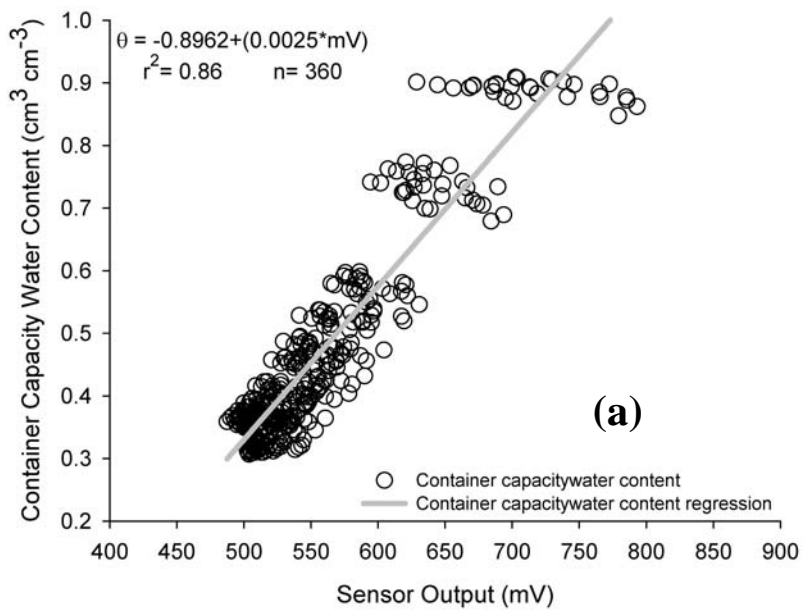
Appendix Fig. B6 a, b. Standard (a) moisture release curve for 20 cm height columns testing **80 pine bark : 20 peat moss mix**, with pressure applied in kilopascals, left had 'y' axis as volumetric water content -- θ -- (VWC), right hand 'y' axis as actual water volume desorbed from the columns throughout the desorption run. Both regression lines are plotted to follow the trend for both axes. Correlation coefficient (r^2) is shown for VWC regression equation depending on matric potential (Ψ_m) and data point count (n). **EC-20** probe volumetric water content calibration (b) with probe output as millivolt on the abscissa and VWC on the ordinate. Correlation coefficient (r^2) is shown for VWC probe calibration equation and data point count (n).



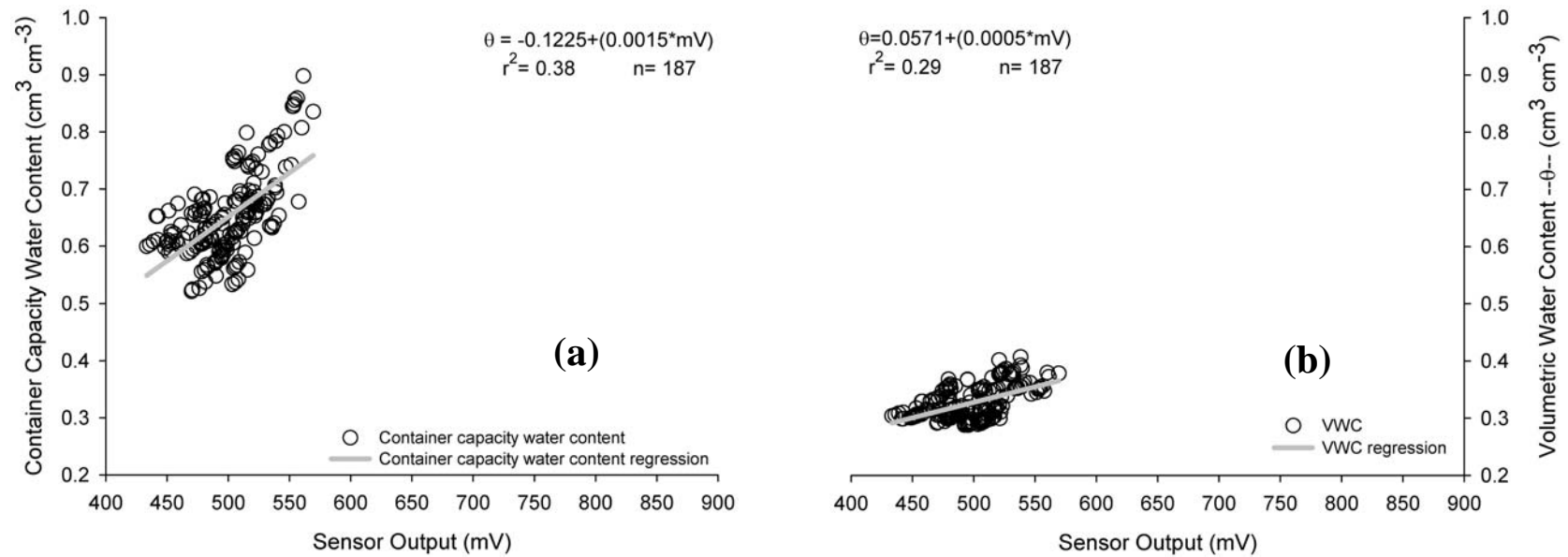
Appendix Fig. B7 a, b. Standard (a) moisture release curve for 20 cm height columns testing **80 peat moss : 20 perlite mix**, with pressure applied in kilopascals, left had 'y' axis as volumetric water content -- θ -- (VWC), right hand 'y' axis as actual water volume desorbed from the columns throughout the desorption run. Both regression lines are plotted to follow the trend for both axes. Correlation coefficient (r^2) is shown for VWC regression equation depending on matric potential (Ψ_m) and data point count (n). **EC-20** probe volumetric water content calibration (b) with probe output as millivolt on the abscissa and VWC on the ordinate. Correlation coefficient (r^2) is shown for VWC probe calibration equation and data point count (n).



Appendix Fig. B8 a, b. Standard (a) moisture release curve for 20 cm height columns testing **100% perlite**, with pressure applied in kilopascals, left hand ‘y’ axis as volumetric water content θ (VWC), right hand ‘y’ axis as actual water volume desorbed from the columns throughout the desorption run. Both regression lines are plotted to follow the trend for both axes. Correlation coefficient (r^2) is shown for VWC regression equation depending on matric potential (Ψ_m) and data point count (n). **EC-20** probe volumetric water content calibration (b) with probe output as millivolt on the abscissa and VWC on the ordinate. Correlation coefficient (r^2) is shown for VWC probe calibration equation and data point count (n).



Appendix Fig. B9 a, b. Comparison of calibration constants for 80% peat : 20% perlite substrate when (a) calculated on a container capacity basis (517 mL) vs. (b) calculated on a total column volume basis (684.1 mL).



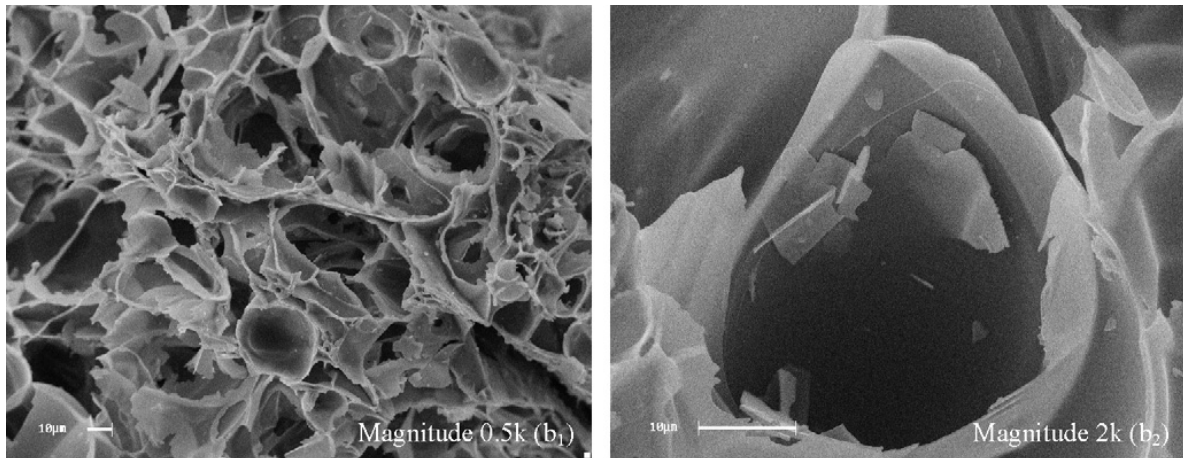
Appendix Fig. B10 a, b. Comparison of calibration constants for 100% perlite when (a) calculated on a container capacity basis (349 mL) vs. (b) calculated on a total column volume basis (684.1 mL).

Appendix C. 1

Representative chemical analyses of Milos (Provatas and Trachilas), Kimolos and Kos perlites, % (After Koukouzas et al., 2000)

	Provatas, Milos		Trachilas, Milos		Kimolos		Kos	
	1	2	3	4	5	6	7	8
SiO ₂	76.10	74.98	76.22	75.19	75.40	73.93	76.80	75.79
TiO ₂	0.14	0.15	0.08	0.08	0.15	0.15	0.13	0.13
Al ₂ O ₃	12.16	12.55	11.83	11.49	12.67	12.67	12.18	11.98
Fe ₂ O ₃	1.19	1.15	0.93	0.95	1.19	1.19	0.75	0.86
MnO	0.05	0.10	0.08	0.08	0.06	0.06	0.06	0.05
MgO	0.27	0.21	0.17	0.21	0.09	0.09	0.03	0.17
CaO	1.21	1.18	0.70	0.73	0.96	0.96	0.57	0.58
Na ₂ O	3.62	3.67	3.25	3.08	3.69	3.69	3.59	3.46
K ₂ O	3.03	2.87	4.51	4.51	3.71	3.71	4.23	4.11
P ₂ O ₅	0.03	0.04	0.02	0.03	0.03	0.03	0.02	0.02
LOI	2.19	2.22	2.37	2.73	2.54	2.54	2.42	2.79
Total	99.99	99.12	100.16	99.09	100.49	100.49	100.78	99.93

Appendix C. 2



SEM images of plain perlite b1 and b2. (After Hosseini et al., 2007)

Glossary

BD: bulk density is the mass in grams of a dried cubic centimeter of substrate. ($\text{g} \cdot \text{cm}^3$)

CC: container capacity describes the amount of water retained by the substrate against the gravitational forces after an irrigation event and after drainage. (% or mL)

TP: Total porosity is the volume of pore space filled either by water or air. (%) Also known as total pore space (TPS)

AFP: air filled-porosity is the percentage of pores filled with air after irrigation and drainage.

EAW: easily-available water is the amount of water released by the substrate with a matric potential (pressure/suction) from 0 to -5 kPa. (%)

WBC: water-buffering capacity is the amount of water released by the substrate with a matric potential from -5 to -10 kPa. (%)

PUW: progressively-unavailable water is the amount of water released by the substrate after 10 kPa. (%)

WUE: water use efficiency is the ability of plants to gain carbon (as total biomass or harvestable yield) per unit of water transpired. ($\text{mol} \cdot \text{mol}$)

Bibliography

- Allaire, S.E., Caron, J., Gallichand, J. 1994. Measuring the saturated hydraulic conductivity of peat substrates in nursery containers. *Can. J. Soil Sci.* 74: 431-437.
- Allaire-Leung, S.E., Caron, J., Parent, L.E. 1999. Changes in physical properties of peat substrates during plant growth. *Can. J. Soil Sci.* 79: 137-139.
- Amente, G., Baker, J.M., Reece, C.F. 2000. Estimation of soil solution electrical conductivity from bulk soil electrical conductivity in sandy soils. *Soil Sci. Soc. Am. J.* 64: 1931-1939.
- Argo, W. R. 1998a. Root medium chemical properties. *HortTechnology* 8, 1-10.
- Argo, W.R. 1998b. Root medium physical properties. *HortTechnology* 8: 11-16.
- Argo, W.R. and Biernbaum, J.A. 1994. Irrigation requirements, root-medium pH, and nutrient concentrations of Easter lilies grown in five peat-based media with and without an evaporation barrier. *J. Amer. Soc. Hort. Sci.* 119: 1151-1156.
- Argo, W.R. and Biernbaum, J.A. 1996a. The effect of lime, irrigation-water source, and water-soluble fertilizer on root-zone pH, EC, and macronutrients management of container root media with impatiens. *J. Amer. Soc. Hort. Sci.* 121: 442-452.
- Argo, W.R. and Biernbaum, J.A. 1996b. Availability and persistence of macronutrients from lime and preplant nutrient charge fertilizers in peat-based root media. *J. Amer. Soc. Hort. Sci.* 121: 453-460.
- Argo, W.R. and Biernbaum, J.A. 1997a. Lime, water source, and fertilizer nitrogen form affect medium pH and nitrogen accumulation and uptake. *HortScience* 32: 71-74.
- Argo, W.R. and Biernbaum, J.A. 1997b. The effect of root media on root-zone pH, calcium, and magnesium management in containers with impatiens. *J. Amer. Soc. Hort. Sci.* 122: 275-284.

- Balendonck, J., Bruins, M.A., Wattimena, M.R., Voogt, W., Huys, A. 2005. WET-sensor pore water EC calibration for three horticultural soils. *Acta Hort.* 691(2): 789-795.
- Bandaranayake, W.A., Parsons, L.R., Borhan, M.S., Holeton, J.D. 2007. Performance of a capacitance-type soil water probe in a well-drained sandy soil. *Soil Sci. Soc. Am. J.* 71: 993-1002.
- Barker, A.V. and Mills, H.A. 1980. Ammonium and nitrate nutrition of horticultural crops. *Hort. Rev.* 2: 395-423.
- Beeson, R.C., Arnold, M.A., Bilderback, T.E., Bolusky, B., Chandler, S., Gramling, H.M., Lea-Cox, J.D., Harris, J.R., Klinger, P.J., Mathers, H.M., Ruter, J.M., Yeager, T.H. 2004. Strategic vision of container nursery irrigation in the next ten years. *J. Environ. Hort.* 22: 113-115.
- Biernbaum, J.A., Argo, W.R., Weesies, B., Weesies, A., Haack, K. 1995. Persistence and replacement of preplant nutrient charge fertilizers from highly leached peat-based root media. *HortScience* 30: 763.
- Bilderback, T.E. and Fonteno, W.C. 1987. Effects of geometry and media physical properties on air and water volumes in containers. *J. Environ. Hort.* 5(4): 180-182.
- Bilderback, T.E., Fonteno, W.C., Johnson, D.R. 1982. Physical properties of media composed of peanut hulls, pine bark, and peat-moss and their effects on azalea growth. *J. Amer. Soc. Hort. Sci.* 107: 522-525.
- Blom, T.J. and Piott, B.D. 1992. Preplant moisture content and compaction of peatwool using two irrigation techniques on potted chrysanthemums. *J. Amer. Soc. Hort. Sci.* 117(2): 220-223.
- Blonquist, J.M., Jones, S.B., Robinson, D.A. 2005. Standardizing characterization of electromagnetic water content sensors: Part 2. Evaluation of seven sensing systems. *Vadose Zone J.* 4: 1059-1069.

- Bogena, H.R., Huisman, J.A., Oberdorster, C., Vereecken, H. 2007. Evaluation of a low-cost soil water content sensor for wireless network applications. *J. of Hydrology* 344: 32-42.
- Brown, J.M., Fonteno, W.C., Cassel, D.K., Johnson, G.A. 1987. Computer tomographic analysis of water distribution in three porous foam media. *Soil Sci. Soc. Am. J.* 51: 1121-1125.
- Brückner, U. 1997. Physical properties of different potting media and substrates mixtures especially air and water capacity. *Acta Hort.* 450: 263-270.
- Bunt, A.C. 1961. Some physical properties of pot-plant compost and their effect on plant growth I. Bulky physical conditioners. *Plant and Soil* 13(4): 322-332.
- Bunt, A.C. 1983. Physical properties of mixtures of peats and minerals of different particle size and bulk density for potting substrates. *Acta Hort.* 150: 143-153.
- Bunt, A.C. 1988. Media and mixes for container-grown plants. Unwin Hyman, London.
- Caron, J., Lemay, I., Dorais, M., Pepin, S. 2006. Improvement of water use efficiency and yield of greenhouse tomato using matric potential sensor. International Annual meeting '06. Joint meeting of the American Society of Agronomy, Crop Science Society of America, Soil Science Society of America (ASA-CSSA-SSSA). Indiana Conv. Center, Indianapolis, USA, November 12-16, 2006. (Abs. 806)
- Caron, J., Riviere, L.M., Guillemain, G. 2005. Gas diffusion and air-filled porosity: Effect of some oversize fragments in growing media. *Can. J. Soil Sci.* 85: 57-65.
- Cattivello, C. 1991. Physical parameters in commercial substrates and their relationships. *Acta Hort.* 294: 183-195.
- Chandler, D.G., Seyfried, M., Murdock, M., McNamara, J.P. 2004. Field calibration of water content reflectometers. *Soil Sci. Soc. Am. J.* 68: 1501-1507.

- Cobos, D. 2009. Permittivity data filtering from Decagon sensors. *pers. comm.* Decagon Devices Inc. Pullman, USA.
- Dane, J.H. and Topp, C. 2002. Methods of soil analysis. Part 4. Physical Methods SSSA, Segoe Road, Madison, WI 53711, USA.
- De Boodt, M. and Verdonck, O. 1972. The physical properties of the substrates in horticulture. *Acta Hort.* 26: 37-44.
- De Boodt, M., Verdonck, O. Cappaert, I. 1974. Method for measuring the water release curve of organic substrates. *Acta Hort.* 37: 2054-2062.
- Decagon Devices. 2008. 5TE Water content, EC, and temperature sensors operator's manual. Version No.3. pp. 31, Pullman, WA.
- Dodd, I.C. 2005. Root-to-shoot signaling: Assessing the roles of 'up' in the up and down world of long-distance signaling in planta. *Plant and Soil* 274: 251-270.
- Drzal, M.S., Fonteno, W.C., Cassel, D.K. 1999. Pore fraction analysis: A new tool for substrate testing. *Acta Hort.* 481: 43-54.
- Flexas, J., Bota, J., Cifre, J., Escalona, J.M., Galmes, J., Gulias, J., Lefi, E.K., Martinez-Canellas, S.F., Moreno, M.T., Ribas-Carbo, M., Riera, D., Sampol, B., Medrano, H. 2004. Understanding down-regulation of photosynthesis under water stress: future prospects and searching for physiological tools for irrigation management. pp. 273-283. *Assoc. Applied Biologists.*
- Fonteno, W.C. 1989. An approach to modeling air water status of horticultural substrates. *Acta Hort.* 238: 67-74.
- Fonteno, W.C., Cassel, D.K., Larson, R.A. 1981. Physical-properties of three container media and their effect on poinsettia growth. *J. Amer. Soc. Hort. Sci.* 106: 736-741.
- Fonteno, W.C., Bailey, D.A., Nelson, P.V. 1995. Properties of greenhouse substrates. *North Carolina flower growers bull.* 40(4): 3-8.

- Food and Agriculture Organization of the United Nations (FAO). 2002. Crops and drops – Making the best of water for agriculture. FAO, Rome, Italy.
- Gabriëls, R., Van Keirsbulck, W., Verdonck, O. 1991. Reference method for physical and chemical characterization of growing media: An international comparative study. *Acta Hort.* 294: 147-160.
- Goh, K.M. and Maas, E.F. 1980. A procedure for determining air and water capacity of soilless media and a method for representing the results for easier interpretation. *Acta Hort.* 99: 81-92.
- Handreck, K. and N. Black. 2002. Growing media for ornamental plants and turf (3rd ed.). Univ. New South Wales Press, Sydney, Australia.
- Hanson, B.R. and Peters, D. 2000. Soil type affects accuracy of dielectric moisture sensors. *California Agriculture* 54: 43-47.
- Hanson, B., Peters, D., Orloff, S. 2000. Effectiveness of tensiometers and electrical resistance sensors varies with soil conditions. *California Agriculture* 54: 47-50.
- Hilhorst, M.A. 2000. A pore water conductivity sensor. *Soil Sci. Soc. Am. J.* 64: 1922-1925.
- Hopmans, J. W. and Rolston, D. E. 2002. SCC107-Introductory soil physics. Chapter 2. Univ. of Cal.
Davis. <http://lawr.ucdavis.edu/classes/ssc107/SSC107Syllabus/chapter2-00.pdf>
(Accessed; 10/20/2009)
- Hosseini, S.N., Borghei, S.M., Vossoughi, M., Taghavinia, N. 2007. Immobilization of TiO₂ on perlite granules for photocatalytic degradation of phenol. *Applied Catalysis B: Environmental* 74: 53-62.
- Incrocci, L., Incrocci, G., Pardossi, A., Lock, G., Nicholl, C., Balendonck, J. 2009. The calibration of WET-sensor for volumetric water content and pore water electrical conductivity in different horticultural substrates. *Acta Hort.* 807: 289-294.

- Inoue, M., Ahmed, B.A.O., Saito, T., Irshad, M., Uzoma, K.C. 2008. Comparison of three dielectric moisture sensors for measurement of water in saline sandy soil. *Soil Use and Management* 24: 156-162.
- Jones, H.G. 1992. *Plants and Microclimate A quantitative approach to environmental plant physiology*, 2nd Ed. Cambridge University Press, Cambridge.
- Jones, H.G. 2004. Irrigation scheduling: advantages and pitfalls of plant-based methods. *J. Exp. Bot.* 55: 2427-2436.
- Jones, H.G. 2007. Monitoring plant and soil water status: established and novel methods revisited and their relevance to studies of drought tolerance. *J. Exp. Botany* 58: 119-130.
- Jones, H.G. 2008. Irrigation scheduling - Comparison of soil, plant and atmosphere monitoring approaches. *Acta Hort.* 792: 391-403.
- Jones, S.B. and Or, D. 2004. Frequency domain analysis for extending time domain reflectometry water content measurement in highly saline soils. *Soil Sci. Soc. Am. J.* 68, 1568-1577.
- Jones, S.B., Blonquist, J.M., Robinson, D.A., Rasmussen, V.P., Or, D. 2005. Standardizing characterization of electromagnetic water content sensors: Part 1. Methodology. *Vadose Zone J.* 4: 1048-1058.
- Karlovich, P.T. and Fonteno, W.C. 1986. Effect of soil-moisture tension and soil-water content on the growth of *Chrysanthemum* in 3 container media. *J. Amer. Soc. Hort. Sci.* 111: 191-195.
- Kelleners, T.J., Robinson, D.A., Shouse, P.J., Ayars, J.E., Skaggs, T.H. 2005b. Frequency dependence of the complex permittivity and its impact on dielectric sensor calibration in soils. *Soil Sci. Soc. Am. J.* 69: 67-76.

- Kelleners, T.J., Seyfried, M.S., Blonquist, J.M., Bilskie, J., Chandler, D.G. 2005a. Improved interpretation of water content reflectometer measurements in soils. *Soil Sci. Soc. Am. J.* 69: 1684-1690.
- Kelleners, T.J., Soppe, R.W.O., Ayars, J.E., Skaggs, T.H. 2004. Calibration of capacitance probe sensors in a saline silty clay soil. *Soil Sci. Soc. Am. J.* 68: 770-778.
- Kiehl, P.A., Liel, J.H., Buerger, D.W. 1992. Growth response of *Chrysanthemum* to various container medium moisture tensions levels. *J. Amer. Soc. Hort. Sci.* 117(2): 224-229.
- Kizito, F., Campbell, C.S., Campbell, G.S., Cobos, D.R., Teare, B.L., Carter, B., Hopmans, J.W. 2008. Frequency, electrical conductivity and temperature analysis of a low-cost capacitance soil moisture sensor. *J. Hydrology* 352: 367-378.
- Koukouzas, N.K., Dunham, A.C., Scott, P.W. 2000. Suitability of Greek perlite for industrial applications. *Transactions of the institution of mining and metallurgy section B-applied earth science* 109: B105-B111.
- Lang, H.J. and Elliott, G.C. 1991. Influences of ammonium: nitrate ratio and nitrogen concentration on nitrification activity in soilless potting media. *J. Amer. Soc. Hort. Sci.* 116: 642-645.
- Lea-Cox, J.D., Ristvey, A.G., Arguedas Rodriguez, F.R., Ross, D.S., Anhalt, J., Kantor, G. 2008. A low-cost multihop wireless sensor network, enabling real-time management of environmental data for the greenhouse and nursery industry. *Acta Hort.* 801: 523-529.
- Lea-Cox, J.D., Stutte, G.W., Berry, W.L., Wheeler, R.M. 1996. Charge balance - a theoretical basis for modulating pH fluctuations in plant nutrient delivery systems. *Life Support Biosphere Sci.* 3:53-59
- Logsdon, S. 2005. Time domain reflectometry range of accuracy for high surface area soils. *Vadose Zone J.* 4: 1011-1019.

- Marschner, H. 1986. Mineral nutrition of higher plants. Academic Press, London.
- Martinez, F.X., Bures, S., Blanca, F., Yuste, M.P., Valero, J. 1991. Experimental and theoretical air/water ratios of different substrate mixtures at container capacity. *Acta Hort.* 294: 241-248
- Milks, R.R., Fonteno, W.C., Larson, R.A. 1989a. Hydrology of horticultural substrates .1. Mathematical-models for moisture characteristics of horticultural container media. *J. Amer. Soc. Hort. Sci.* 114: 48-52.
- Milks, R.R., Fonteno, W.C., Larson, R.A. 1989b. Hydrology of horticultural substrates .2. Predicting physical-properties of media in containers. *J. Amer. Soc. Hort. Sci.* 114: 53-56.
- Milks, R.R., Fonteno, W.C., Larson, R.A. 1989c. Hydrology of horticultural substrates .3. Predicting air and water-content of limited-volume plug cells. *J. Amer. Soc. Hort. Sci.* 114: 57-61.
- Nadler, A. 1981. Field application of the 4-electrode technique for determining soil solution conductivity. *Soil Sci. Soc. Am. J.* 45: 30-34.
- Nadler, A. 1982. Estimating the soil-water dependence of the electrical-conductivity soil solution electrical-conductivity bulk soil ratio. *Soil Sci. Soc. Am. J.* 46: 722-726.
- Nadler, A. and Frenkel, H. 1980. Determination of soil solution electrical-conductivity from bulk soil electrical-conductivity measurements by the 4-electrode method. *Soil Sci. Soc. Am. J.* 44: 1216-1221.
- Nelson, P.V. 1991. Greenhouse operations and management. 4th ed. Prentice Hall, Englewood Cliffs, NJ.
- Nemali, K.S., Montesano, F., Dove, S.K., van Iersel, M.W. 2006. Calibration and performance of moisture sensors in soilless substrates: ECH₂O and theta probes. *Sci. Hort.* 112: 227-234.

- Niemiera, A.X. and Wright, R.D. 1986. The influence of nitrification on the medium solution and growth of holly, azalea, and juniper in pine bark medium. *J. Amer. Soc. Hort. Sci.* 111: 708-712.
- Nkongolo, N.V., Caron, J. 1999. Bark particle sizes and the modification of the physical properties of peat substrates. *Can. J. Soil Sci.* 79: 111-116.
- Noborio, K., Horton, R., Tan, C. S. 1999. Time domain reflectometry probe for simultaneous measurement of soil matric potential and water content. *Soil Sci. Soc. Am. J.* 63: 1500-1505.
- Or, D. 2001. Who invented the tensiometer? *Soil Sci. Soc. Am. J.* 65: 1-3.
- Orozco, R., Gschwander, S., Marfa, O. 1997. Substrate classification from particle size analysis. *Acta Hort.* 450: 397-404.
- Paquet, J.M., Caron, J., Banton, O. 1993. In situ determination of water desorption characteristics of peat substrates. *Can. J. Soil Sci.* 73: 329-339.
- Parsons, L.R. and Bandaranayake, W.M. 2009. Performance of a new capacitance soil moisture probe in a sandy soil. *Soil Sci. Soc. Am. J.* 73: 1378-1385.
- Pepin, S., Dorais, M., Gruyer, N., Ménard, C. 2008. Defining irrigation set points for organically-grown greenhouse tomato crops using growth and physiological responses to soil matric potential. *Plants and Soils: Montreal '08: Joint meeting of the CSHS, CSA and Northeastern Branch ASA-CSSA-SSSA, McGill University, Montréal, Canada, July 13-16, 2008. (Oral presentation)*
- Persson, K.M. and Berndtsson, R. 1998. Texture and electrical conductivity effects on temperature dependency in time domain reflectometry. *Soil Sci. Soc. Am. J.* 62: 887-893.
- Peterson, J. C. 1981. Modify your pH perspective. *Florist's Review* 169, 34-35, 92-93.

- Plauborg, F., Iversen, B.V., Laerke, P.E. 2005. In situ comparison of three dielectric soil moisture sensors in drip irrigated sandy soils. *Vadose Zone J.* 4: 1037-1047.
- Polyakov, V., Fares, A., Ryder, M.H. 2005. Calibration of a capacitance system for measuring water content of tropical soil. *Vadose Zone J.* 4: 1004-1010.
- Raviv, M. and Lieth, J.H. 2008. *Soilless culture: theory and practice*. 1st Ed. Elsevier Science, Amsterdam.
- Raviv, M., Medina, S., Shamir, Y., Ner, Z. 1993. Very low medium moisture tension – A feasible criterion for irrigation control of container-grown plants. *Acta Hort.* 342: 111-120
- Raviv, M., Wallach, R., Blom, T. J. 2004. The effect of physical properties of soilless media on plant performance – a review. *Acta Hort.* 644: 251-259.
- Rhoades, J.D., Chandivi, F., Lesch, S.M. 1999. Soil salinity assessment methods and interpretation of electrical conductivity measurements. FAO, Rome, Italy. Vol 57 152p
- Rhoades, J.D., Manteghi, N.A., Shouse, P.J., Alves, W.J. 1989. Soil electrical-conductivity and soil-salinity - new formulations and calibrations. *Soil Sci. Soc. Am. J.* 53: 433-439.
- Rhoades, J.D., Raats, P.A.C., Prather, R.J. 1976. Effects of liquid-phase electrical-conductivity, water-content, and surface conductivity on bulk soil electrical-conductivity. *Soil Sci. Soc. Am. J.* 40: 651-655.
- Rippy, J.F.M., and Nelson, P.V. 2007. Cation exchange capacity variation among Alberta, Canada, moss peats. *HortScience* 42: 349-352.
- Robinson, D.A., Lebron, I., Lesch, S.M., Shouse, P. 2004. Minimizing drift in electrical conductivity measurements in high temperature environments using the EM-38. *Soil Sci. Soc. Am. J.* 68: 339-345.

- Scoggins, H.L. and van Iersel, M.W. 2006. In Situ Probes for Measurement of Electrical Conductivity of soilless substrates: Effects of Temperature and Substrate Moisture Content. *HortScience* 40: 210-214
- Seyfried, M.S. and Murdock, M.D. 2001. Response of a new soil water sensor to variable soil, water content, and temperature. *Soil Sci. Soc. Am. Proc.* 65: 28-34.
- Seyfried, M.S. and Murdock, M.D. 2004. Measurement of soil water content with a 50-MHz soil dielectric sensor. *Soil Sci. Soc. Am. J.* 68: 394-403.
- Seyfried, M.S., Grant, L.E., Du, E., Humes, K. 2005. Dielectric loss and calibration of the hydra probe soil water sensor. *Vadose Zone J.* 4: 1070-1079.
- Smith, R.A., Schwarz, G.E., Alexander, R.B. 1997. Regional interpretation of water-quality monitoring data. *Water Res. Res.* 33: 2781-2798.
- Smith-Rose, R.L. 1933. The electrical properties of soils for alternating currents at radio frequencies. *Proc. R. Soc. London.* 140:359.
- Stevenson, D.S. 1982. Unreliabilities of pressure plate 1500 kilopascal data in predicting soil water contents at which plants become wilted in soil-peat mixes. *Can. J. Soil Sci.* 62: 415-419.
- Stver, R.C. and Koranski, D. 1997. Plug and transplant production. A grower's guide., Ball Publishing, Batavia, Ill.
- Thompson, R.B., Gallardo, M., Fernandez, M.D., Valdez, L.C., Martinez-Gaitan, C. 2007. Salinity effects on soil moisture measurement made with a capacitance sensors. *Soil Sci. Soc. Am. J.* 71: 1647-1657.
- Tilt, K.M., Bilderback, T.E., Fonteno, W.C. 1987. Particle-size and container size effects on growth of 3 ornamental species. *J. Amer. Soc. Hort. Sci.* 112: 981-984.
- Topp, G.C. and Zebchuk, W. 1979. Determination of soil-water desorption curves for soil cores. *Can. J. Soil Sci.* 59: 19-26.

- Topp, G.C., Davis, J.L., Annan, A.P. 1980. Electromagnetic determination of soil-water content – measurements in coaxial transmission-lines. *Water Resources Research* 16: 574-582.
- Topp, G.C., Zegelin, S., White, I. 2000. Impacts of the real and imaginary components of relative permittivity on time domain reflectometry measurements in soils. *Soil Sci. Soc. Am. J.* 64: 1244-1252.
- U. S. Dept. Agr. 2007. Nursery crops 2006 summary. National Agricultural Statistics Serv. Washington, DC. Sp Cr 6-3 (07).
- Verdonck, O. 1983. Reviewing and evaluation of new materials used as substrates. *Acta Hort.* 150: 467-474.
- Verdonck, O., Penninck, R., De Boodt, M. 1983. The physical properties of different horticultural substrates. *Acta Hort.* 150: 155-160.
- Wallach, R., da Silva, F.F., Chen, Y. 1992. Hydraulic characteristics of tuff (scoria) used as container medium. *J. Amer. Soc. Hort. Sci.* 117: 415-421.
- Waller, P.L. and Harrison, A.M. 1991. Estimation of pore space and the calculation of air volume in horticultural substrates. *Acta Hort.* 294: 29-39.
- Williams, B.J., Peterson, J.C., Utzinger, J.D. 1988. Liming reactions in sphagnum peat-based growing media. *J. Amer. Soc. Hort. Sci.* 113: 210-214.
- Wright, R.D. 1983. Leachate pour-through extraction. *HortScience* 18: 624-624.
- Wright, R.D. 1986. The pour-through nutrient extraction procedure. *HortScience* 21: 227-229.
- Yeager, T.H. and Barrett, J.E. 1985. Phosphorus and sulphur leaching from an incubated superphosphate-amended container medium. *HortScience* 20: 671-672.
- Zhang, Z.B. and Zhang, J.H. 2007. Water-saving agriculture: an urgent issue. *Journal of Integrative Plant Biology* 49: 1409.